Statistical Issues in Imaging Studies

Hongtu Zhu, Ph.D.

Department of Biostatistics and Biomedical Research Imaging Center

University of North Carolina at Chapel Hill

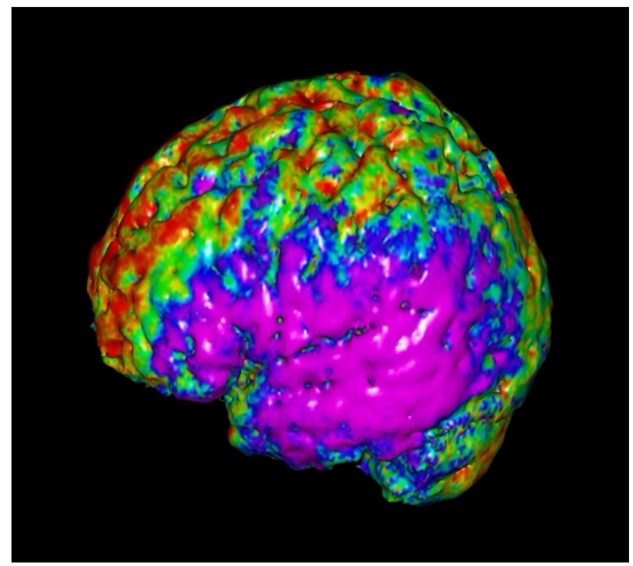

UNC Biostatistics and Imaging Analysis Lab

2 Faculty Members

10 Ph.d Students

5 Postdoctor Fellows

2 Visitor Scholars

4 Past members

UNC Biostatistics and Imaging Analysis Lab

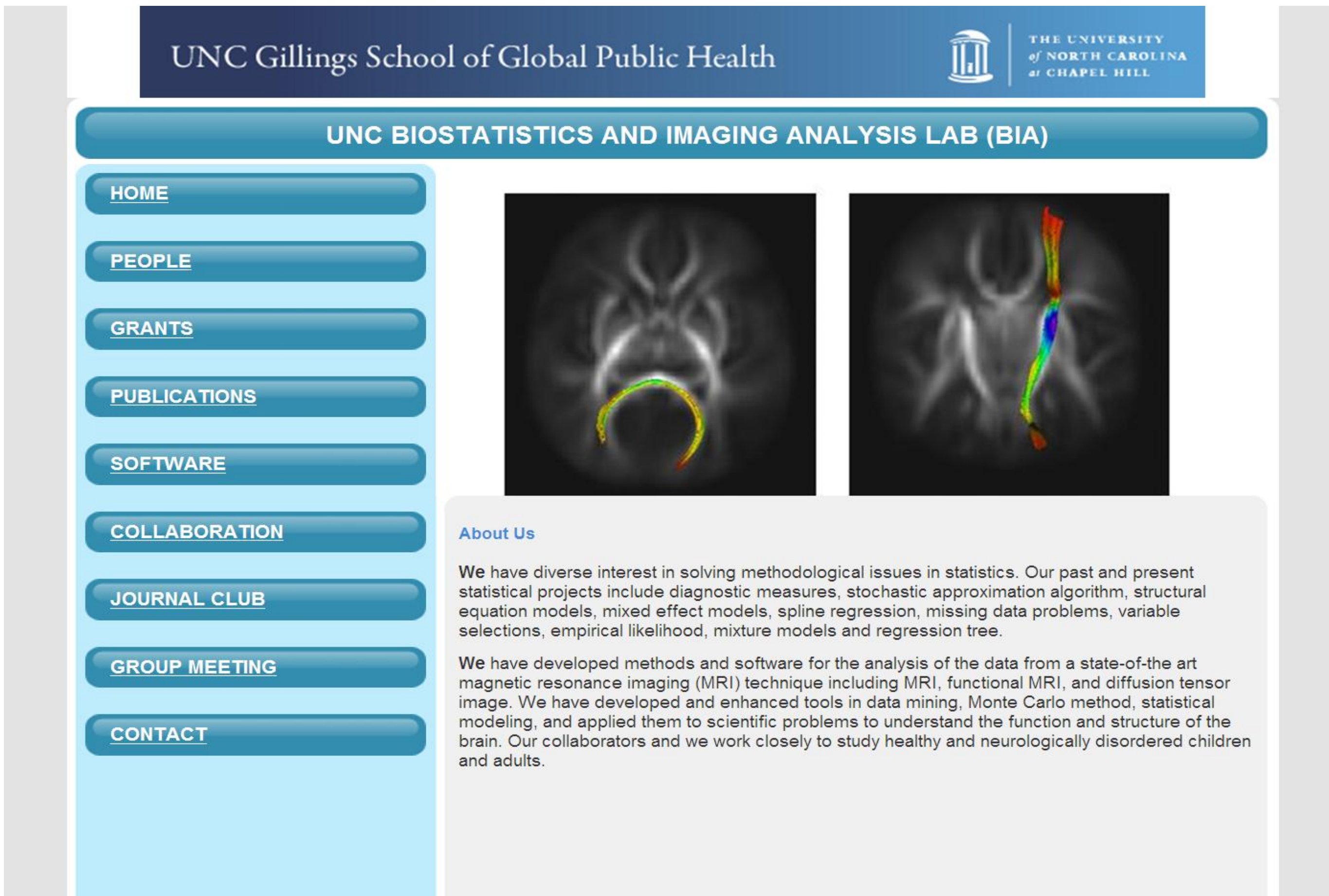

UNC Biostatistics and Imaging Analysis Lab

Sequence Evaluation

Sequence Optimization

Reconstruction

Smoothing

Population Analysis

Data Mining

Imaging Genetics

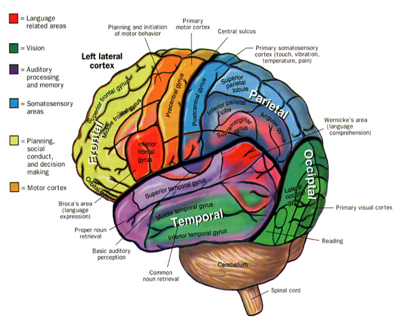

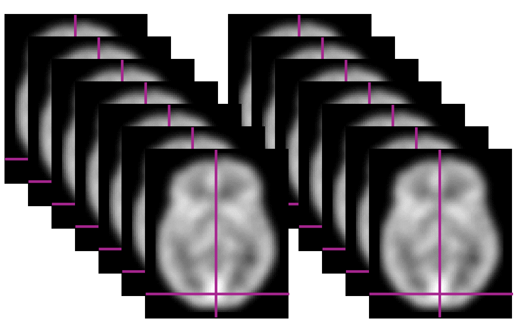

group 1 | group 2

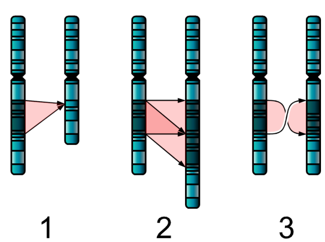

Outline

- Evaluating Imaging Sequence Accuracy
- Imaging Sequence Optimization
- Reconstructing Diffusion Tensor Images
- Smoothing Diffusion Tensor Field
- Analyzing Tract-based Diffusion Tensor Statistics
- Multiscale Adaptive Regression Models
- Brain Connectivity Analysis

Evaluating Imaging Sequence Accuracy

Statistical Methods in Diagnostic Medicine

ARFI Beam Sequence Performance as Evaluated by Trained Readers: Plaque Detection

PI. Caterina M. Gallippi

Methods of Acoustic Radiation Force Impulse (ARFI) Ultrasound

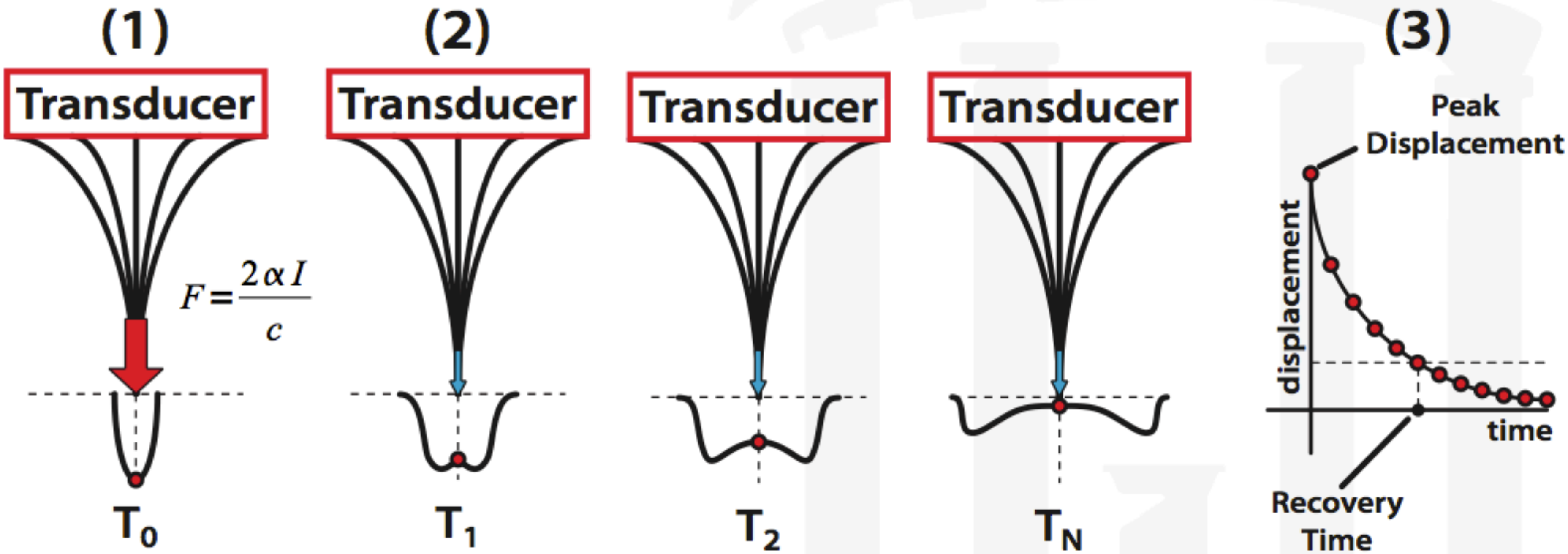

(1) ARFI Excitation Pulse (~70µs) induces axial displacment

(2) Conventional B-Mode pulses track induced displacement

(3) Displacements are calculated to create a displacement profile for every pixel witin the image.

Methods of Shear Wave Elasticity Imaging (SWEI)

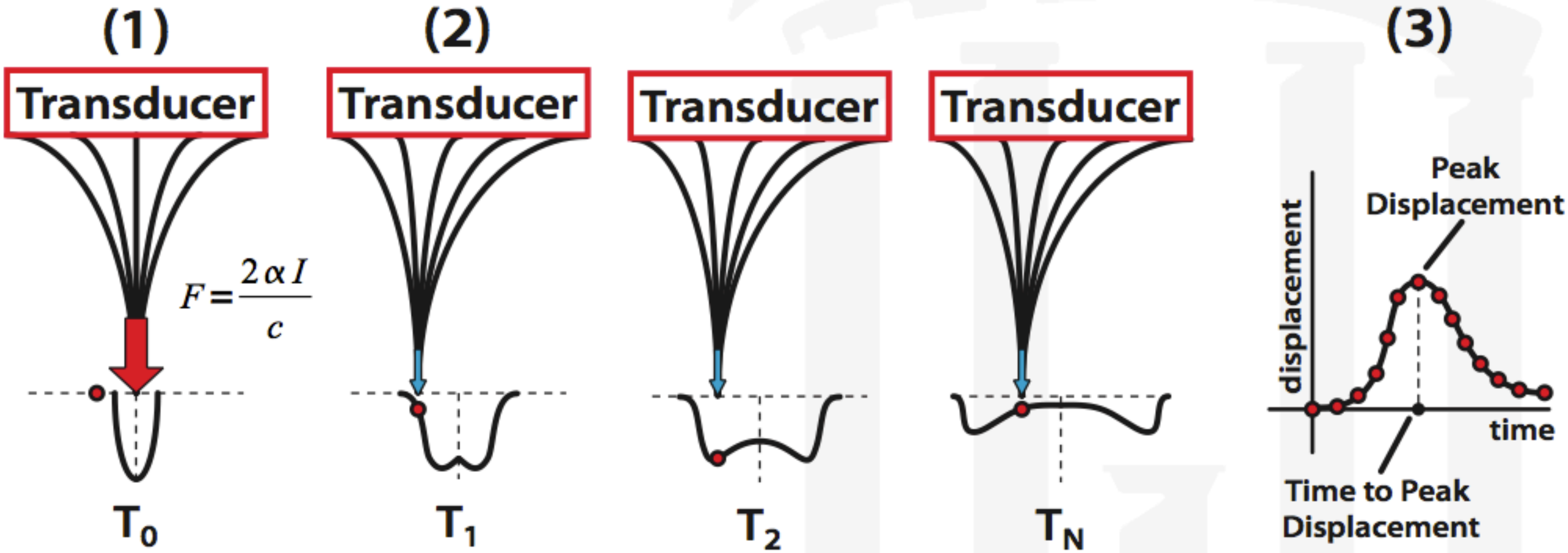

(1) ARFI Excitation Pulse (~70μs) induces axial displacment

(2) Tracking Away From Region of Excitation Tracks ARFI-induced Shear Waves

(3) Displacement Profiles Are Created

Hypothesis

Select ARFI/SWEI beam sequences will yield higher sensitivity and specificity for atherosclerotic plaque detection in peripheral arteries.

General Methods: Beam Sequences

- 3 Types of Excitation

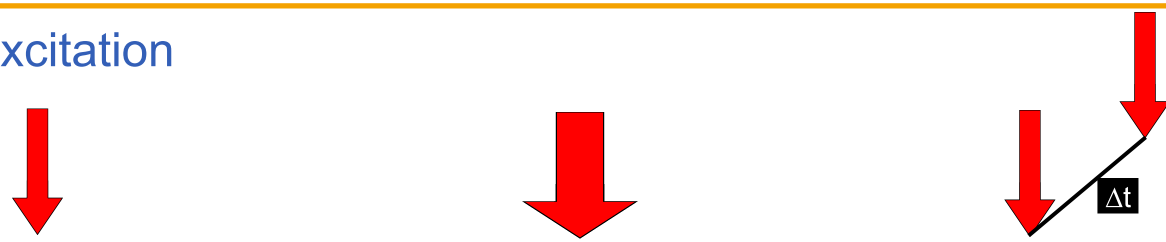

Single F/1.5
(SP1.5)

Single F/3
(SP3)

Double F/1.5
(DP)

- 3 Types of Tracking

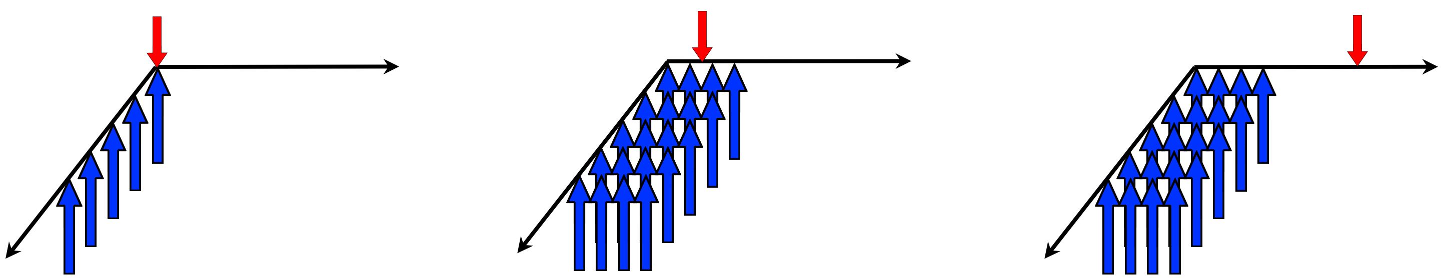

Single A-line RX
(SRx)

4:1 Parallel RX
(ParRx)

SWEI

- Combine for 9 Total Sequences

Reader Study

- Automatically Generated Images
  - ♦ Lumen masking & Color scaling
- 12 Trained Readers
  - ♦ Various levels of experience with ARFI
  - ♦ Only 6 evaluated each Image Set
- Validation
  - ♦ Phantom results compared with known truth
  - ♦ Ex vivo results compared with pathologist rating of spatially matched histology
- Statistics
  - ♦ Latent Variable Models to compare ordinal responses
  - ♦ Generated receiver operating characteristic (ROC) curves
  - ♦ Calculated mean area under the curve (AUC)

Reader GUI

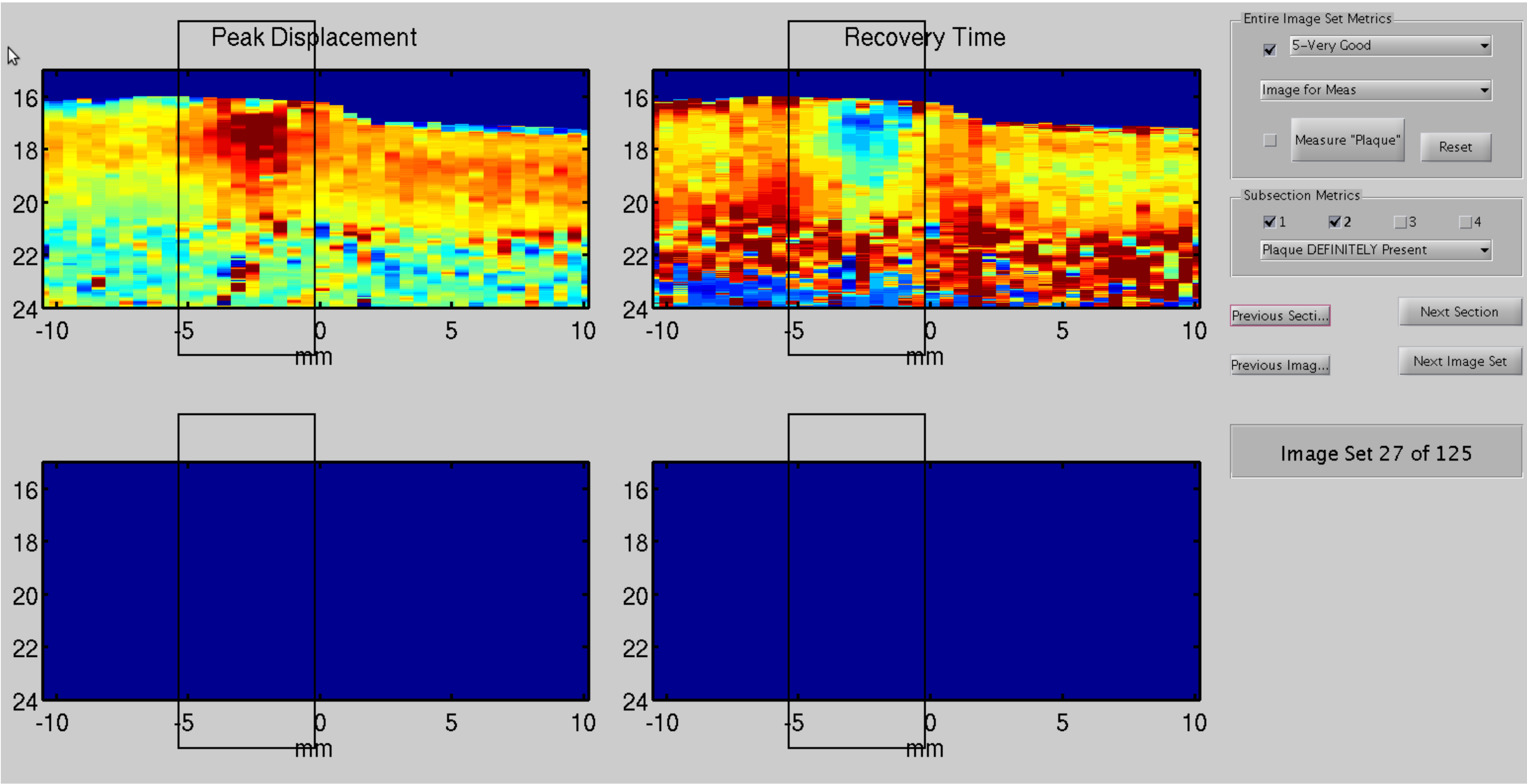

Peak Displacement
Recovery Time
mm
Entire Image Set Metrics
5-Very Good
Image for Meas
Measure "Plaque"
Reset
Subsection Metrics
1
2
3
4
Plaque DEFINITELY Present
Previous Secti...
Next Section
Previous Imag...
Next Image Set
Image Set 27 of 125

Custom Phantom Structure

- ~4mm Layer
- Hard or Soft Inclusions
  - ♦ ~110 kPa & ~190 kPa
- 2.5 or 5mm Width
- Imaging in 3 Locations
  - ♦ Centered (0mm Offset)
  - ♦ -3mm Lateral Offset
  - ♦ -6mm Lateral Offset
- 2 Acquisitions

- 250 Total Image Sets

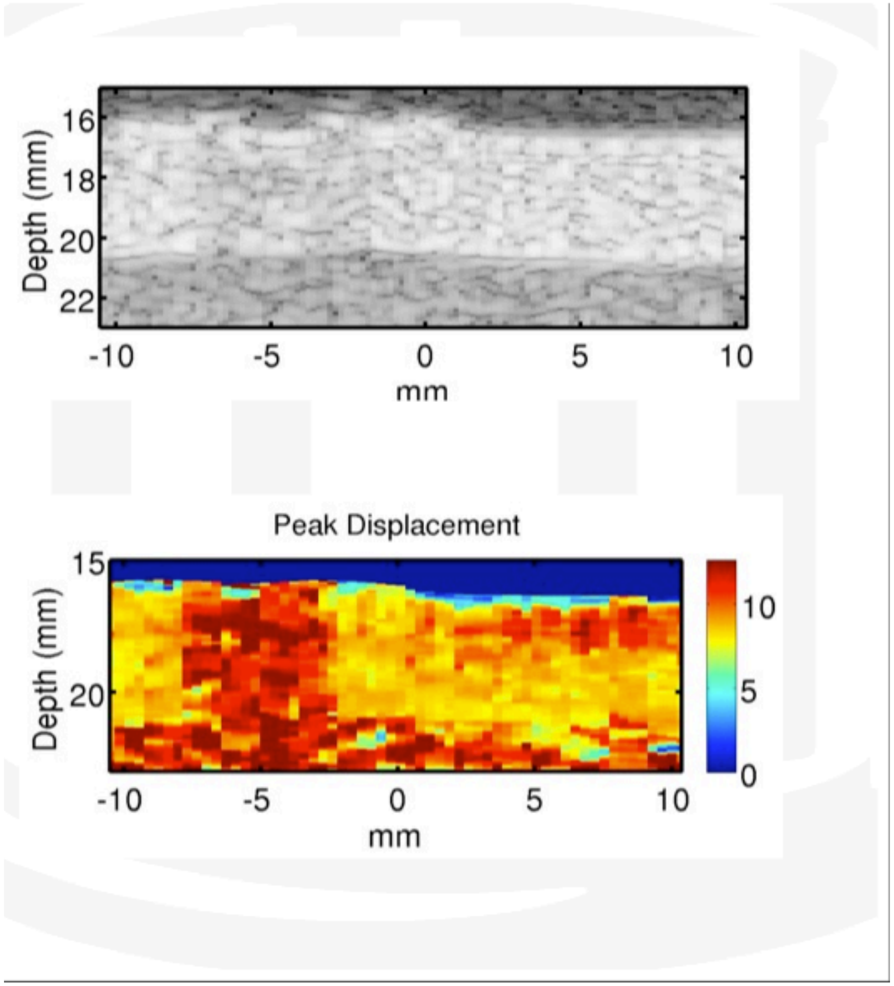

Results: Phantom, All Locations

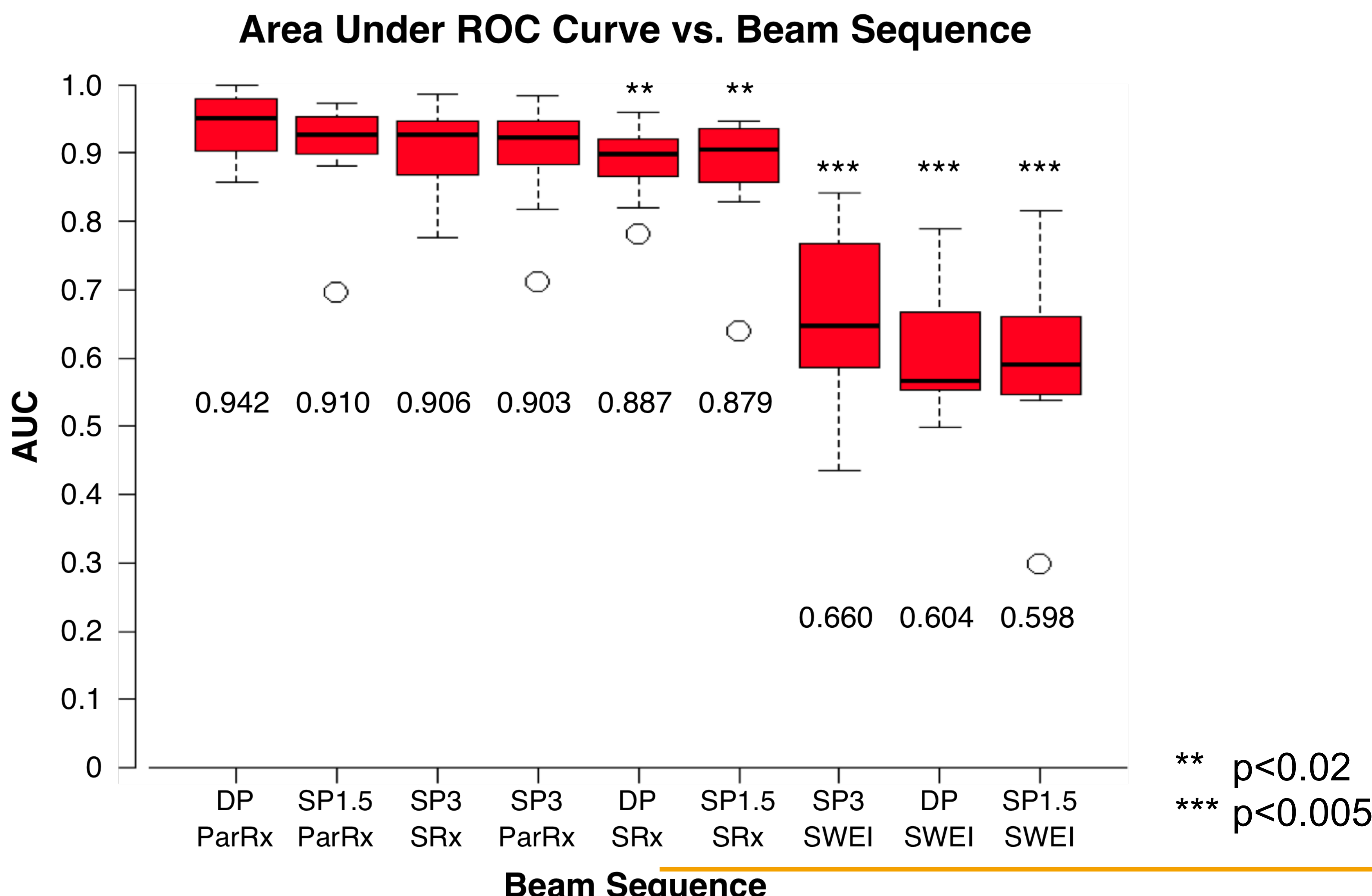

Results: Phantom, -6 mm Lateral Offset

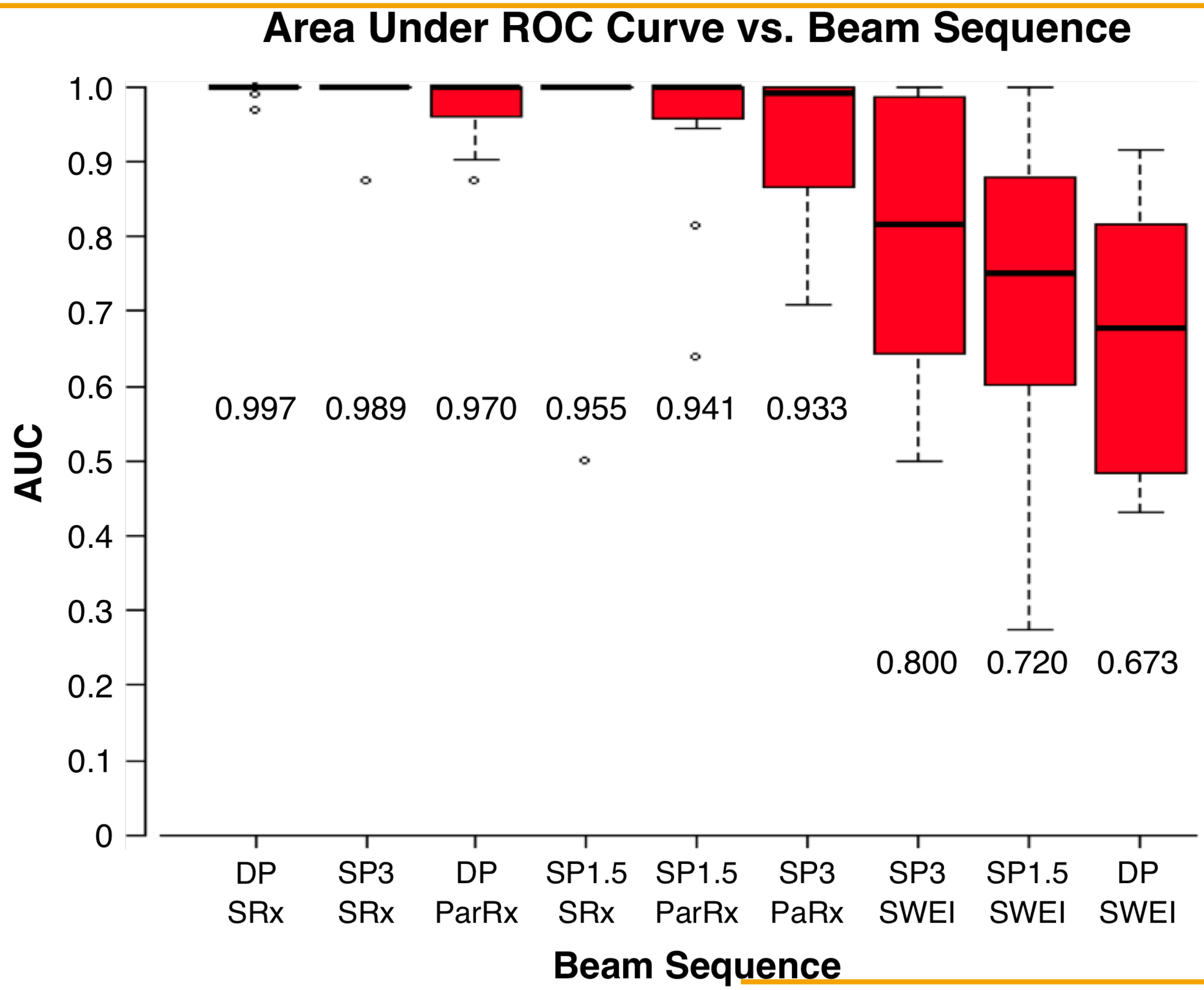

Conclusions

- Robust Method for Statistically Comparing Beam Sequences
- Plaque Detection was better when tracking in ROE
  - ♦ Both in Phantoms and Ex Vivo
  - ♦ Even when accounting for optimal positioning
- Ranking of sequence performance remained consistent between phantom and ex vivo studies
  - ♦ SP1.5-SRx
  - ♦ SP3-SRx
  - ♦ SP3-ParRx
  - ♦ DP-SRx
  - ♦ DP-ParRx
  - ♦ SP3-SWEI
  - ♦ SP1.5-SWEI

Imaging Sequence Optimization

Experimental Design

How to design an optimal imaging acquisition scheme to achieve the best signal-to-noise ratio for a given scan time?

Acquisition Scheme
(Imaging Parameters)

Noisy Images

Images Reconstruction

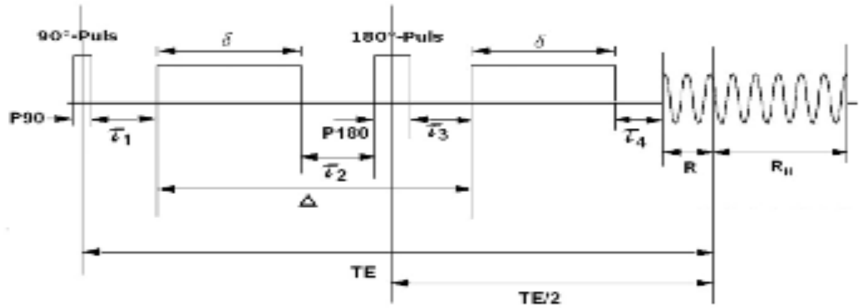

Puled-gradient spin-echo (PGSE) sequence

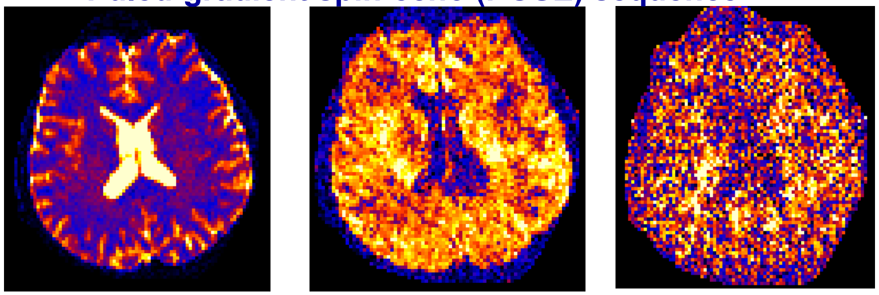

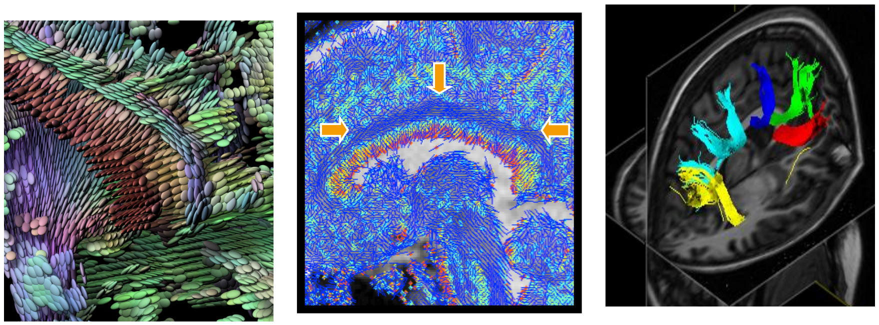

STATISTICAL MODEL

Gradient Orientations & b factors

Design Criterion

Global Optimization

$$S \approx S_0 e^{-bg^T Dg} = f(x,\theta)$$

$$p(S,b,g \mid S_0,D)$$

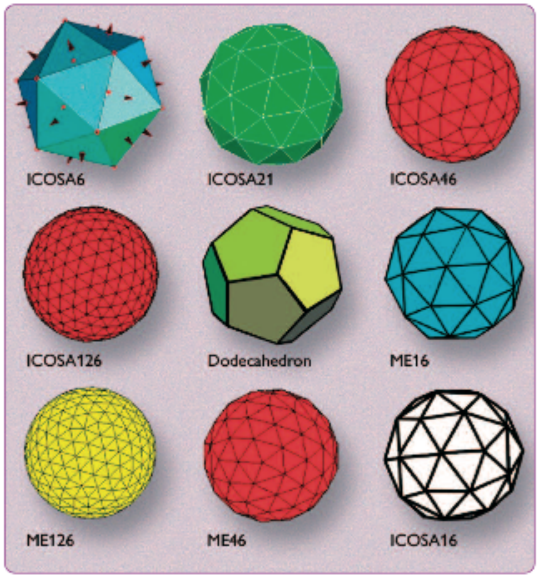

Gradient directions (Hasan & Narayana, 2005, MedicaMundi)

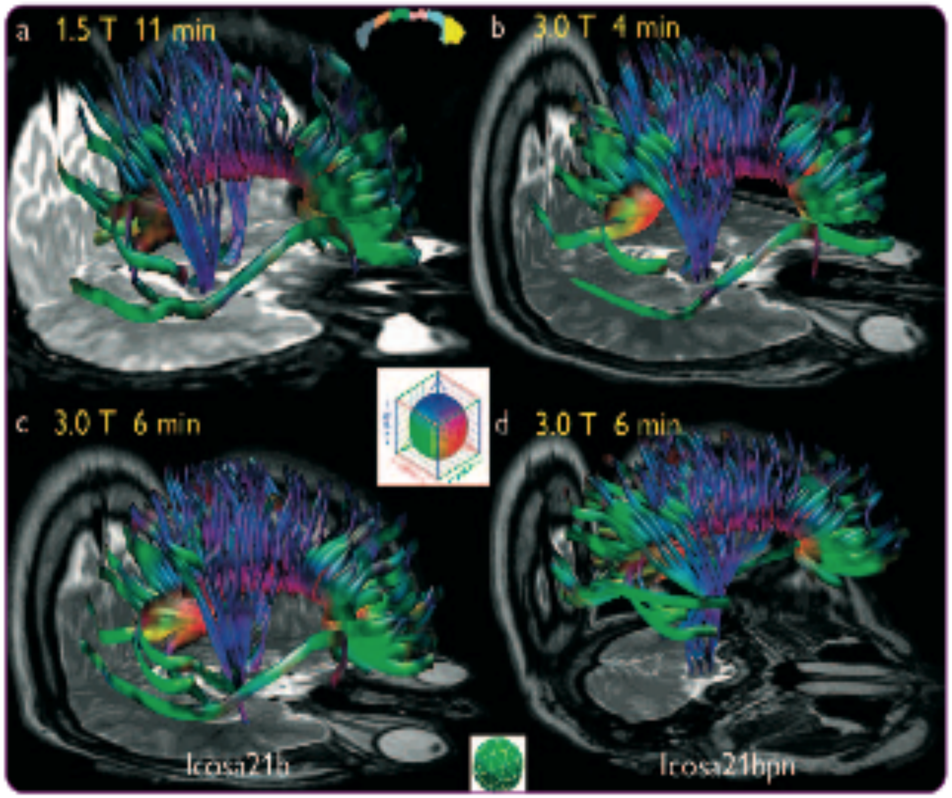

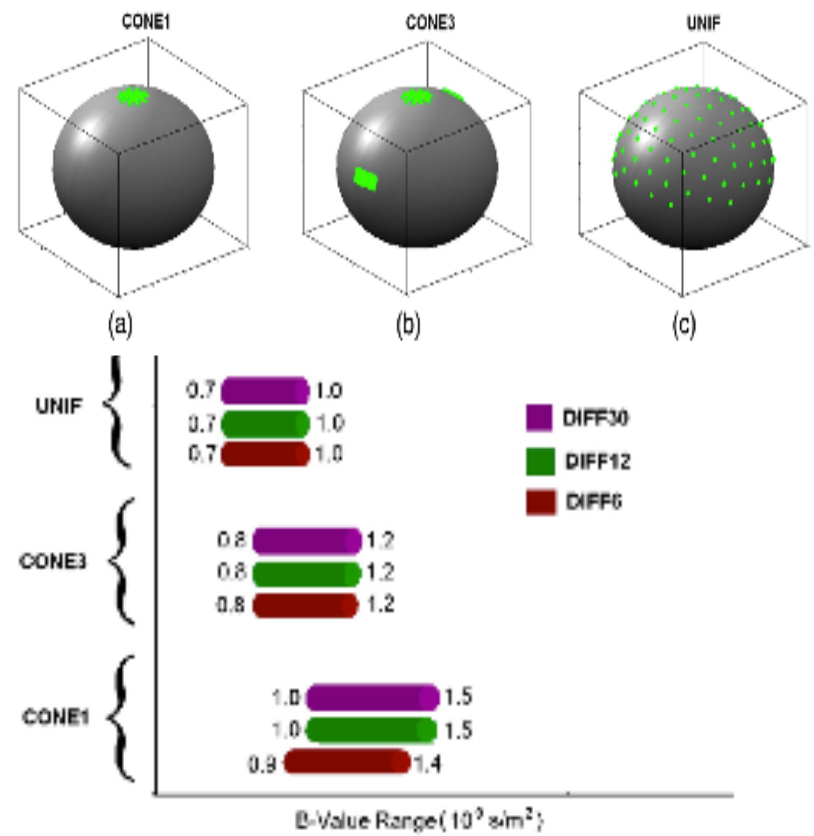

Hasan & Narayana (2005), *MedicaMundi*.

Gao, Zhu, Lin. (2008). *Neuroimage.*

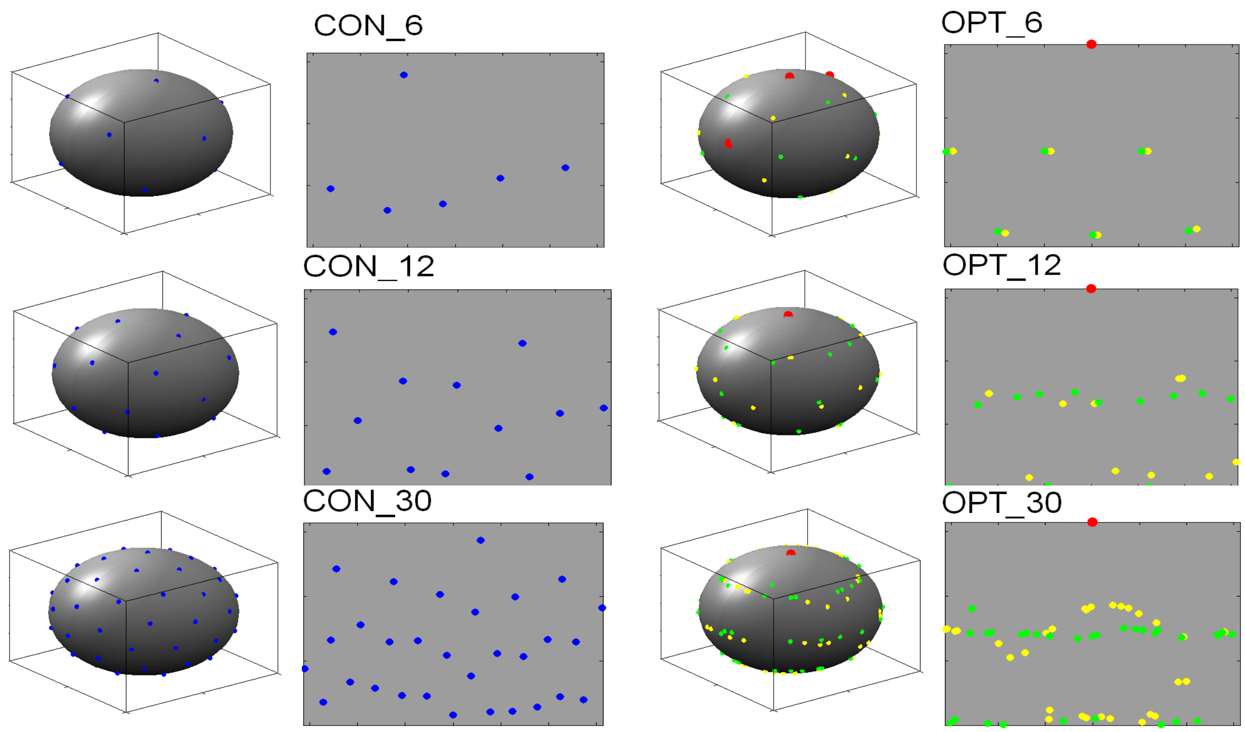

Conventional gradient schemes (a) and optimized schemes (b) based on LS and WLS estimation for uniform fiber case.

Gao, Zhu, Lin. (2008). *Neuroimage.*

Reconstructing Diffusion Tensor Images

Estimation Theory

How to obtain accurate estimates of diffusion tensor and its derived quantities?

Data

$$\{(S_i(v), b_i, g_i) : i = 1, \ldots, n; v \in V\}$$

Rician Regression or Log-linear Model

$$S_i(v) = S_0(v)\exp(-b_i g_i^T D(v) g_i) + \text{noise}$$

Estimated Diffusion Tensor

$$\hat{D}(v)$$

Estimated Eigenvalues or Eigenvectors

$$\{(\hat{\lambda}_k, \hat{e}_k) : k = 1,2,3\}$$

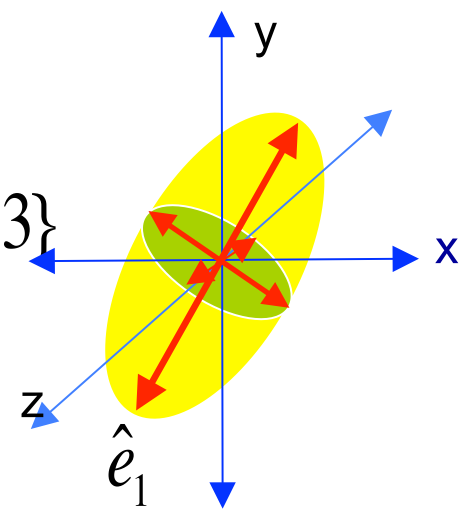

Sorting Bias

$$\hat{D}(v) = \hat{\lambda}_1 \hat{e}_1 \hat{e}_1^T + \hat{\lambda}_2 \hat{e}_2 \hat{e}_2^T + \hat{\lambda}_3 \hat{e}_3 \hat{e}_3^T$$

$$P(\hat{\lambda}_1 > \hat{\lambda}_2 > \hat{\lambda}_3) = 1$$

$$E(\hat{\lambda}_1) > \lambda_1$$

$$E(\hat{\lambda}_3) < \lambda_3$$

$$E(\hat{\lambda}_2) \approx \lambda_2$$

True Diffusion Tensor

$$D(v) = \lambda_1 e_1 e_1^T + \lambda_2 e_2 e_2^T + \lambda_3 e_3 e_3^T$$

$$\lambda_1 \geq \lambda_2 \geq \lambda_3$$

D=diag(0.7, 0.7, 0.7)

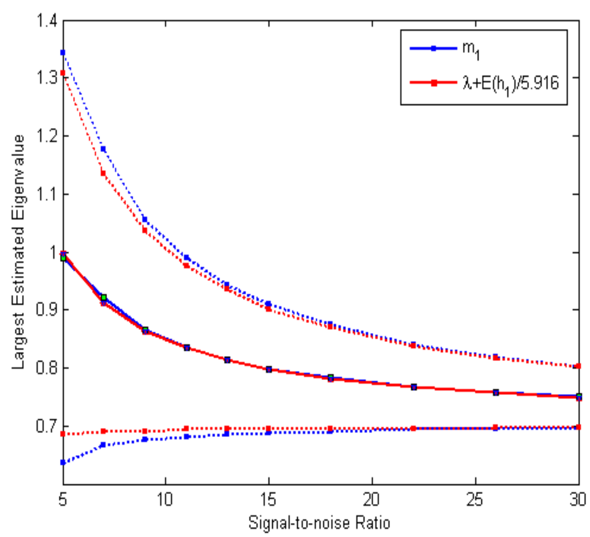

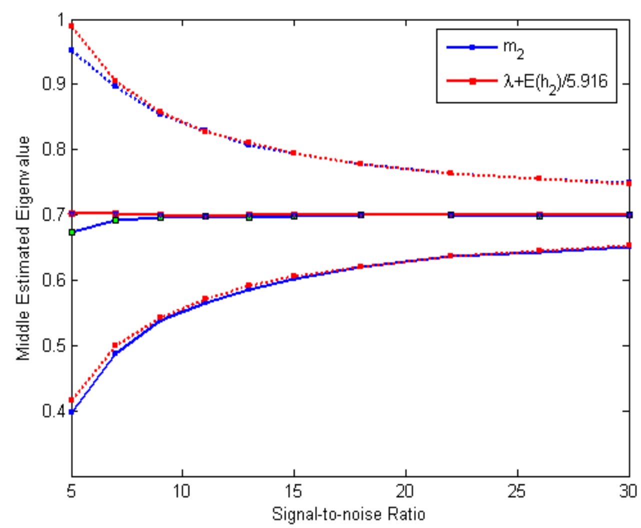

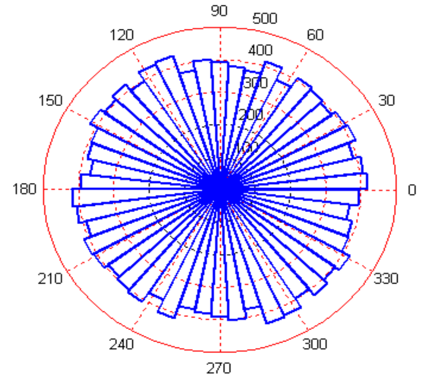

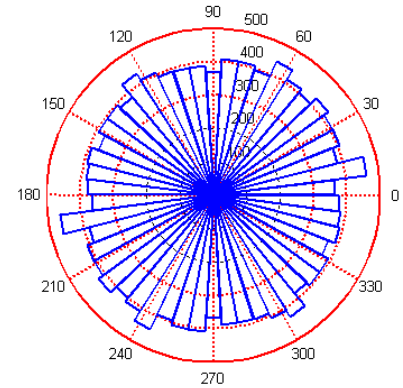

$\theta \in [0, 2\pi]$ and $\phi \in [0, \pi]$ are associated with the spherical coordinate $(1, \theta, \phi)$ of $\mathbf{e}_1$.

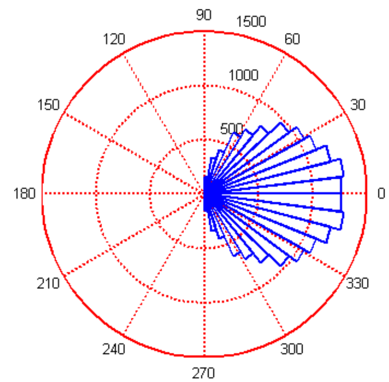

$$SNR = S_0 / \sigma = 22$$

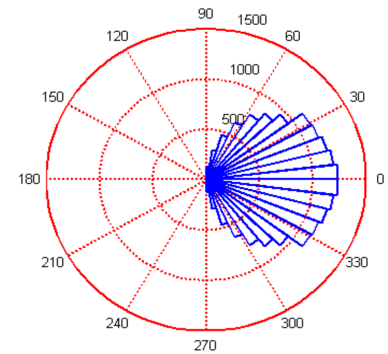

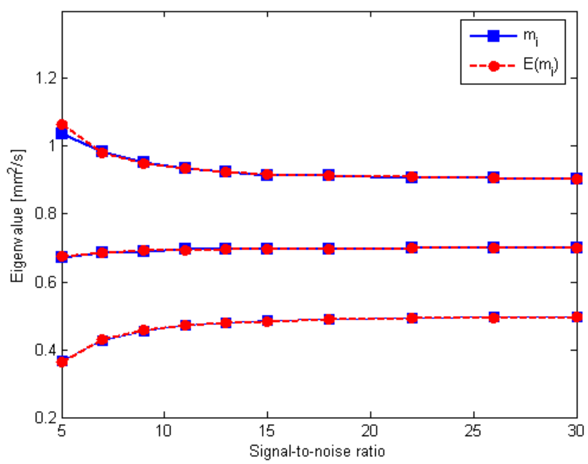

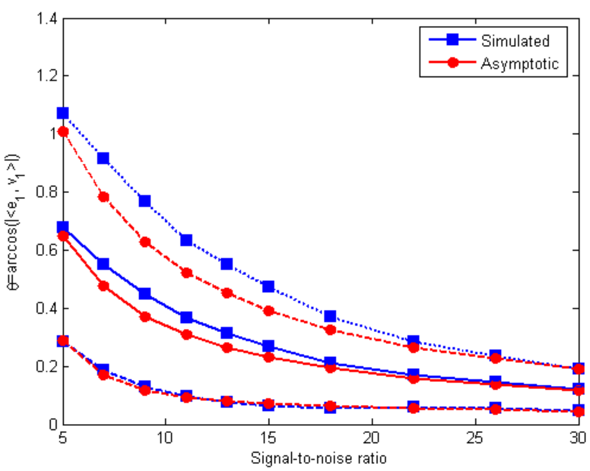

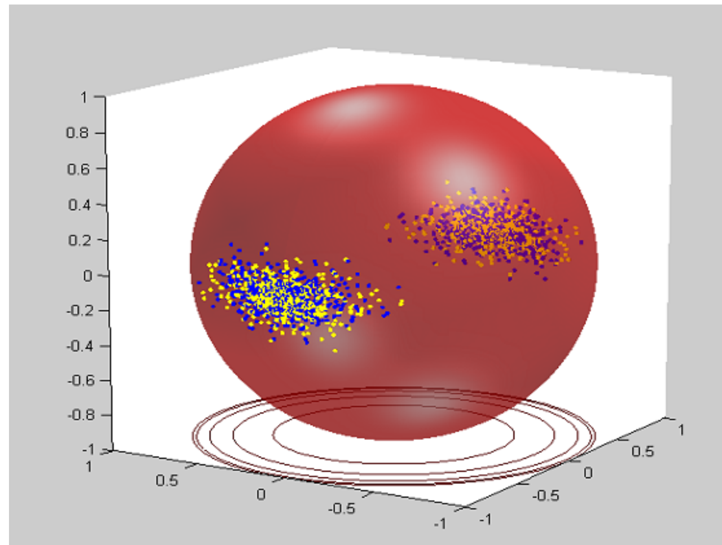

$$SNR = S_0 / \sigma = 22$$

$$D = diag[0.9, 0.7, 0.5]$$

Quantifying Uncertainty by using bootstrap methods

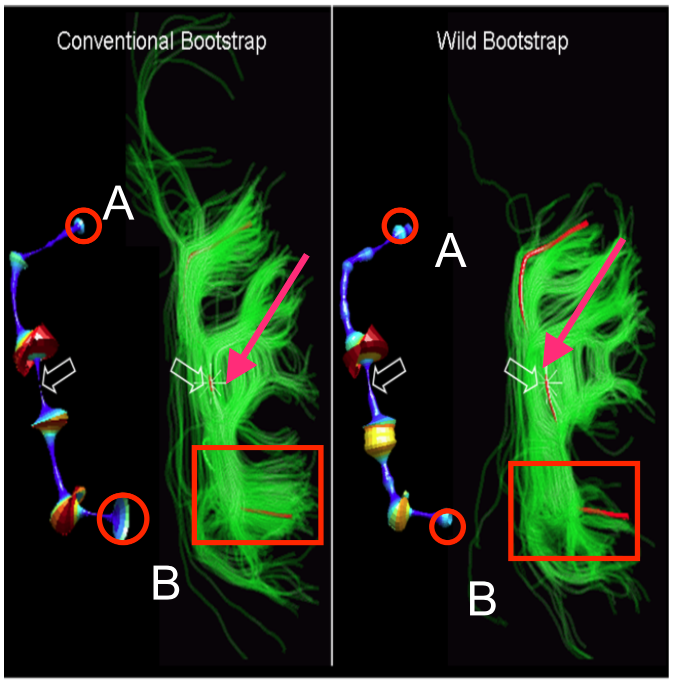

Repetition Wild

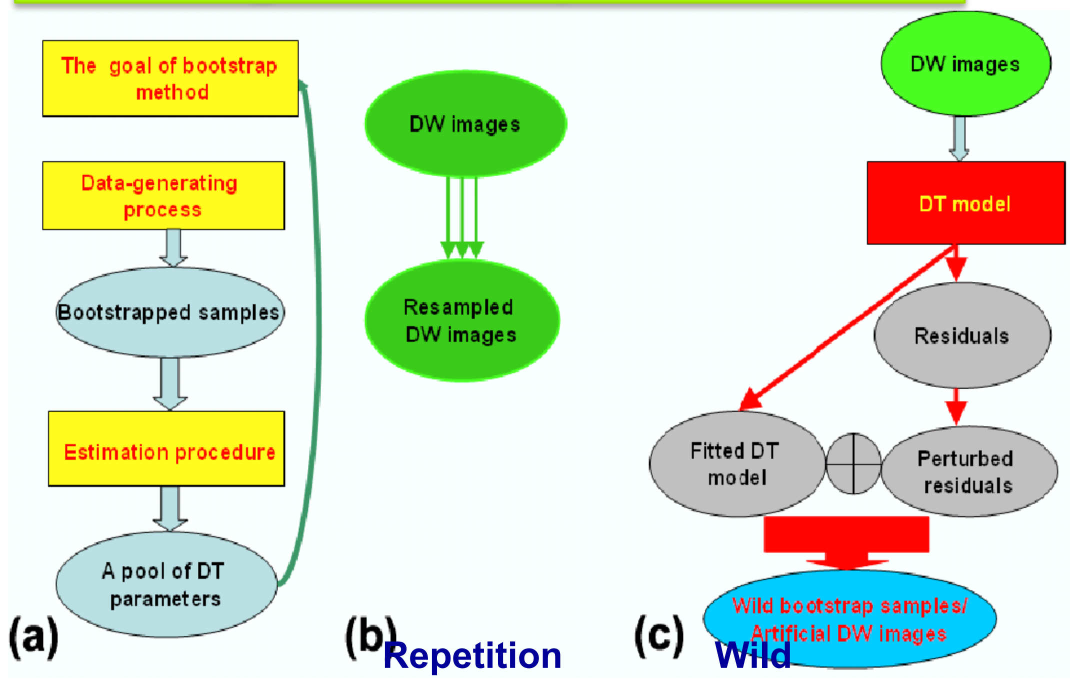

Bootstrap

Yuan, Zhu, Ibrahim, Lin, Peterson. (2008). IEEE TMI

Gold Standard

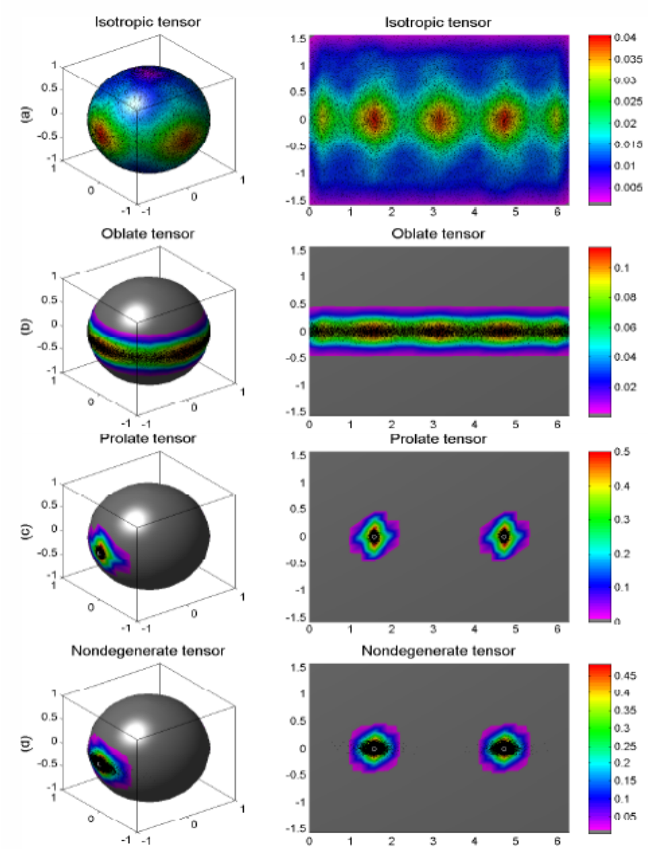

Repetition Bootstrap

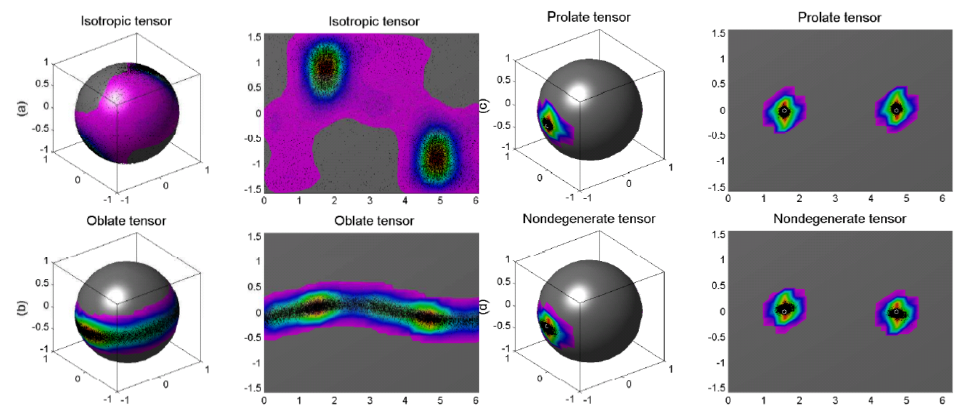

Wild Bootstrap

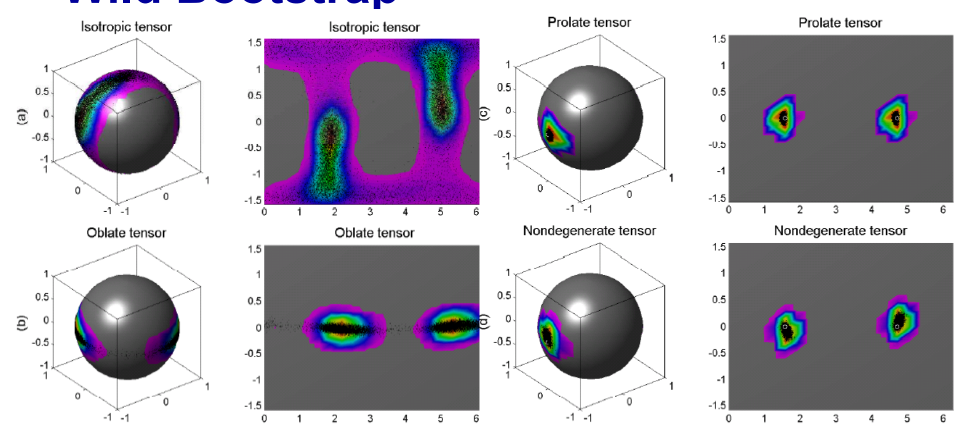

Smoothing Diffusion Tensor Field

Nonparametric Regression

How to smooth diffusion tensor along fiber tracts or in 3D volume?

Data $(x_1, S_1), \cdots, (x_n, S_n)$ $S(x)$

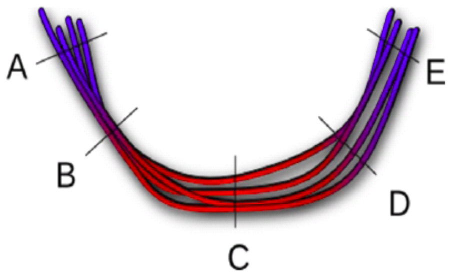

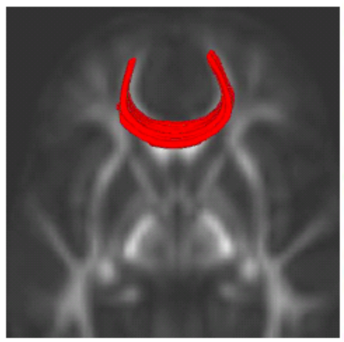

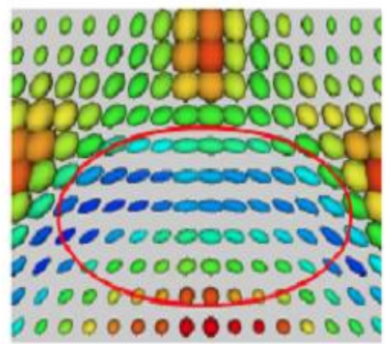

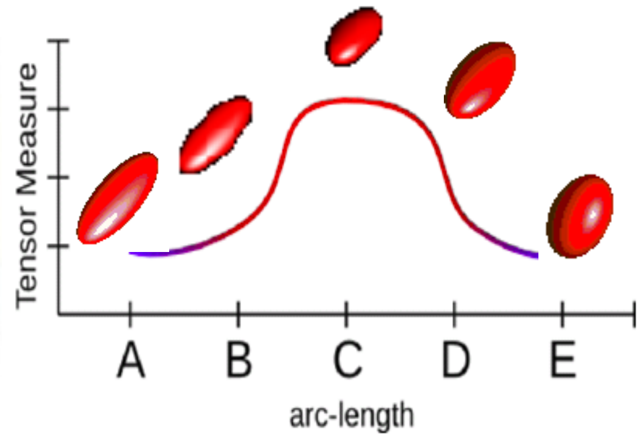

Styner, M. (2008).

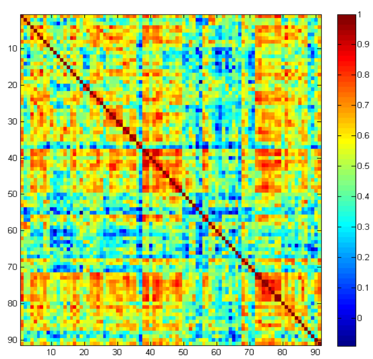

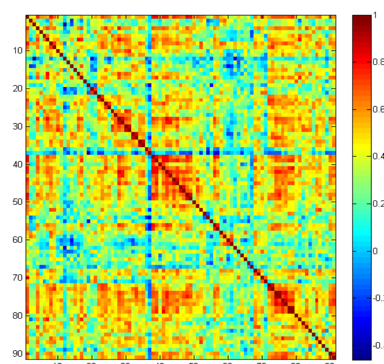

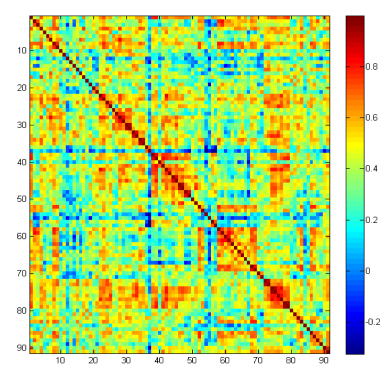

$$M = Sym(m)^+$$

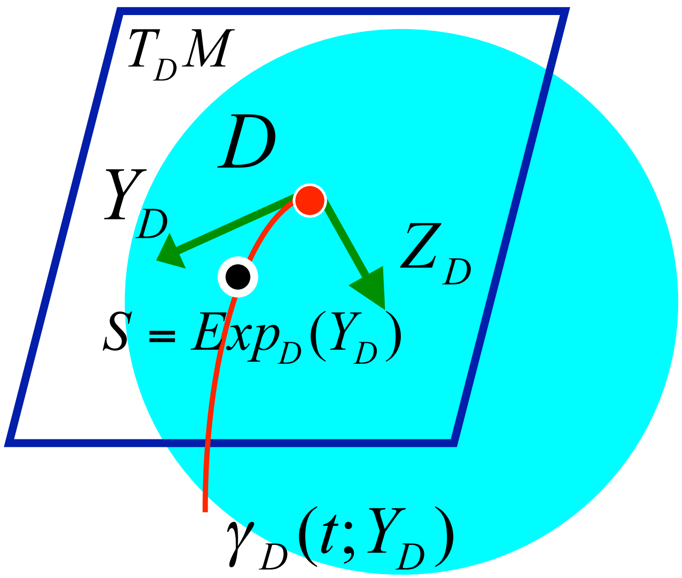

Inner product $<< Y_D, Z_D >>$

Geodesic

Riemannian exponential/logarithm maps

- Affine invariant metric

$$<< Y_D, Z_D >>_{D,R} = \mathrm{tr}(Y_D D^{-1} Z_D D^{-1})$$

- Log-Euclidean metric

$$<< Y_D, Z_D >>_{D,L} = \mathrm{tr}(R_D(Y_D) R_D(Z_D))$$

$$R_D : T_D M \rightarrow T_{I_m} M$$

Local polynomial kernel regression to nonparametrically estimate an intrinsic mean of S given x.

Local linear regression performs better than **local constant** regression.

Statistical inferences depend on a specific inner product defined on the tangent space.

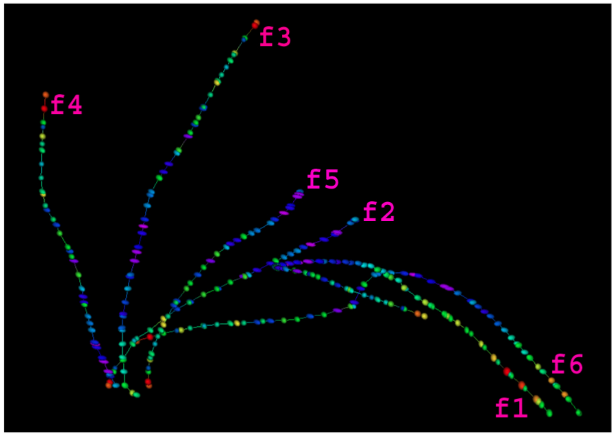

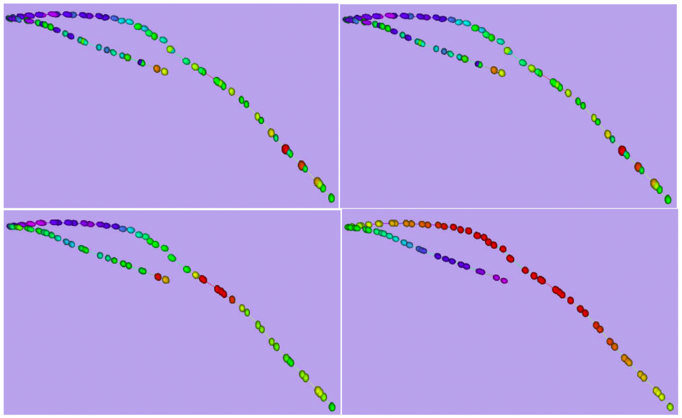

Local Polynomial Kernel Regression

$$\mathrm{Log}_{D(x_0)}(D(x)) \in T_{D(x_0)}Sym^+(m)$$

$$\phi_{D(x_0)}(.) : T_{D(x_0)}Sym^+(m) \to T_{I_m}Sym^+(m)$$

$$Y(x) = \phi_{D(x_0)}(\mathrm{Log}_{D(x_0)}(D(x)))$$

$$\mathrm{Log}_{D(x_0)}(D(x))) = \phi^{-1}_{D(x_0)}(Y(x)) \approx \phi^{-1}_{D(x_0)}(Y(x_0) + \sum_{k=1}^{K} Y^{(k)}(x_0)(x - x_0)^k)$$

$$D(x) = \mathrm{Exp}_{D(x_0)}(\phi^{-1}_{D(x_0)}(Y(x))) \approx \mathrm{Exp}_{D(x_0)}(\phi^{-1}_{D(x_0)}(\sum_{k=1}^{K} Y^{(k)}(x_0)(x - x_0)^k))$$

Simulation Studies

Data model

$$S_i = C(x_i)\exp(E_i)C(x_i), \qquad E_i \sim MN(0,\Omega)$$
$$x_i \sim N(0,0.25)$$
$$D(x) = C(x)^2$$

$$C(x) = \begin{pmatrix} -0.1x & 0.2x & \sin(x) \\ 0.2x & 0.6x & -0.4x \\ \sin(x) & -0.4x & 0.5x \end{pmatrix}$$

Correlation

$$\Sigma_1 = \begin{pmatrix} 0.3 & 0.049 & 0.052 \\ 0.049 & 0.2 & 0.0424 \\ 0.052 & 0.0424 & 0.1 \end{pmatrix} \quad \Sigma_2 = 2\Sigma_1, \quad \Sigma_3 = 4\Sigma_1, \quad \Sigma_4 = 8\Sigma_1$$

Data $\{(x_i,S_i) : i = 1,\cdots,n\}$ for $n = 50$ or 100

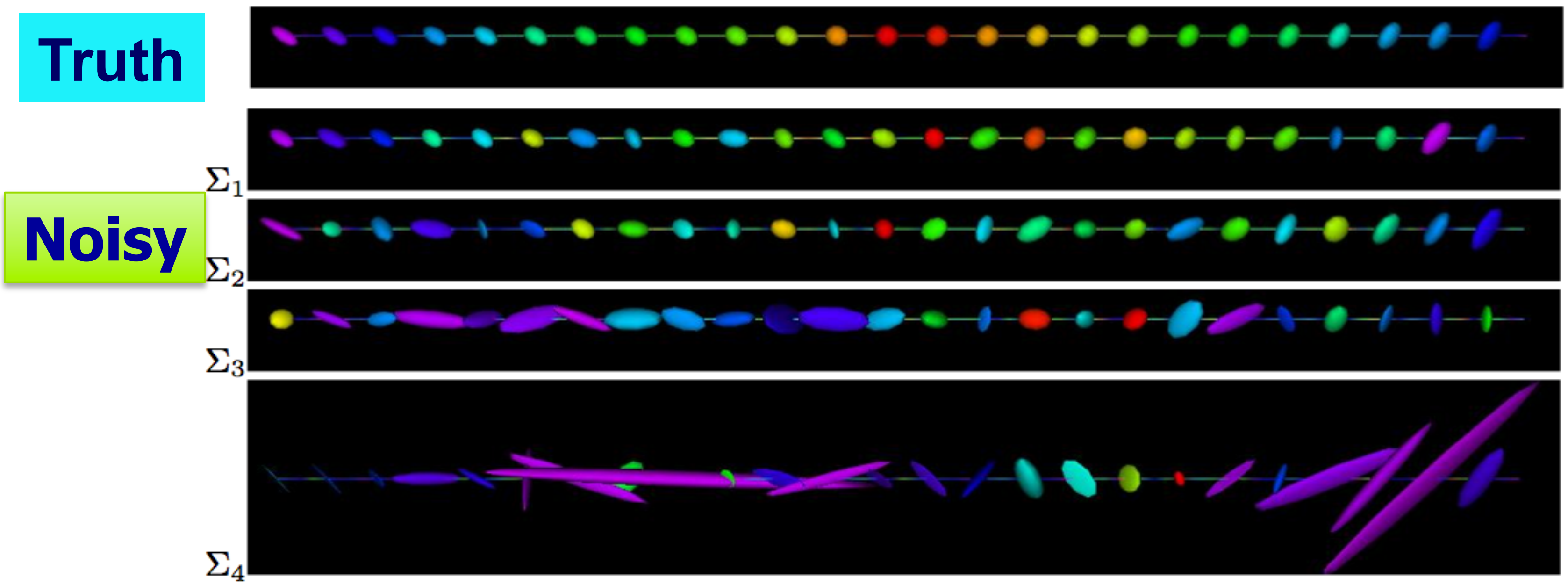

Fig. 1. Ellipsoidal representations of the true (the first row) and simulated SPD matrix data along the design points under the four different noise distributions (the second to the fifth rows: Σ_1-Σ_4) colored with FA values.

Truth

Log-Euclidean Local Linear

Riemannian Local Linear

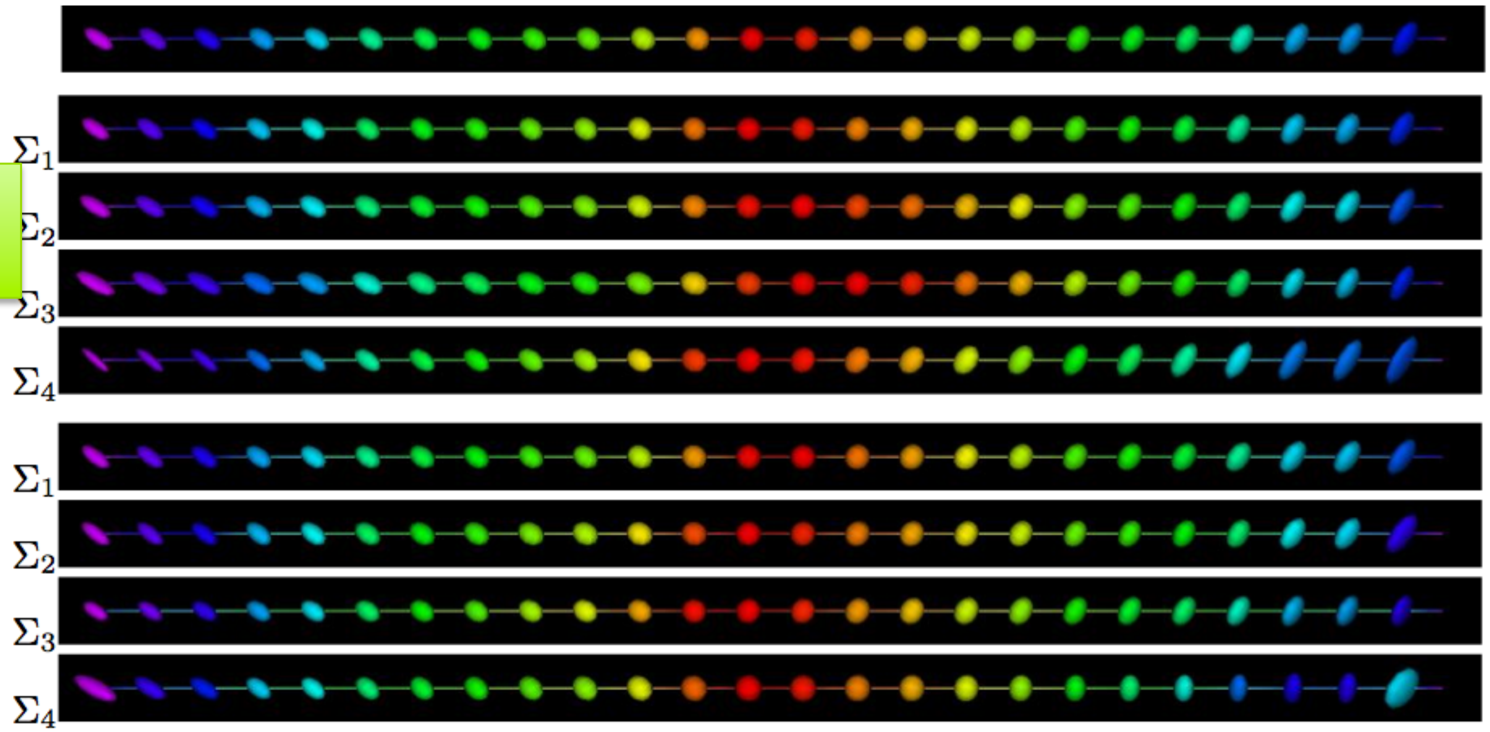

Fig. 2. Ellipsoidal representations of the true (the first row) and estimated SPD matrix data along the design points under the four different noise levels colored with FA values. The second to the fifth rows (Log-Euclidean metric): Σ_1-Σ_4, the sixth to the ninth rows (the Riemannian metric): Σ_1-Σ_4.

Simulation 1.

• Compare the performance of the **local linear** with the **local constant**

• Assess the performance using the Average Geodesic Distance (AGD) for each replication j=1, … , N with N as the number of replications, denoted by

$$\mathrm{AGD} = (nN)^{-1}\sum_{j=1}^{N}\sum_{i=1}^{n} d(\hat{D}_j(x_i), D(x_i))$$

where $\hat{D}_j(x_i)$ and $D(x_i)$ are, respectively, the estimated and true diffusion tensors at x_i

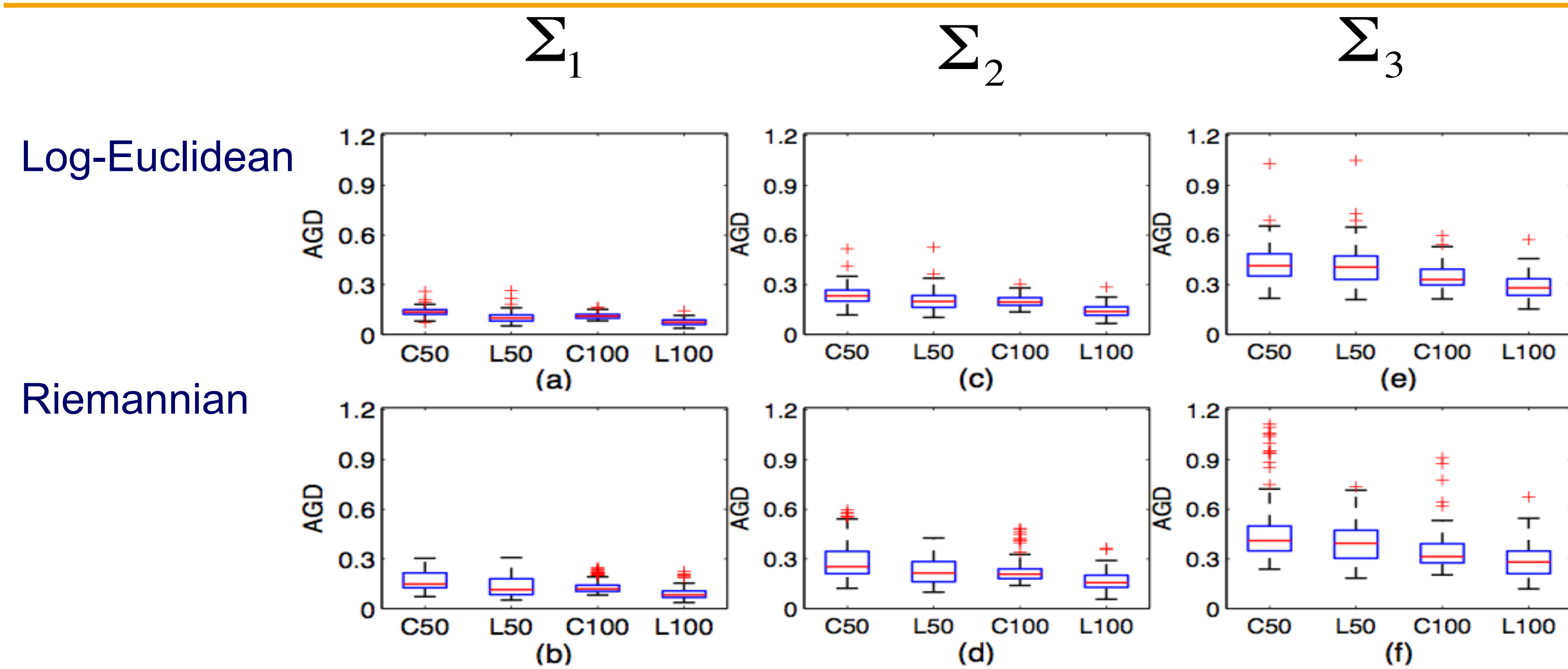

Fig. 3. Boxplots of the AGD using the intrinsic local constant and linear estimators under the log-Euclidean (the first row) and Riemannian (the second row) metrics based on 100 replications under the three covariance matrices (a)-(b) Σ_1, (c)-(d) Σ_2, and (e)-(f) Σ_3. C50 and C100 represent the intrinsic local constant estimators at sample sizes 50 and 100, respectively. L50 and L100 represent the intrinsic local linear estimators at sample sizes 50 and 100, respectively.

Log-Euclidean

Riemannian

Log-Euclidean

Riemannian

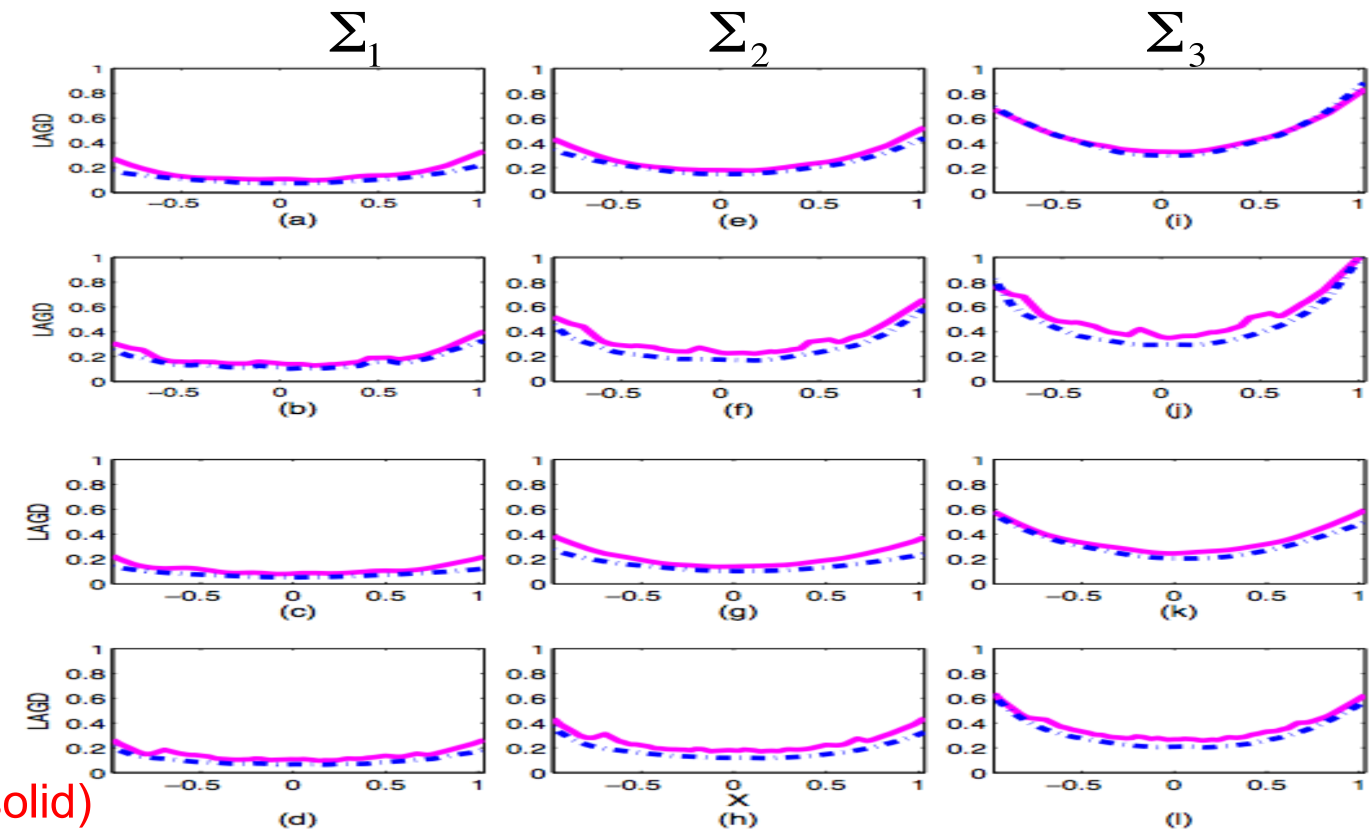

Local constant (solid)

Local linear (dashed)

Fig. 4. The LAGD curves at each sample point using the intrinsic local constant (solid line) and linear (dash-dotted line) estimators under the three covariance matrices (a)-(d) Σ_1, (e)-(h) Σ_2, (i)-(l) Σ_3 for sample sizes 50 (the top two rows) and 100 (the bottom two rows). The first and third rows correspond to the log-Euclidean metric while the second and fourth rows correspond to the Riemannian metric.

Simulation 2. High noisy level

Compare the performance of the local linear under two metrics

Σ_4

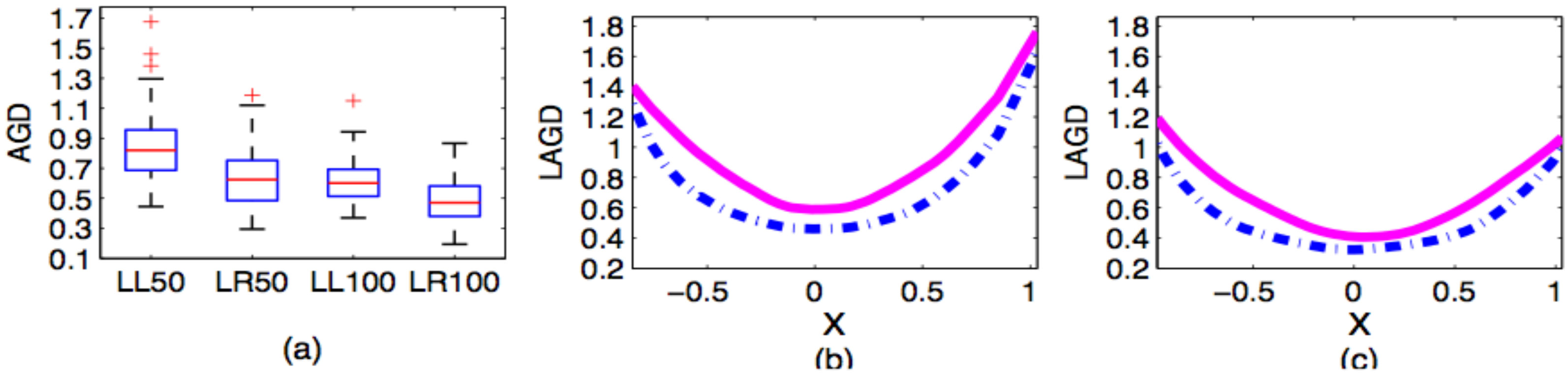

Riemannian (dashed) Log-Euclidean (solid)

Fig. 5. (a) Boxplots of the AGD's using the linear regressions based on 100 replications under the covariance matrix Σ_4, under the Log-Euclidean and Riemannian metrics, respectively. (b) and (c) LAGD curves at each sample point using the local linear regressions under the affine invariant (dash-dotted line) and Log-Euclidean (solid line) metrics under the the covariance matrix Σ_4 at sample size 50 (b) and 100 (c), respectively. LL50 (LR50) and LL100 (LR100), respectively, represent the local linear regressions under Log-Euclidean (Riemannian) metrics at sample sizes 50 and 100.

Simulation 3.

- Value of developing the LPK smoothing method

- Two different methods for smoothing FA values

M1. Calculate FA values from `noisy' SPDs and then use the local linear method to smooth the FA values

M2. Use the local linear method to smooth SPDs and then calculate FA values from the smoothed SPDs

- Calculate the Mean Absolute Deviation Error (MADE):

$$\mathrm{MADE} = (nN)^{-1} \sum_{j=1}^{N} \sum_{i=1}^{n} |\hat{\mathrm{FA}}_j(x_i) - \mathrm{FA}_j(x_i)|$$

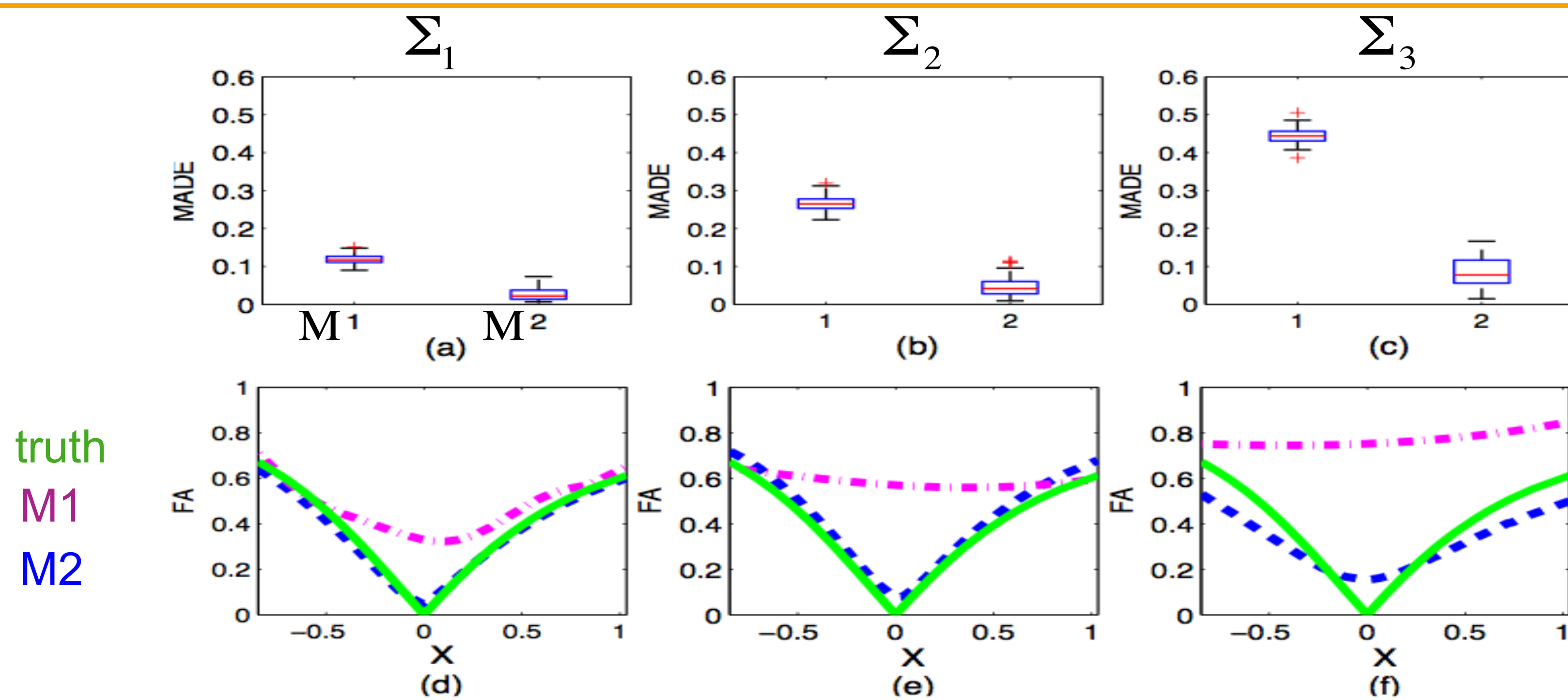

Fig. 6. Boxplot of the MADE's using the two smoothing methods based on 100 replications under the covariance matrices (a) Σ_1, (b) Σ_2, and (c)Σ_3 at sample size 50. Smoothed FA curves for the realizations with median MADE under the covariance matrices: (d) Σ_1, (e) Σ_2, and (f) Σ_3. The true FA curve (the solid line), the estimated FA curve using the first method (the dash-dotted line) and the estimated FA curve using the second method (the dashed line). This shows that the more intrinsic approach is much better.

Smoothing DTs along a select tract

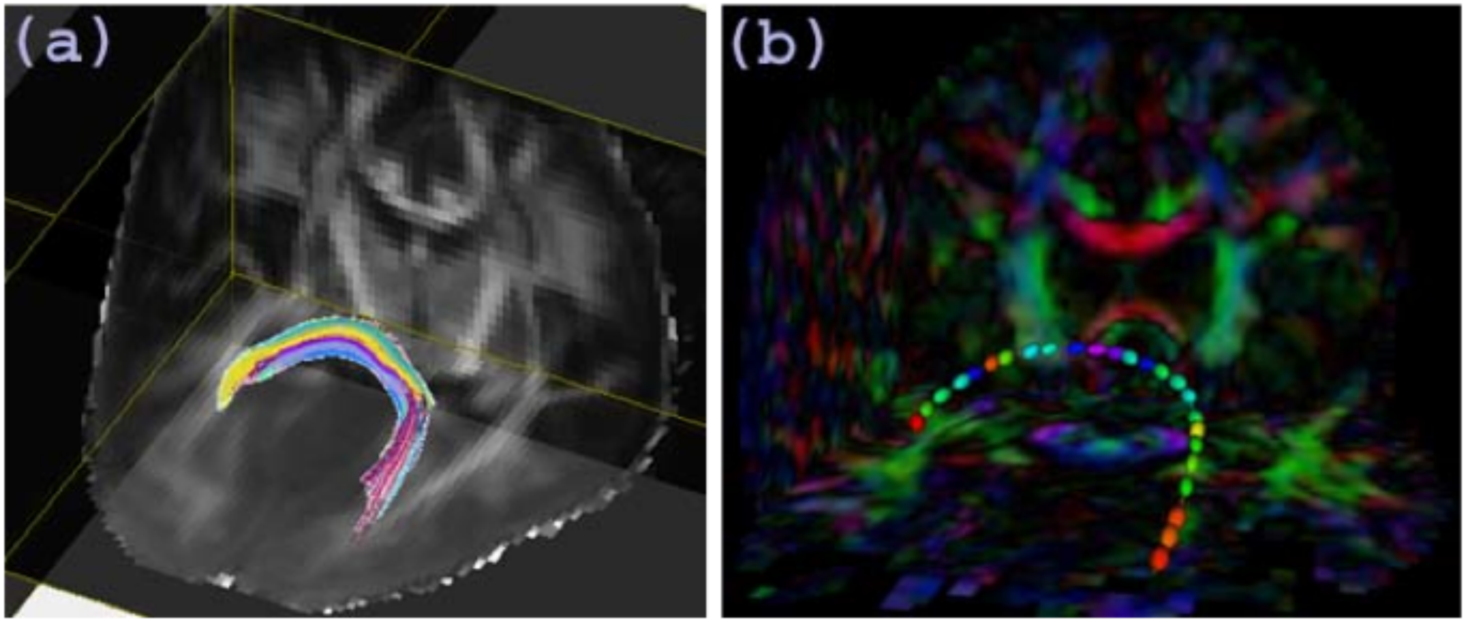

Fig. 7. (a)The splenium of the corpus callosum in the analysis of HIV DTI data. (b)The ellipsoidal representation of full tensors on the fiber tract from a selected subject.

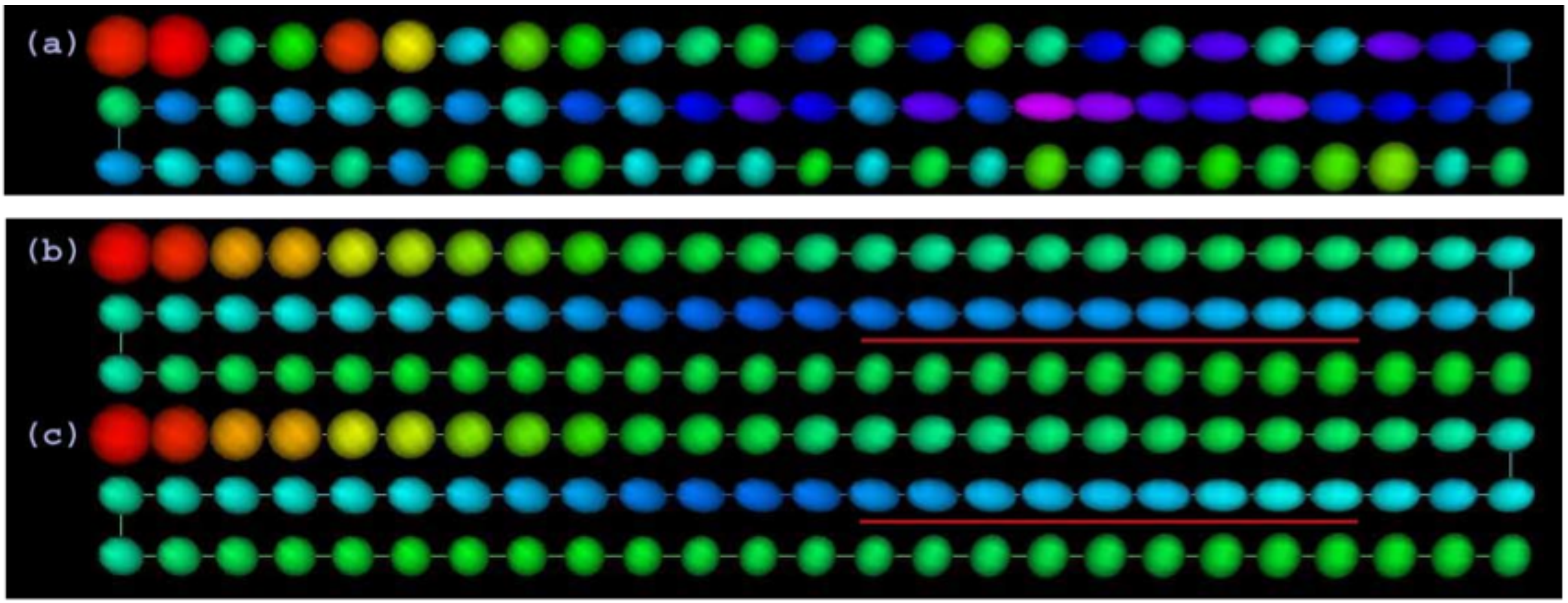

Fig. 8. (a) Ellipsoidal representations of the diffusion tensor data and estimated tensors using the intrinsic local linear regression under the (b)log-Euclidean and (c) Riemannian metrics along the fiber tract f1 colored with FA values. The estimated tensors in the middle right part (highlighted in the red line) are more anisotropic using the method under the Log-Euclidean metric.

Local Polynomial Kernel Regression for SPD

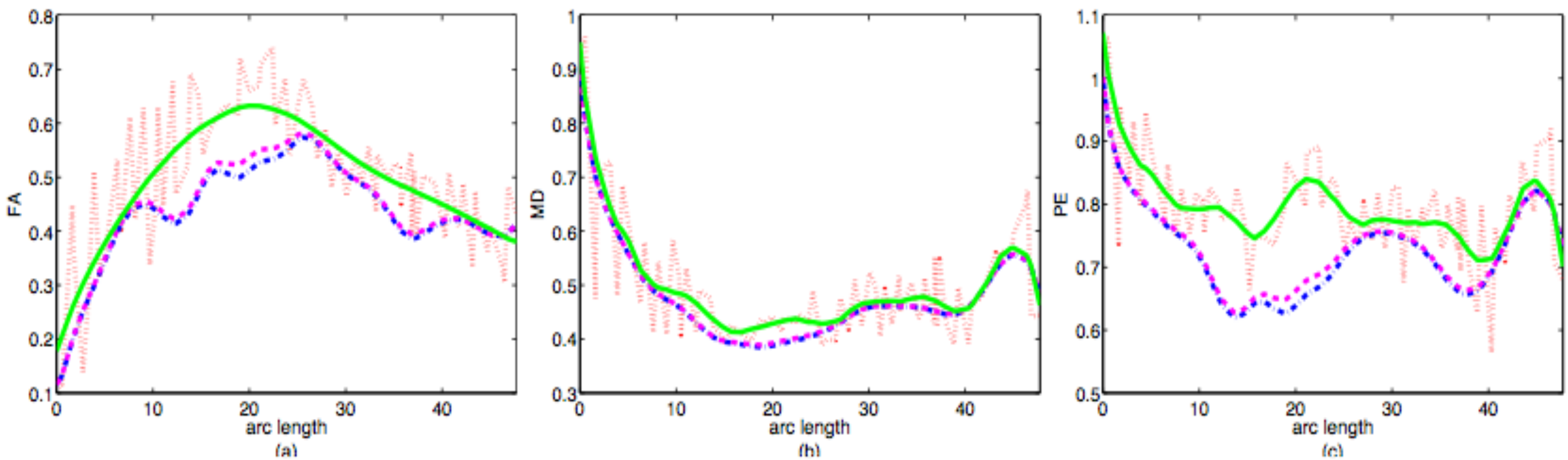

Fig. 9. (a) FA's , (b) MD's and (c) PE's derived from the raw tensor data (dot line) and estimated tensors using the intrinsic local linear regression under the Riemannian (dash-dot line) and log-Euclidean (dash line) metrics as the function of arc-length along the tract f1. Estimated FA function along the fiber tract f1 by using the standard local linear regression for scalars (solid line).

Smoothing Covariance matrices along age

16 subjects resting state fcMRI
32 ROIs

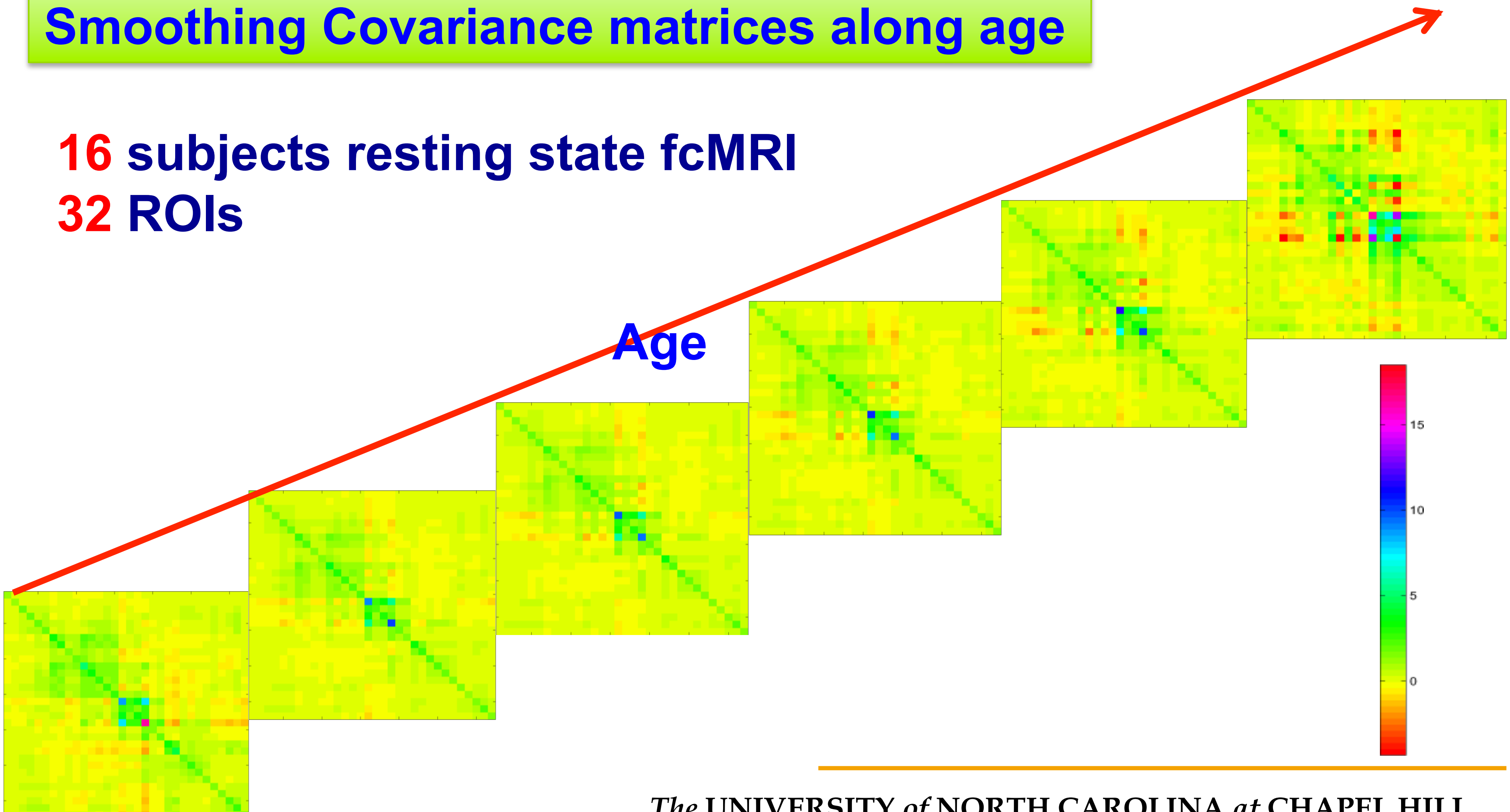

Analyzing Tract-based Diffusion Tensor Statistics

Multivariate Varying Coefficient Model

How to compare diffusion tensors or tensor quantities along fiber tracts?

Neonatal Brain Development

PI: John H. Gilmore

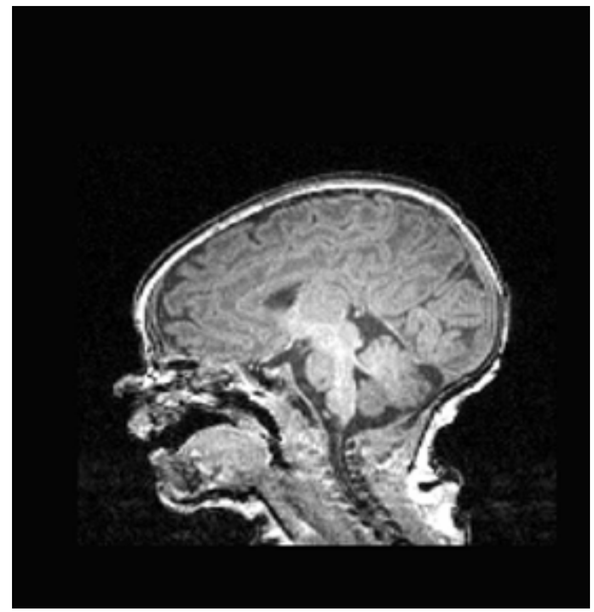

www.google.com

Early Brain Development

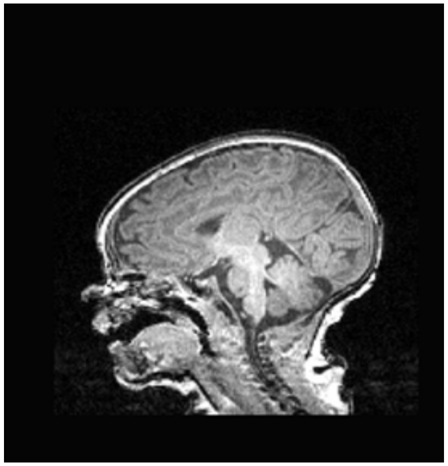

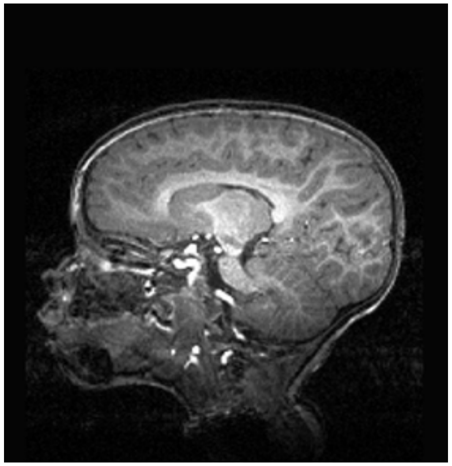

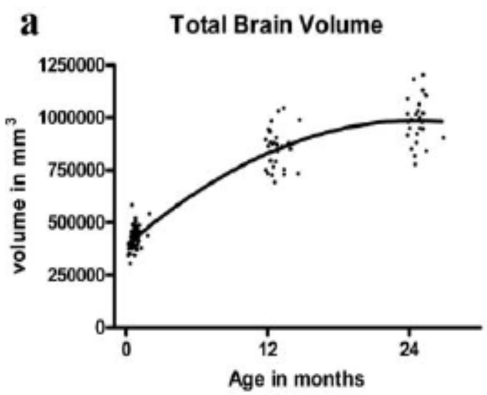

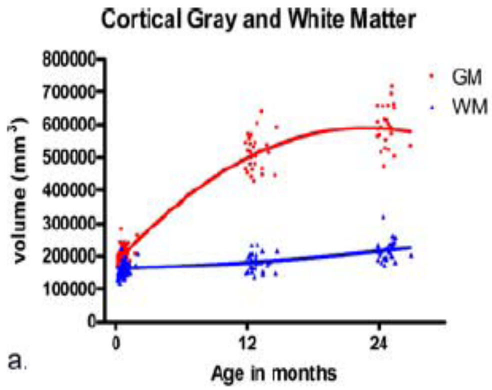

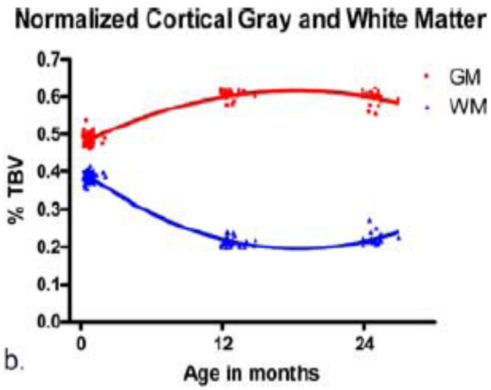

White Matter Maturation

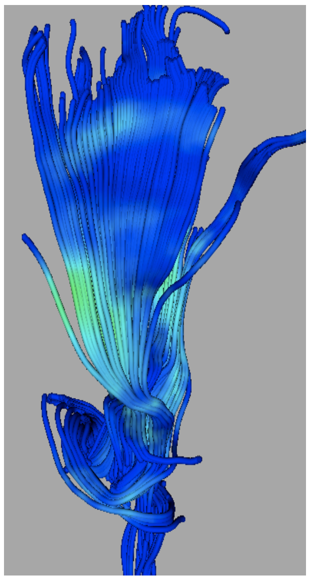

Week 2

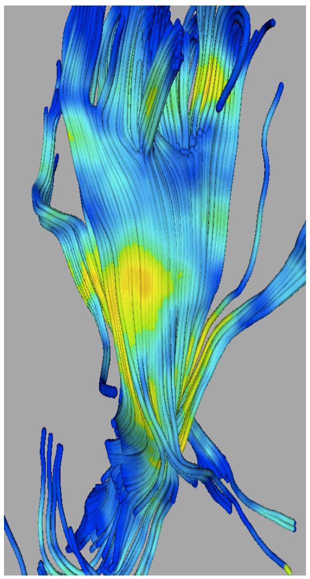

Year 1

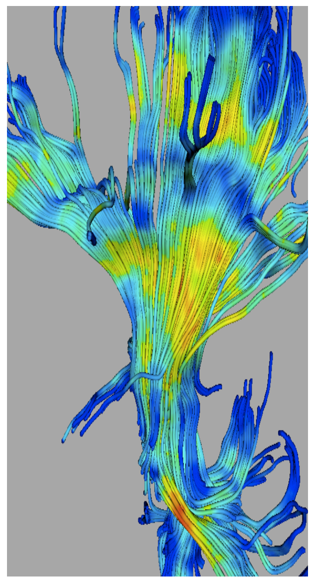

Year 2

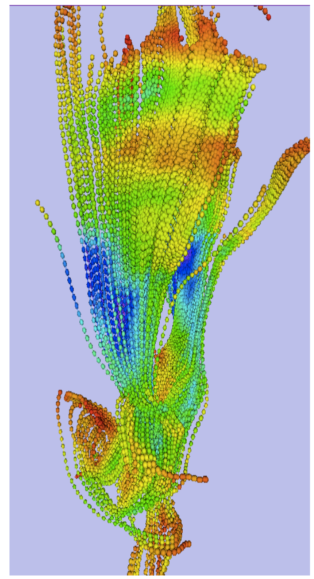

Week 2

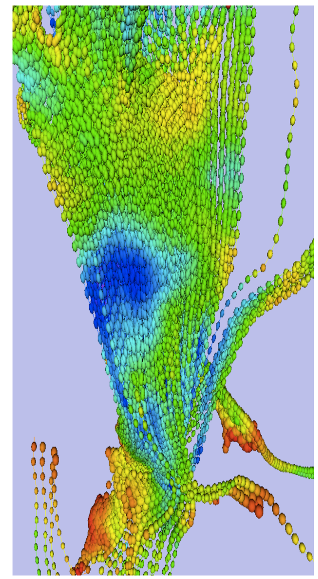

Year 1

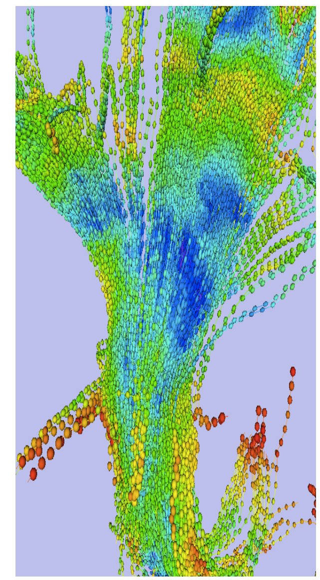

Year 2

Sample Data

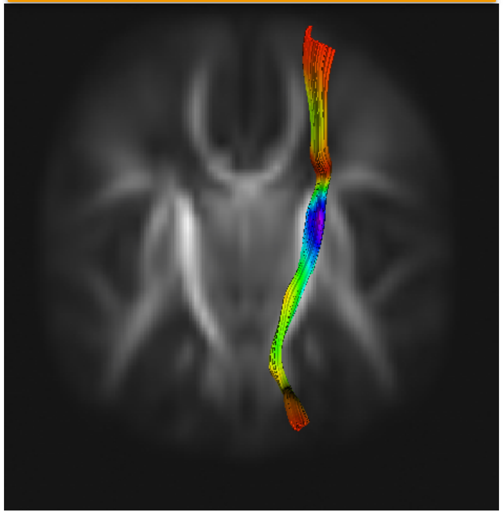

Right internal capsule: a collection of axons connecting the cerebral cortex and the brain stem

diffusion properties or diffusion tensors

$$Y_i(s_j) = (y_{i,1}(s_j), \cdots, y_{i,m}(s_j))^T$$

grids $\{s_1, \cdots, s_{n_G}\}$

covariates $x_1, \cdots, x_n$

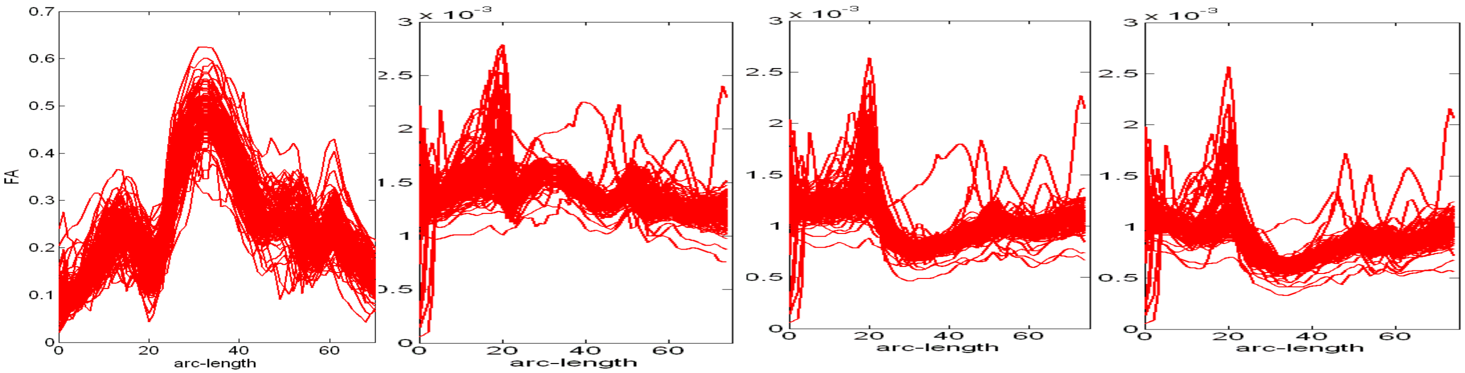

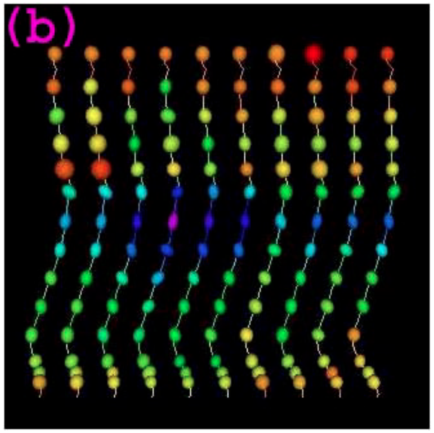

Tract-based FA as a function of Age

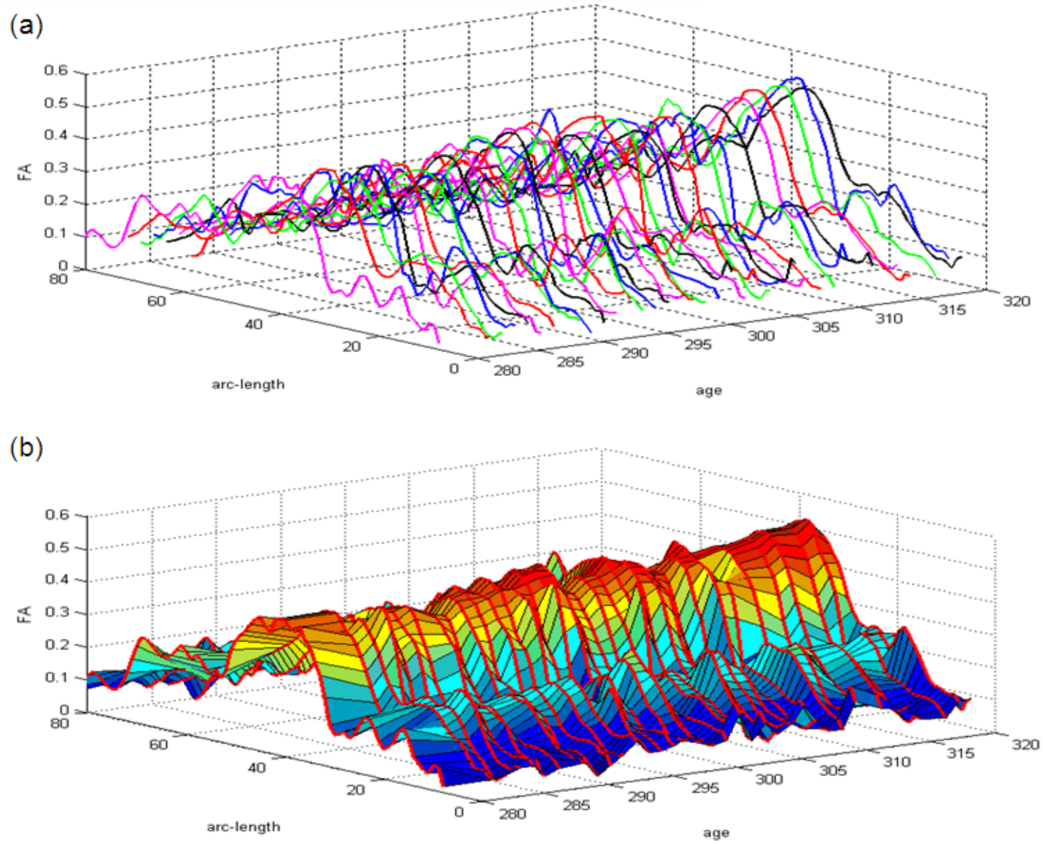

Varying Coefficient Model

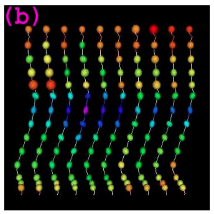

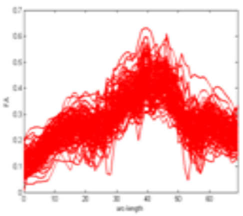

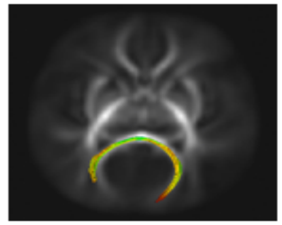

Multivariate varying coefficient model

$$y_{i,k}(s) = \mathbf{x}_i^T B_k(s) + \eta_{i,k}(s) + \epsilon_{i,k}(s)$$

Weighted least square estimation

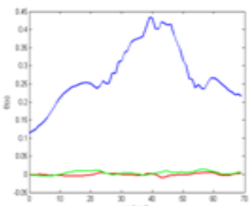

$$B_k(s_j) = B_k(s) + \dot{B}_k(s)(s_j - s)$$

Functional principal component analysis

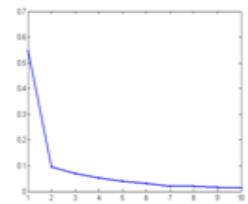

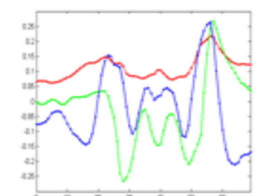

$$\hat{\Sigma}_{\eta,kk}(s,t) = \sum_{l=1} \hat{\lambda}_{k,l}\hat{\psi}_{k,l}(s)\hat{\psi}_{k,l}(t)$$

Confidence bands

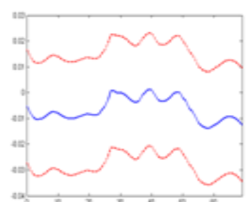

Resampling methods

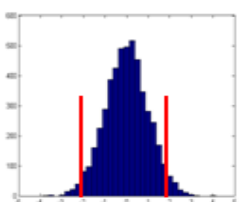

$$P(\sup_{s\in[0,L_0]} |G_{kl}(s)| \le C_{kl}(\alpha)) = 1 - \alpha$$

Hypothesis test

$$H_0 : \mathbf{C}\mathrm{vec}(B(s)) = \mathbf{b}_0(s)$$

$$H_1 : \mathbf{C}\mathrm{vec}(B(s)) \neq \mathbf{b}_0(s)$$

Resampling methods

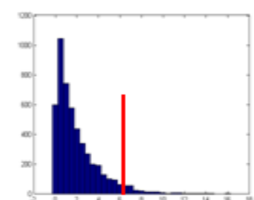

$$S_n = n\int_0^{L_0} \mathbf{d}(s)^T[\mathbf{C}(\hat{\Sigma}_\eta(s,s)\otimes\hat{\Omega}_X^{-1})\mathbf{C}^T]^{-1}\mathbf{d}(s)ds \quad p = G^{-1}\sum_{g=1}^{G} 1(S_n^{(g)} \ge S_n)$$

PI: John H. Gilmore

Sujects:
125 healthy infants (75:53 M:F)
Gestational age (298+/-17.6 days)

Aims:
Gender Effects
Age Effects

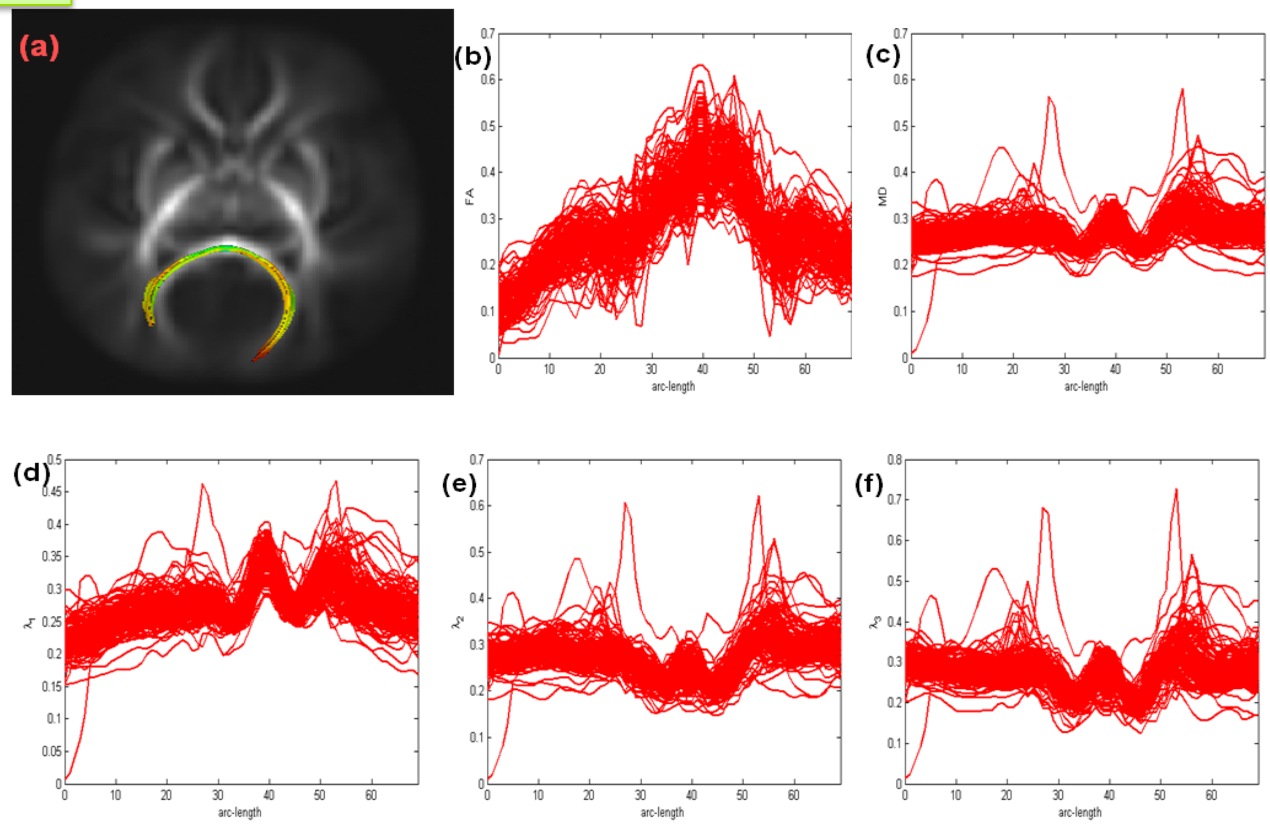

Splenium

Global and Local p-values for Gender and Age Effects

	Right Internal Capsule					Splenium				
	FA	MD	Lambda1	Lambda2	Lambda3	FA	MD	Lambda1	Lambda2	Lambda3
Gender	.169	.354	.241	.314	.376	.683	.063	.048	.057	.302
Age	<.001	<.001	<.001	<.001	<.001	.103	.008	.003	.007	.010

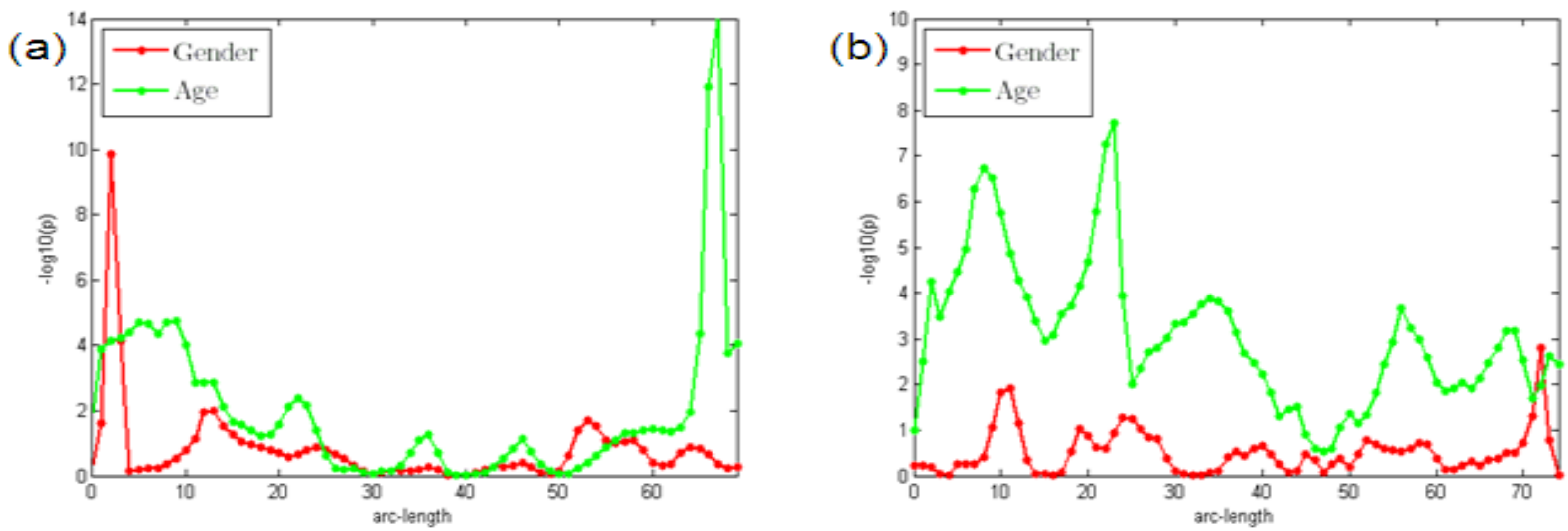

Functional Prinicipal Components

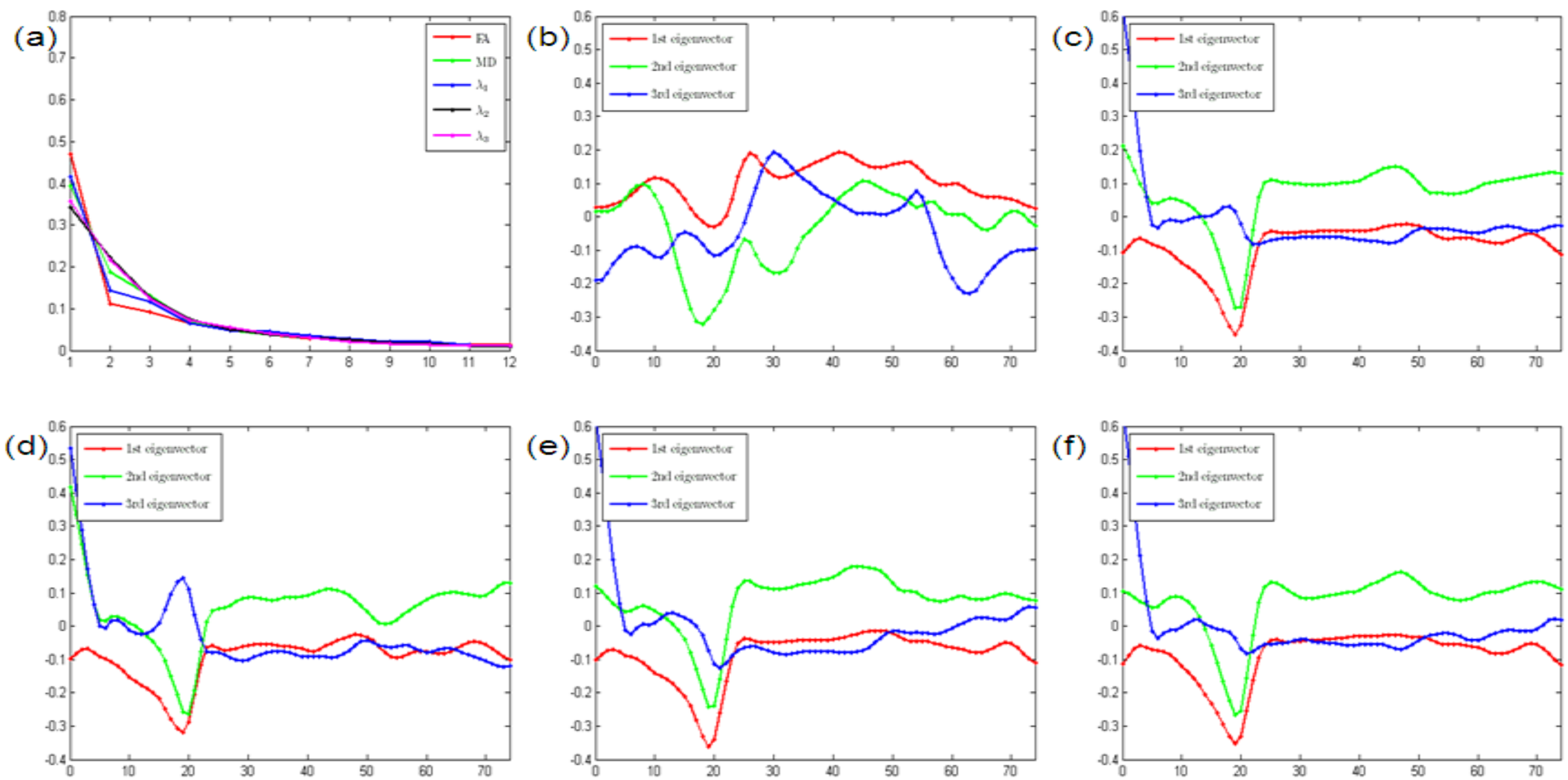

Simultaneous Confidence Bands

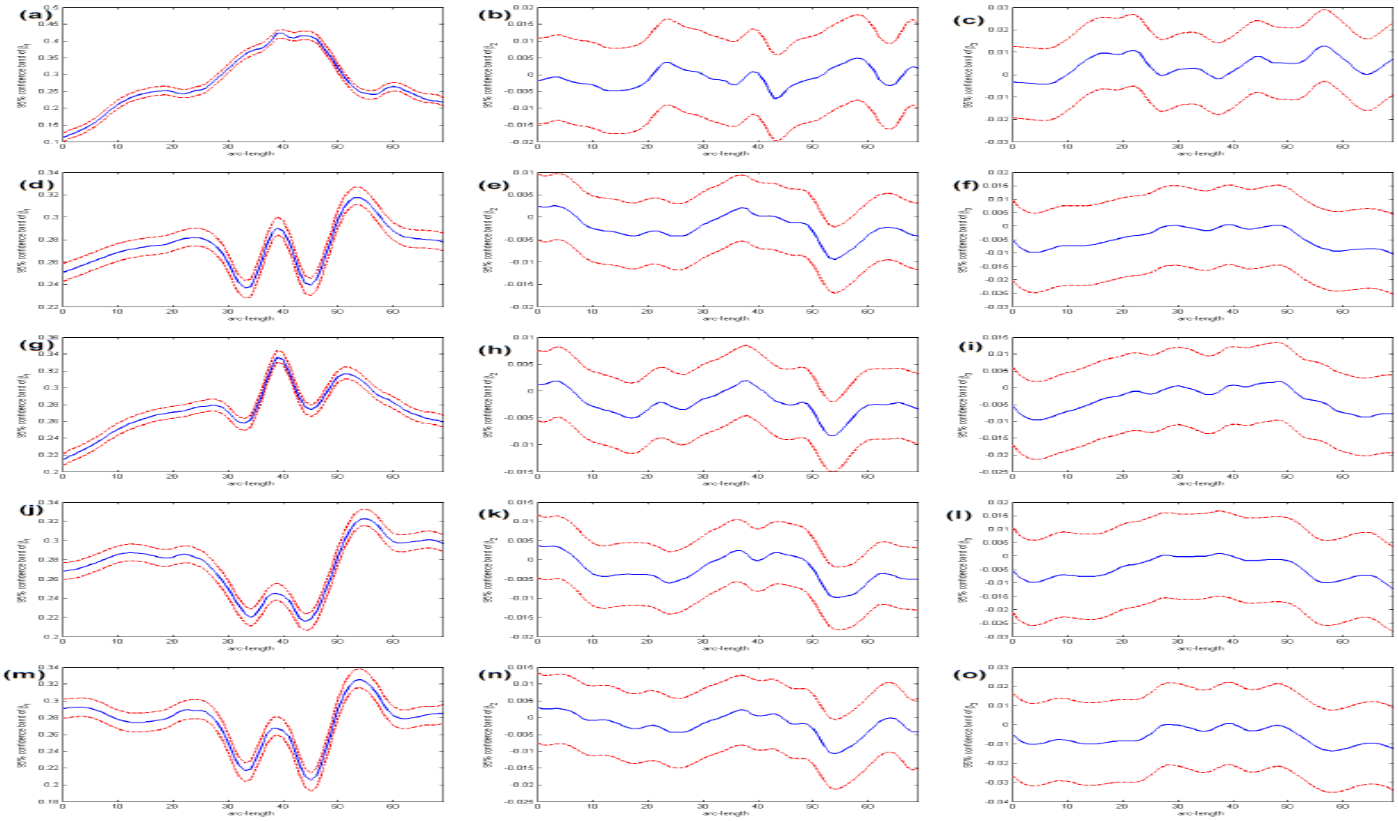

Multiscale Adaptive Regression Models

Regression Analysis and Nonparametric Smoothing Methods

How to spatially and adaptively compare imaging measures across subjects in 3D volume or 2D surface?

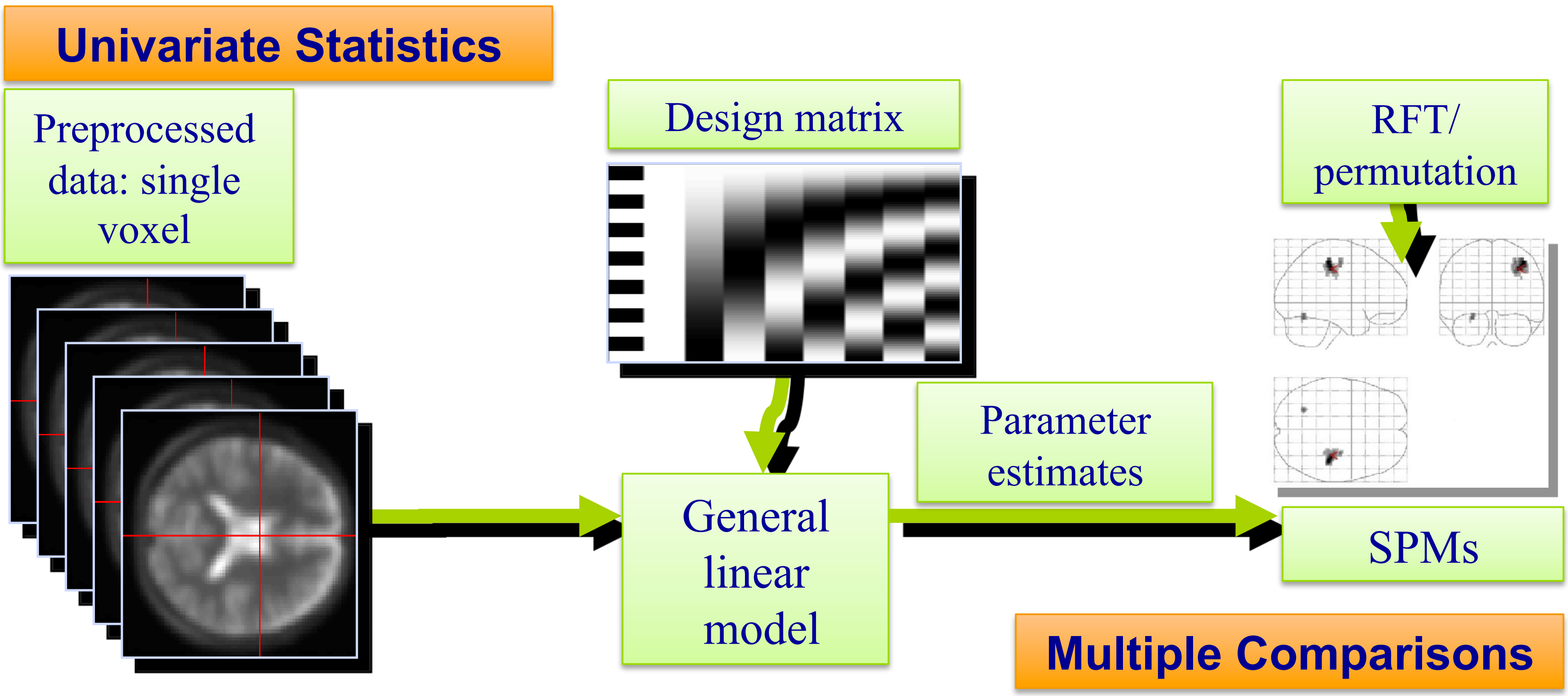
Univariate Statistics
Preprocessed data: single voxel
Design matrix
RFT/ permutation
Parameter estimates
General linear model
SPMs
Multiple Comparisons

All voxels are treated as **independent units.**

Initial smoothing step before the voxel-wise approach often blurs the image data near the edges of activated regions.

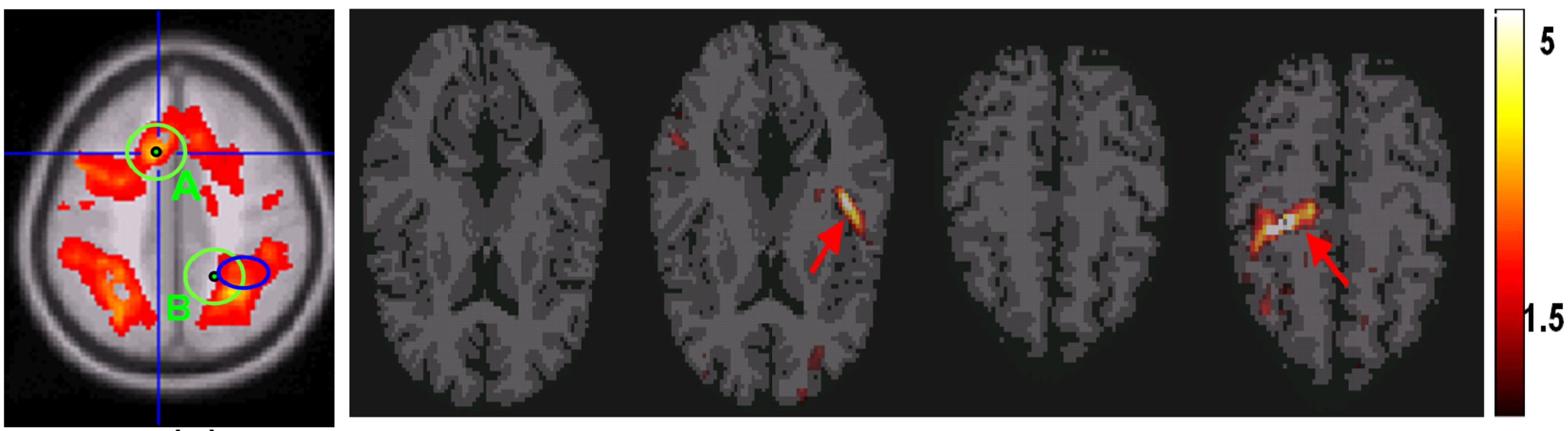

(a) (b) (c) (d)

Multiscale Adaptive Regression Model

- Learning Voxel Feature
- Local Feature Adaptation
- Adaptive Estimation and Testing
- Automatic Stop
- Nice Asymptotic Results

Identifying homogeneous regions

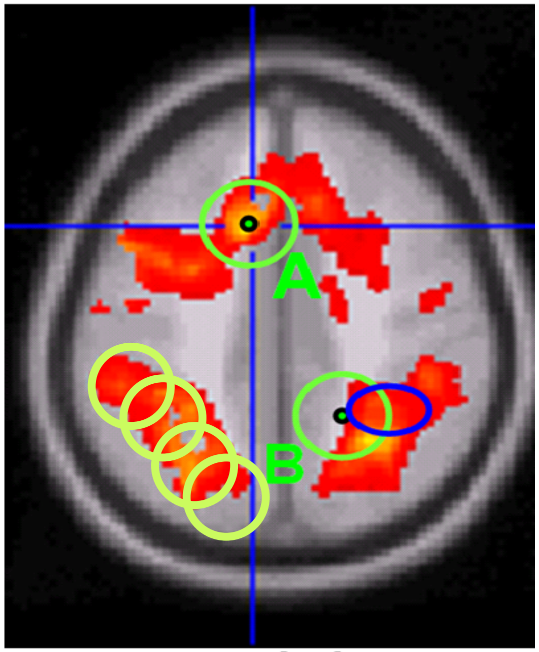

Drawing a sphere with radius r0 at each voxel

Calculating the similarities between the current voxel and its neighboring voxels.

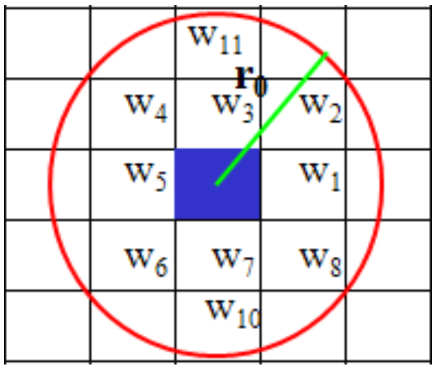

Being Hierarchical

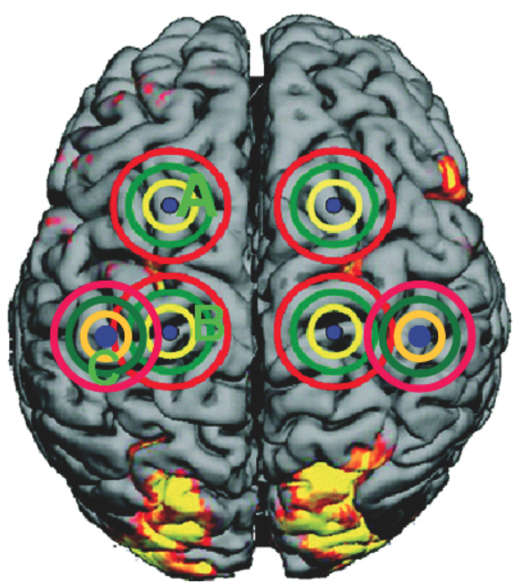

Drawing nested spheres with increasing radiuses at each voxel

$$h_0 = 0 < h_1 < \cdots < h_S = r_0$$

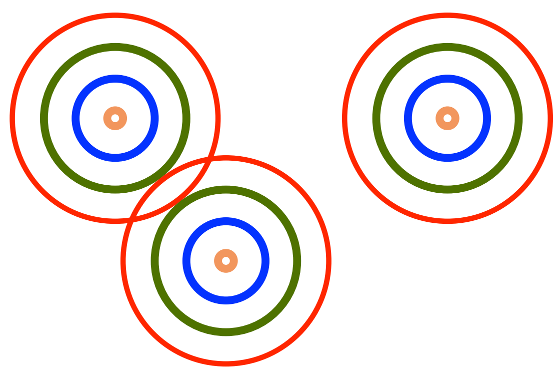

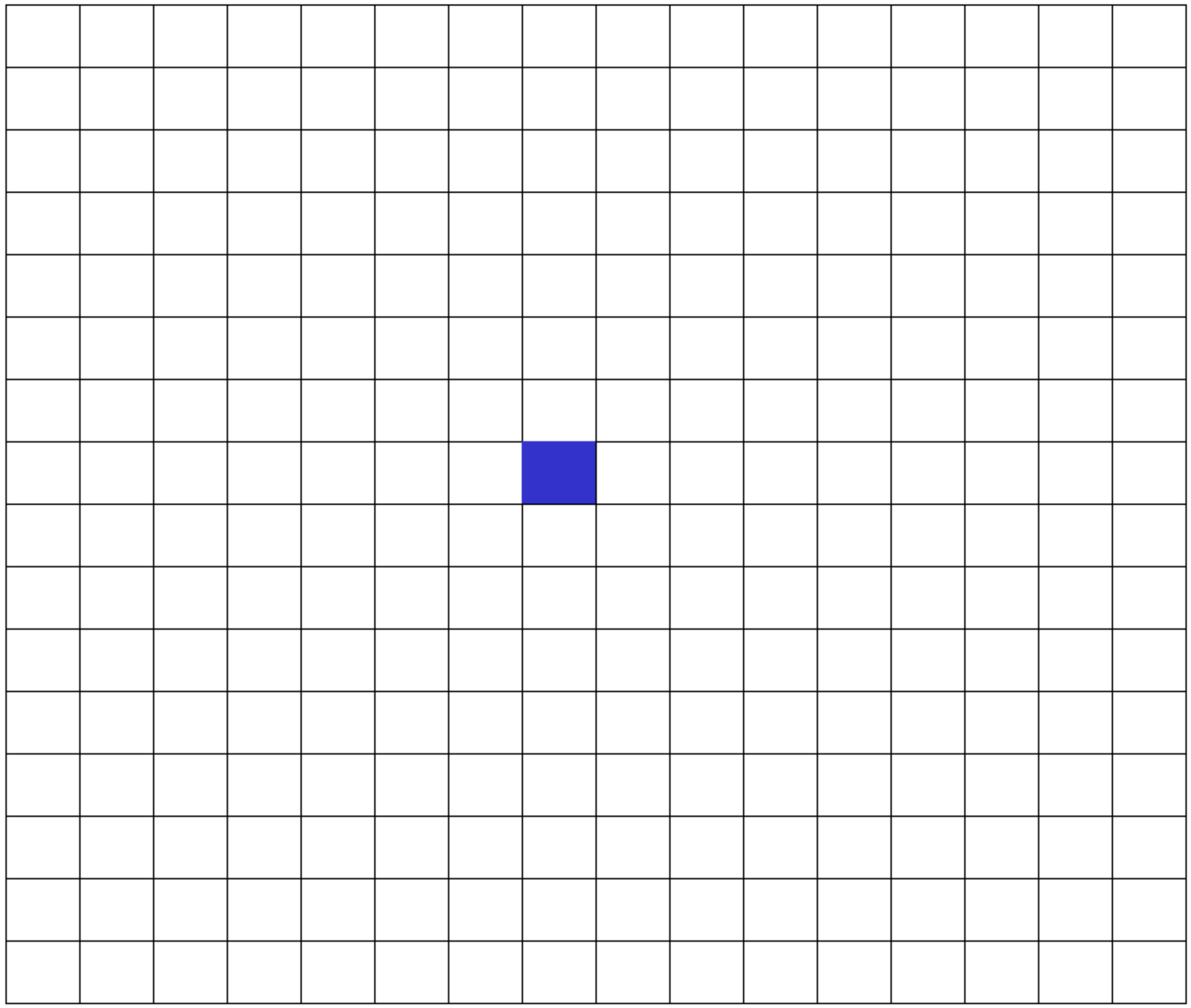

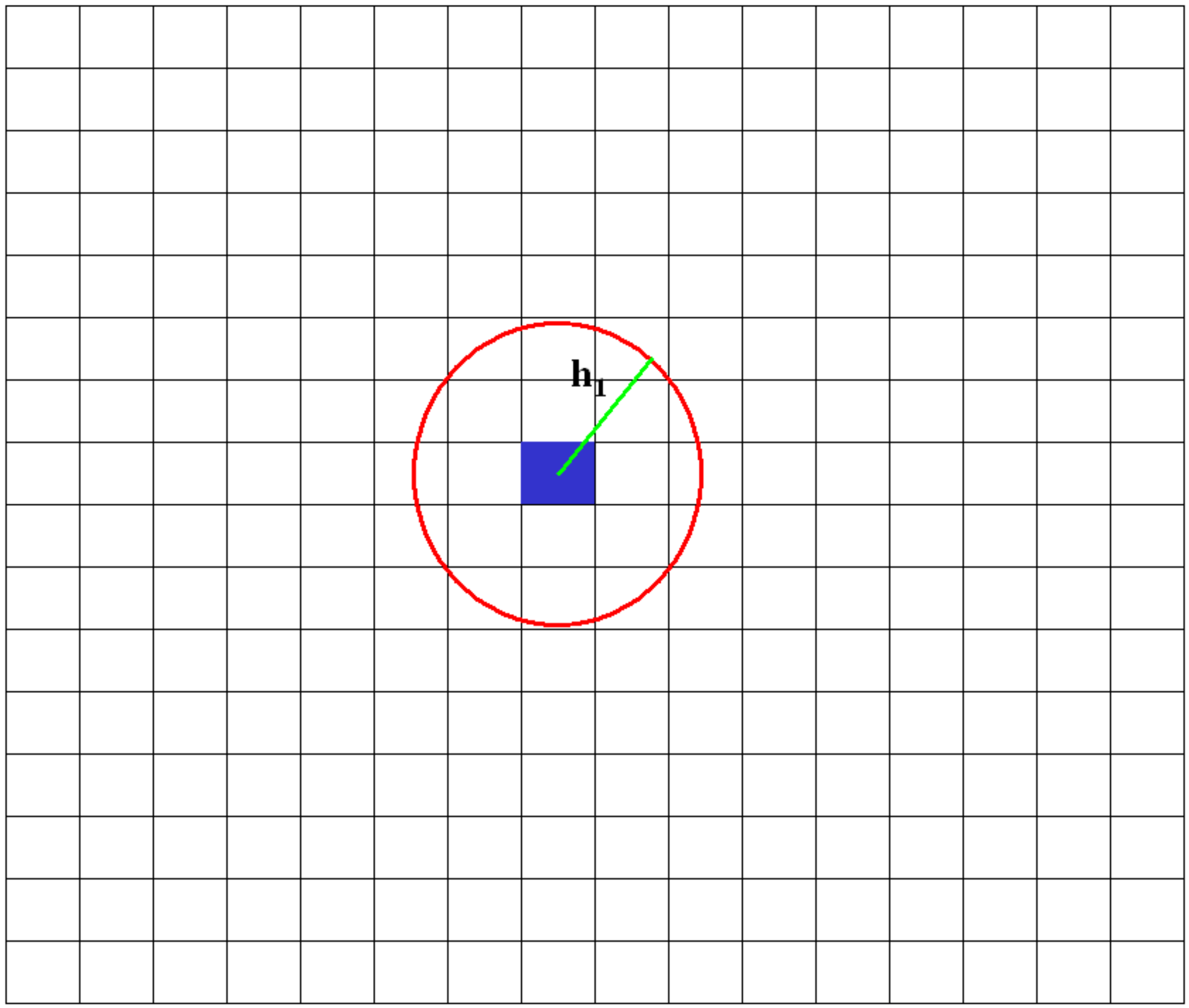
h_1

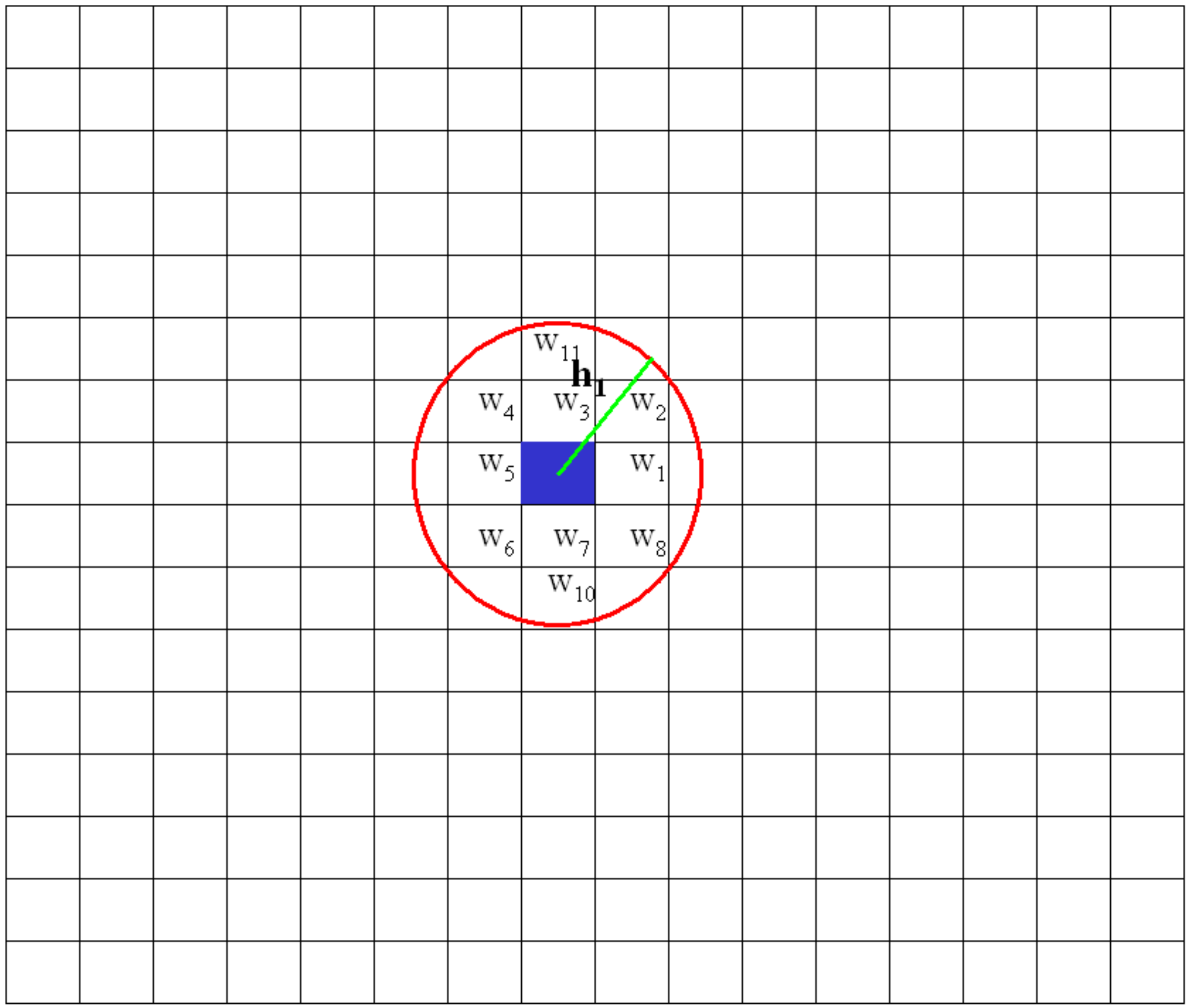

W11
h1
W4
W3
W2
W5
W1
W6
W7
W8
W10

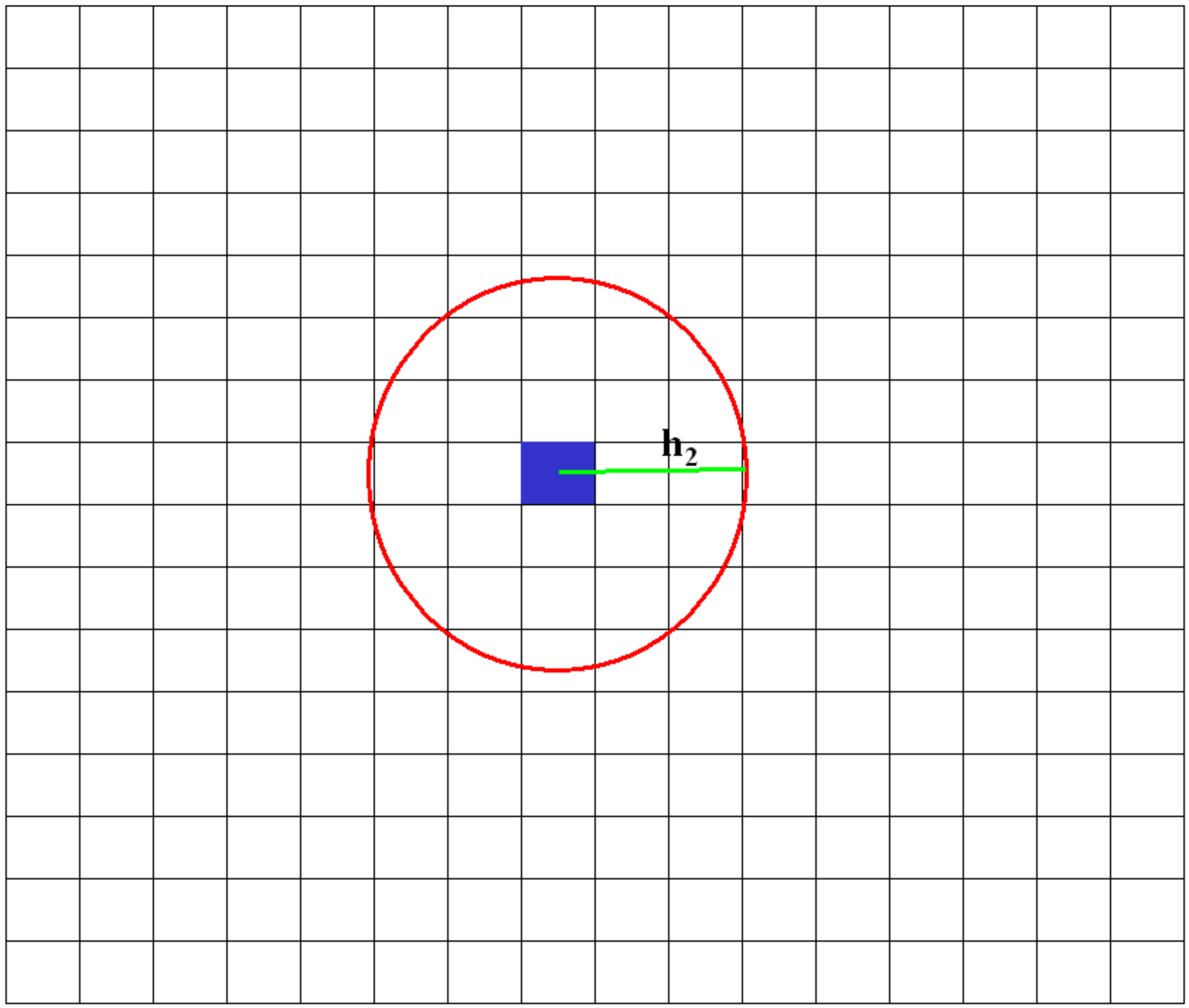
h2

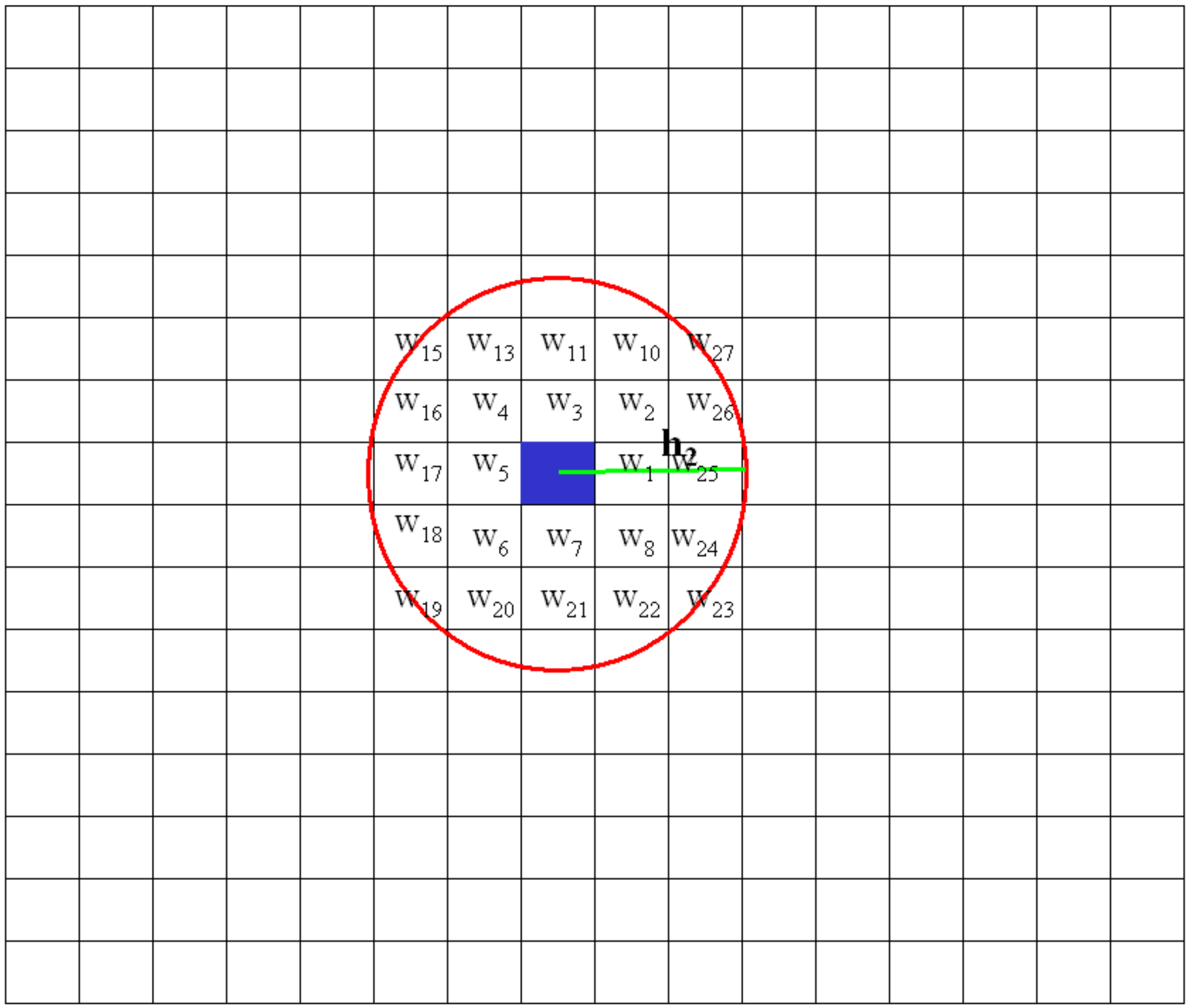

W15
W13
W11
W10
W27
W16
W4
W3
W2
W26
h2
W17
W5
W1
W25
W18
W6
W7
W8
W24
W19
W20
W21
W22
W23

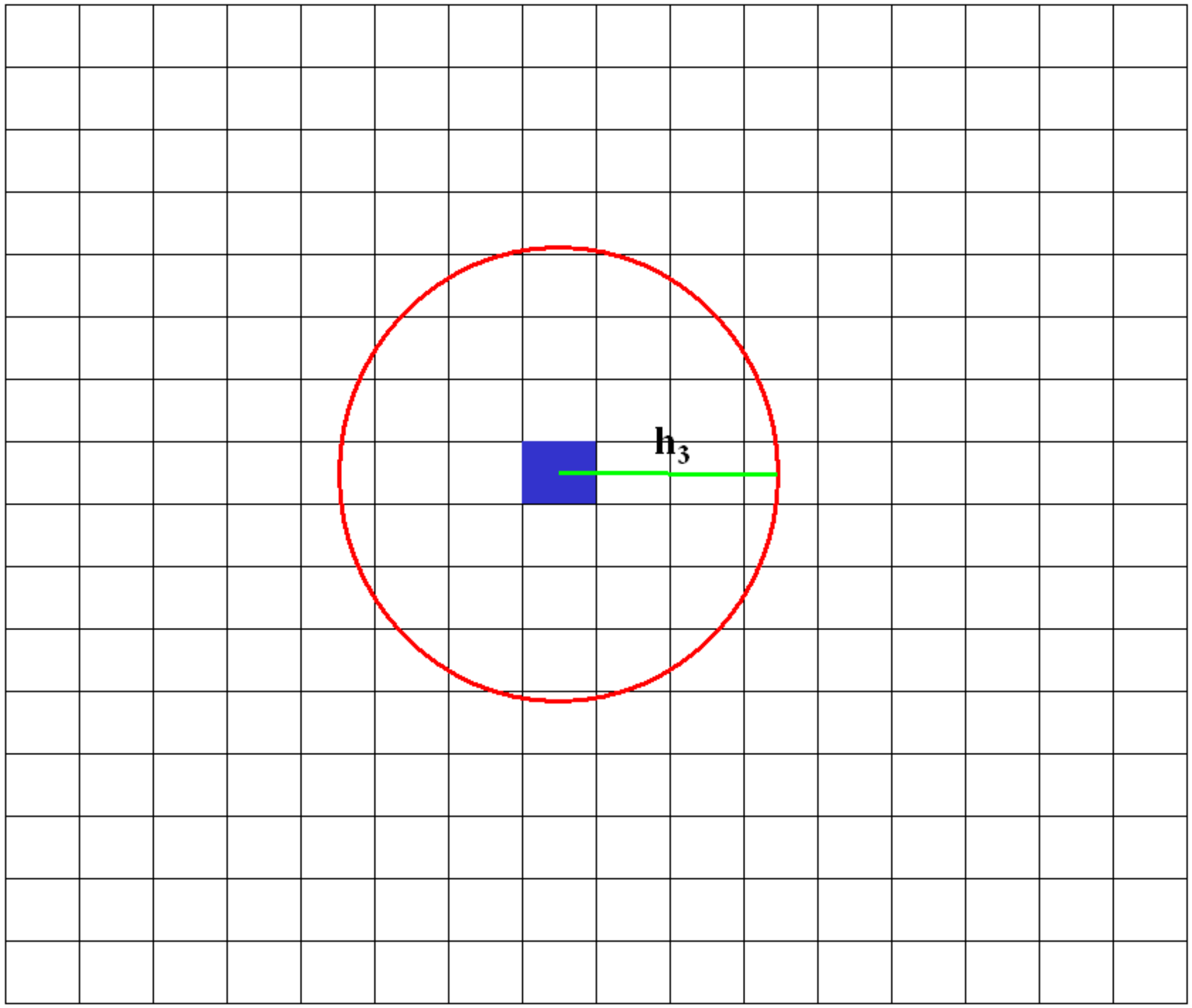
h_3

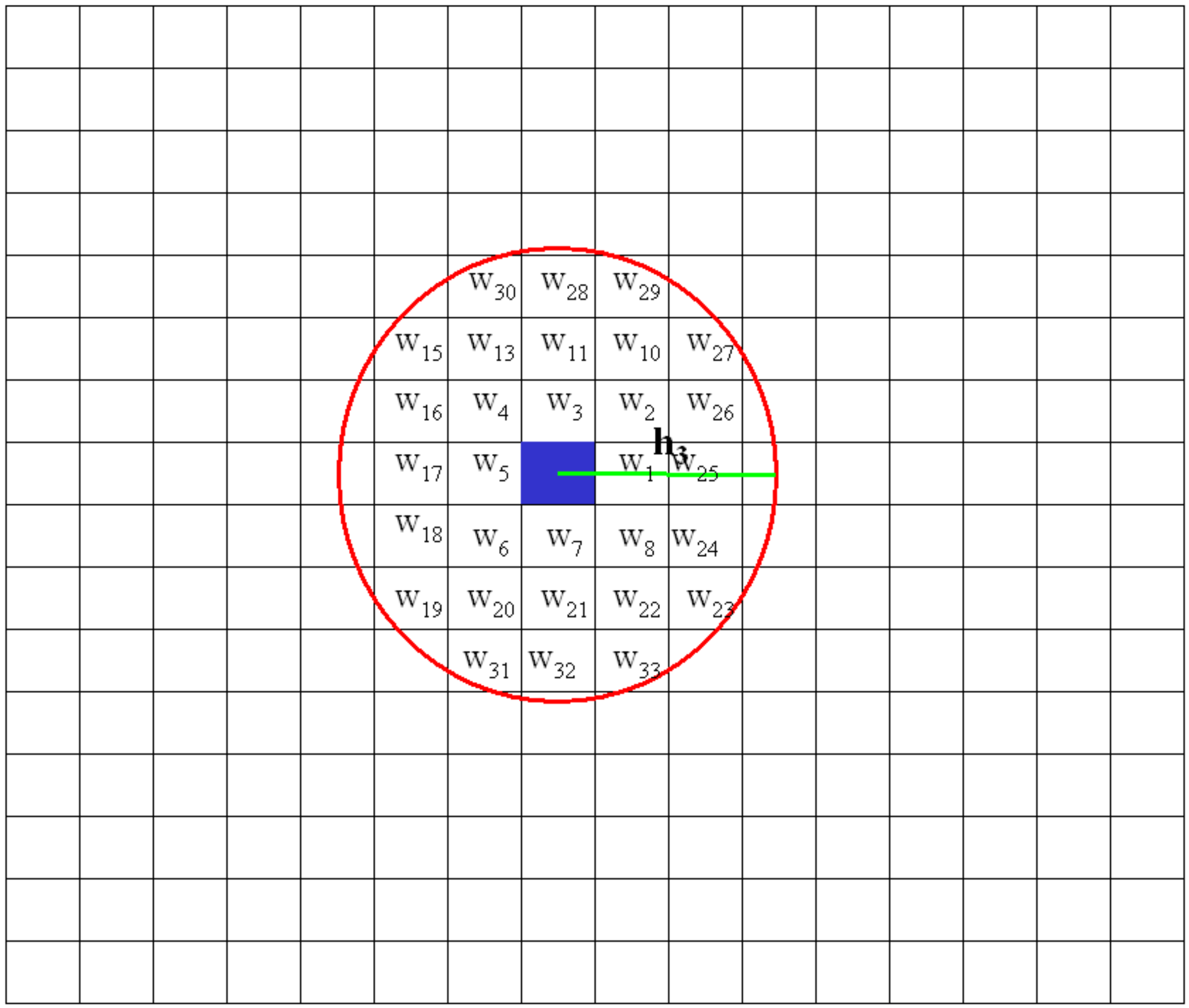

w_{30} w_{28} w_{29}
w_{15} w_{13} w_{11} w_{10} w_{27}
w_{16} w_4 w_3 w_2 w_{26}
h_3
w_{17} w_5 w_1 w_{25}
w_{18} w_6 w_7 w_8 w_{24}
w_{19} w_{20} w_{21} w_{22} w_{23}
w_{31} w_{32} w_{33}

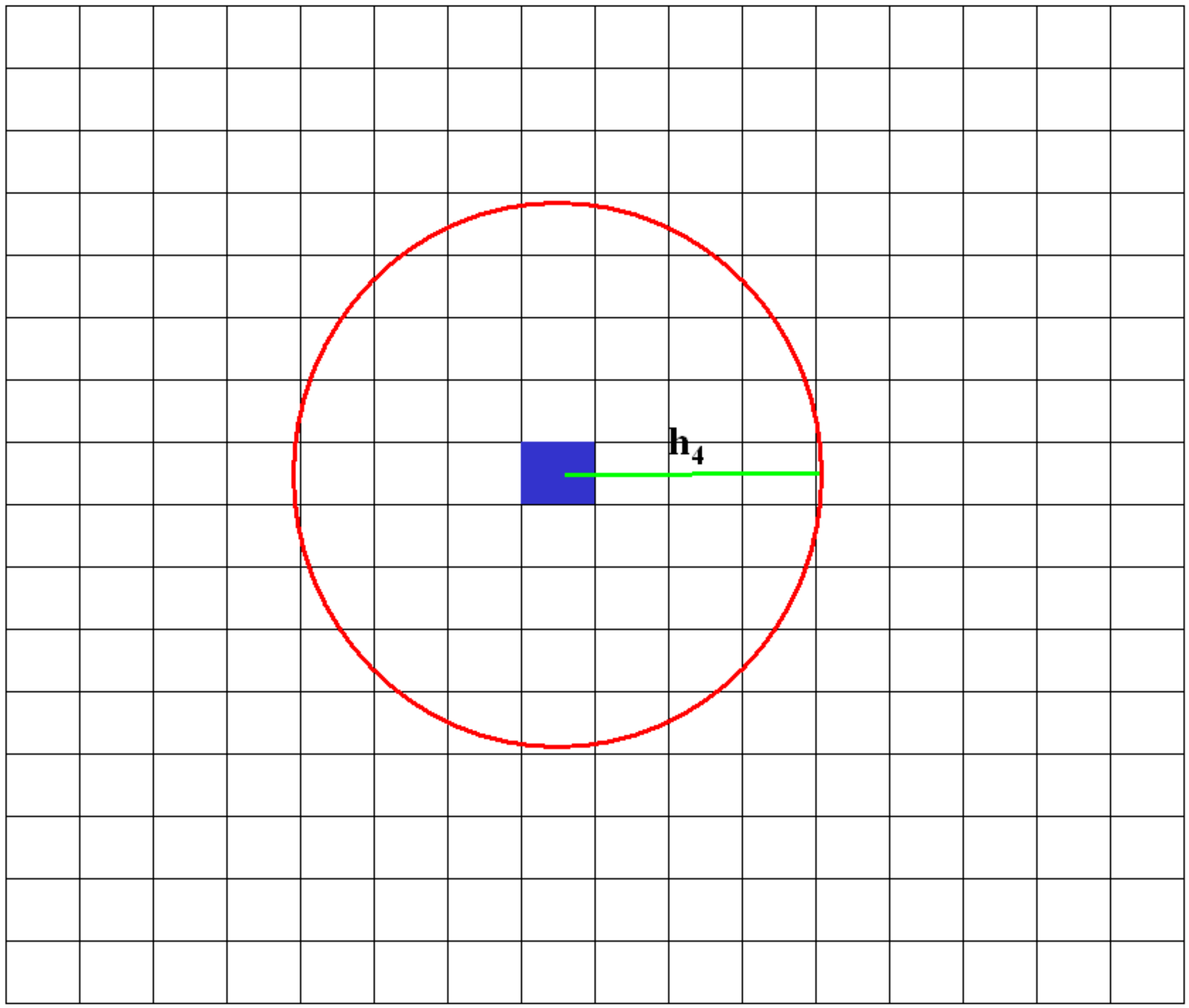
h_4

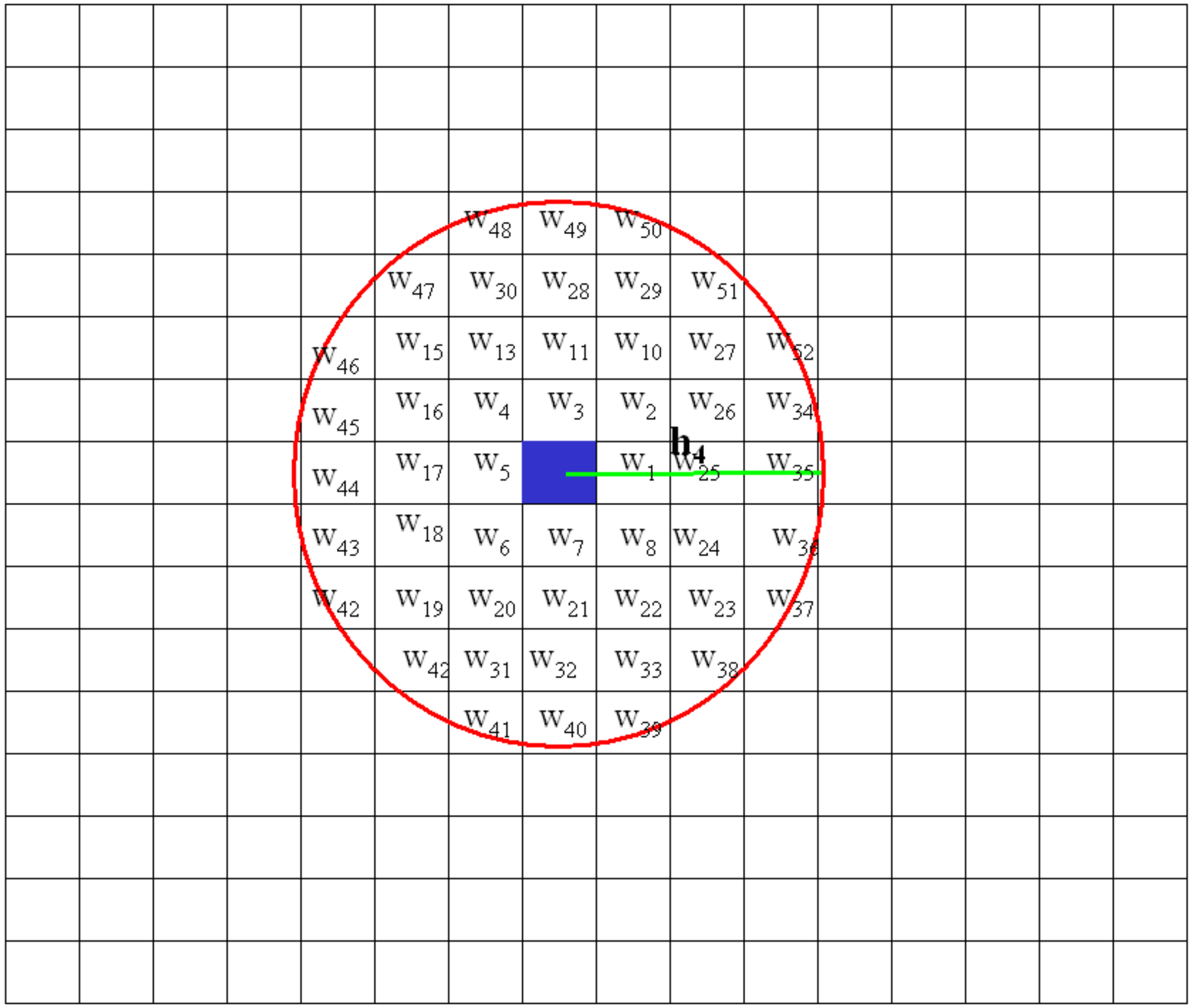

W48 W49 W50
W47 W30 W28 W29 W51
W46 W15 W13 W11 W10 W27 W52
W45 W16 W4 W3 W2 W26 W34
h4
W44 W17 W5 W1 W25 W35
W43 W18 W6 W7 W8 W24 W36
W42 W19 W20 W21 W22 W23 W37
W42 W31 W32 W33 W38
W41 W40 W39

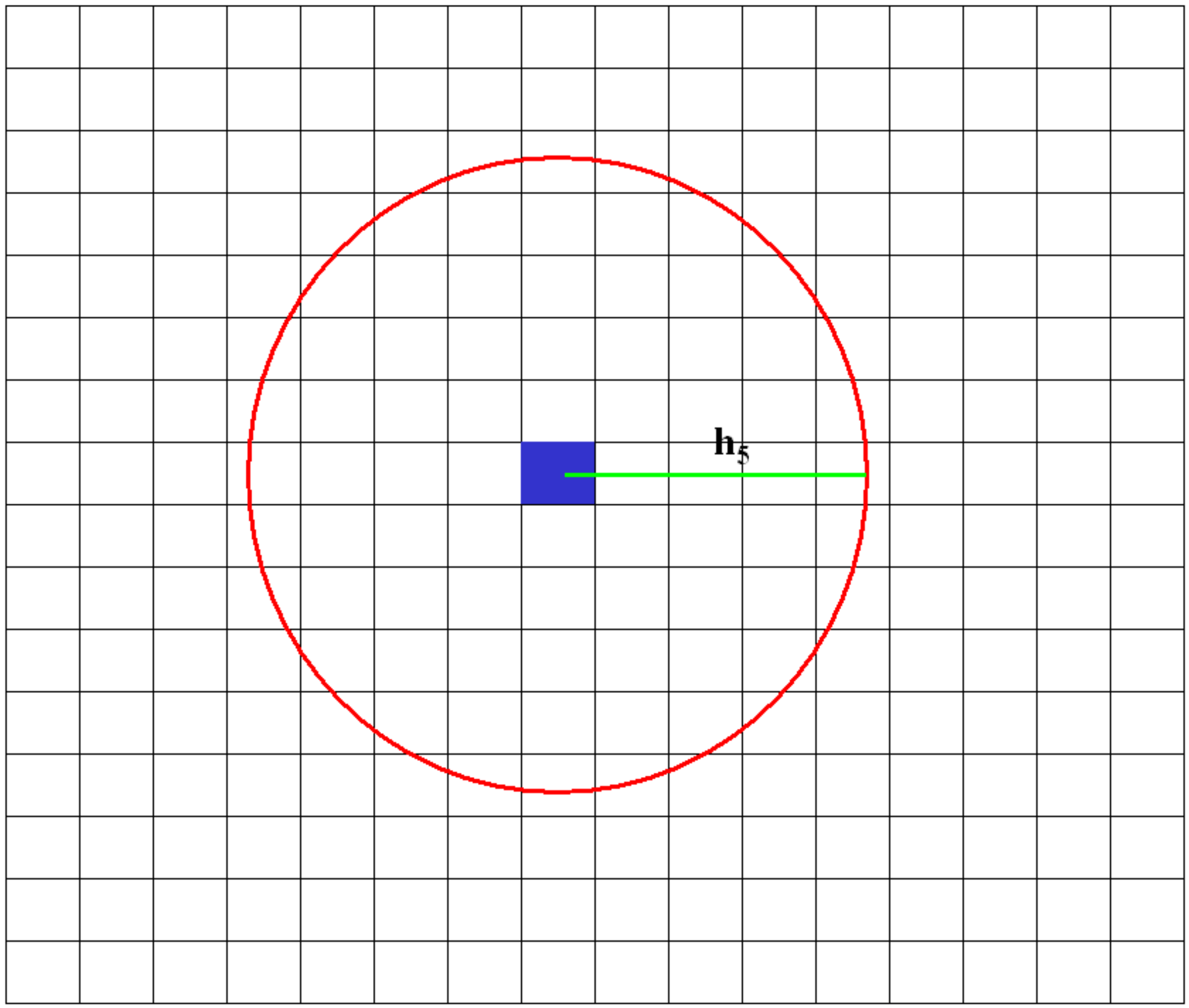
h_5

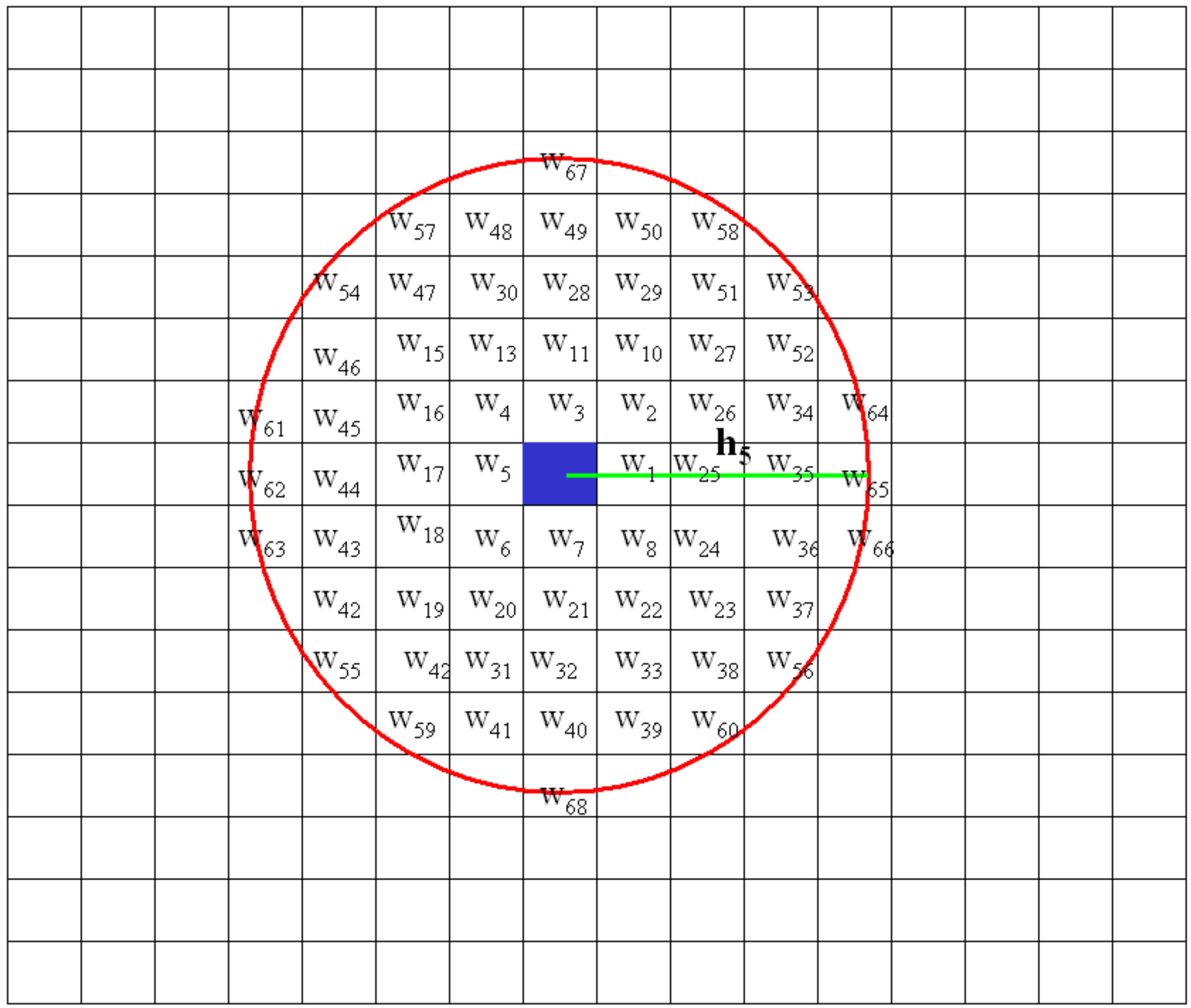

W_{67}
W_{57} W_{48} W_{49} W_{50} W_{58}
W_{54} W_{47} W_{30} W_{28} W_{29} W_{51} W_{53}
W_{46} W_{15} W_{13} W_{11} W_{10} W_{27} W_{52}
W_{61} W_{45} W_{16} W_{4} W_{3} W_{2} W_{26} W_{34} W_{64}
h_5
W_{62} W_{44} W_{17} W_{5} W_{1} W_{25} W_{35} W_{65}
W_{63} W_{43} W_{18} W_{6} W_{7} W_{8} W_{24} W_{36} W_{66}
W_{42} W_{19} W_{20} W_{21} W_{22} W_{23} W_{37}
W_{55} W_{42} W_{31} W_{32} W_{33} W_{38} W_{56}
W_{59} W_{41} W_{40} W_{39} W_{60}
W_{68}

Simulation Studies

Model $y_i(d) = x_i^T \beta(d) + \varepsilon_i(d)$

Error $\varepsilon_i(d) \sim N(0,1)$ $\varepsilon_i(d) \sim \chi^2(3) - 3$

$n = 60$ or $n = 80$

Covariates $x_i = (1, x_{i2}, x_{i3})^T$

$x_{i2} \sim \text{Bernoulli}(0.5)$

$x_{i3} \sim \text{Uniform}[1,2]$

Coefficients $\beta(d) = (\beta_1(d), \beta_2(d), \beta_3(d))^T$

$\beta_1(d) = \beta_2(d) = 0$

ROIs

ROI	*black*	*blue*	*red*	*yellow*	*white*
$\beta_3(d)$	0.0	0.2	0.4	0.6	0.8

64x64 phantom image

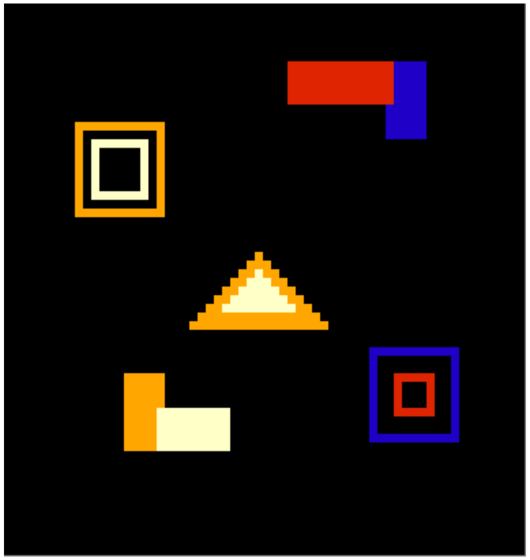

		$\chi^2(3)-3$						$N(0,1)$					
		$n=60$			$n=80$			$n=60$			$n=80$		
$\beta_2(d)$		h_0	h_5	h_{10}	h_0	h_5	h_{10}	h_0	h_5	h_{10}	h_0	h_5	h_{10}
0.0	BIAS	0.00	0.00	0.01	0.00	0.00	0.00	0.00	0.00	0.00	0.00	0.00	0.00
	RMS	0.48	0.35	0.26	0.41	0.31	0.22	0.20	0.15	0.11	0.17	0.13	0.09
	SD	0.47	0.34	0.24	0.41	0.30	0.21	0.19	0.14	0.10	0.17	0.12	0.09
	RE	1.03	1.05	1.06	1.02	1.03	1.04	1.03	1.05	1.06	1.02	1.03	1.04
0.2	BIAS	0.00	-0.03	-0.07	0.01	-0.02	-0.06	0.00	-0.03	-0.05	0.00	-0.02	-0.05
	RMS	0.46	0.34	0.24	0.39	0.29	0.21	0.19	0.14	0.11	0.16	0.12	0.09
	SD	0.46	0.33	0.24	0.40	0.29	0.21	0.19	0.14	0.10	0.16	0.12	0.09
	RE	1.01	1.01	1.01	0.99	1.00	1.01	1.02	1.04	1.06	1.02	1.02	1.03
0.4	BIAS	-0.01	-0.05	-0.09	0.01	-0.02	-0.06	0.00	0.00	-0.01	0.00	0.00	0.00
	RMS	0.46	0.34	0.25	0.40	0.30	0.22	0.19	0.15	0.12	0.16	0.13	0.10
	SD	0.46	0.33	0.24	0.40	0.29	0.21	0.19	0.14	0.11	0.16	0.12	0.09
	RE	1.01	1.02	1.03	1.01	1.02	1.03	1.03	1.05	1.07	1.00	1.01	1.02
0.6	BIAS	0.00	-0.05	-0.09	0.00	-0.04	-0.07	0.00	0.01	0.02	0.00	0.00	0.01
	RMS	0.46	0.35	0.26	0.40	0.30	0.23	0.19	0.15	0.12	0.16	0.13	0.10
	SD	0.46	0.34	0.25	0.40	0.30	0.22	0.19	0.14	0.11	0.16	0.13	0.10
	RE	1.01	1.03	1.04	1.01	1.02	1.03	1.02	1.04	1.06	1.01	1.03	1.04
0.8	BIAS	0.00	-0.04	-0.06	0.00	-0.02	-0.05	0.00	-0.01	-0.02	0.00	0.00	-0.01
	RMS	0.47	0.35	0.26	0.40	0.30	0.23	0.19	0.15	0.11	0.17	0.13	0.10
	SD	0.46	0.34	0.25	0.40	0.30	0.22	0.19	0.14	0.11	0.16	0.12	0.09
	RE	1.02	1.03	1.04	1.01	1.02	1.03	1.02	1.04	1.05	1.03	1.05	1.06

$\hat{\beta}_3(d,h_0)$

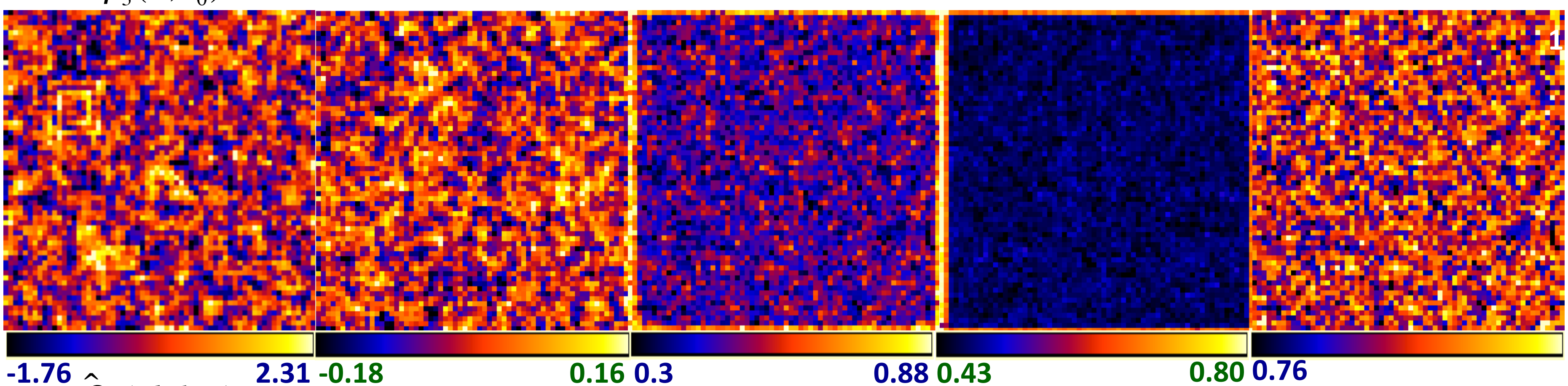

$\hat{\beta}_3(d,h_{10})$

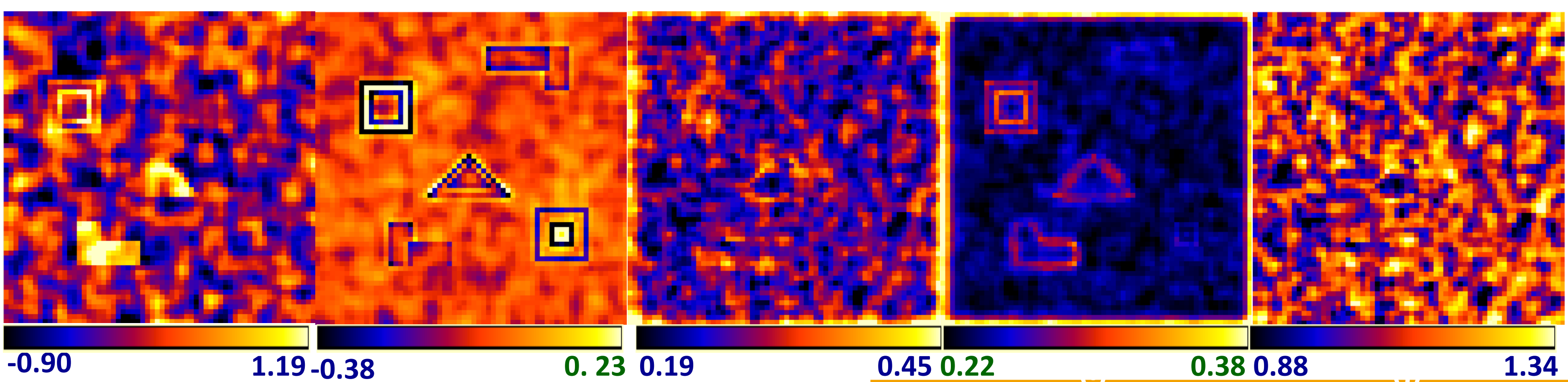

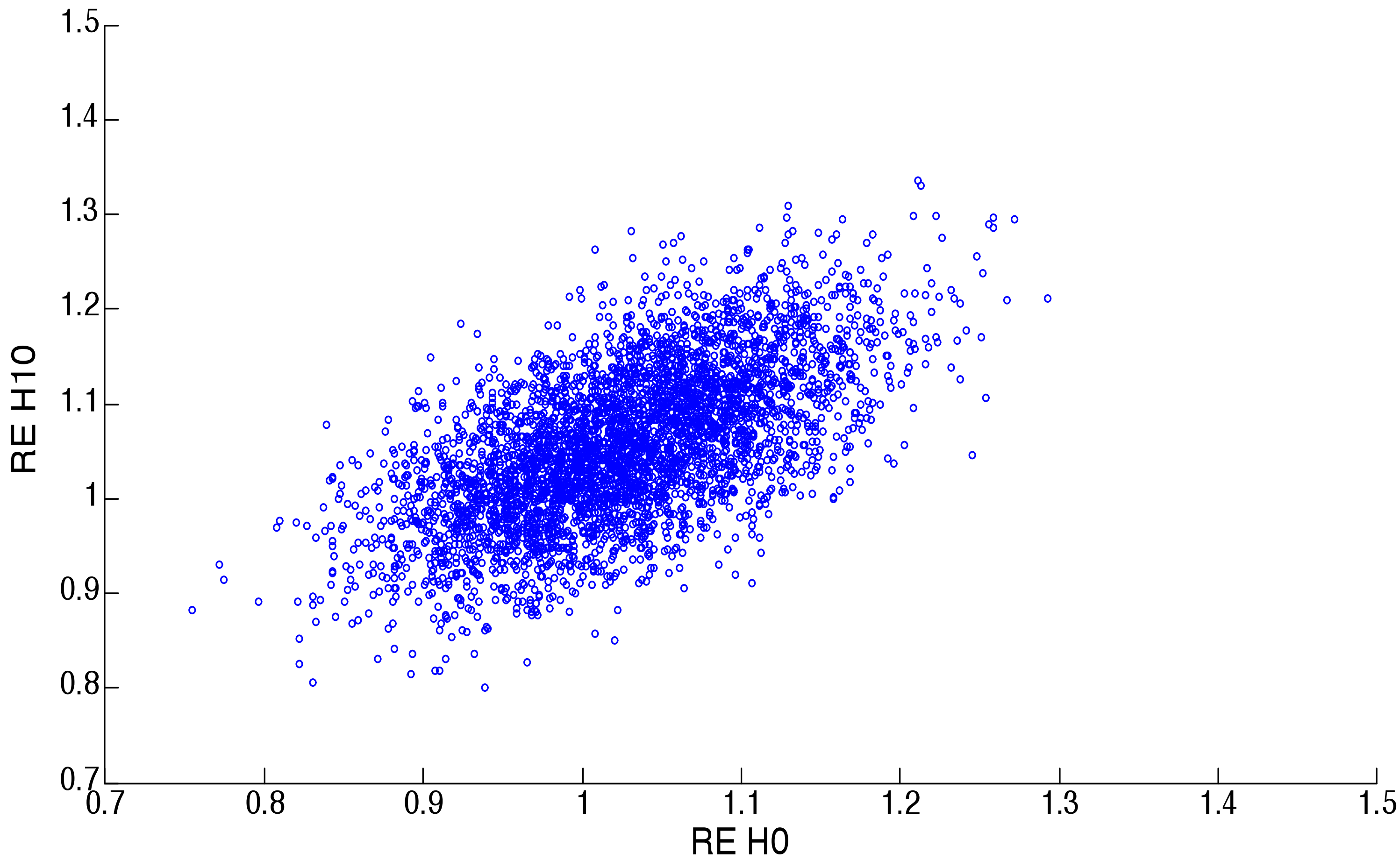

1.5
1.4
1.3
1.2
1.1
1
0.9
0.8
0.7
RE H10
0.7
0.8
0.9
1
1.1
1.2
1.3
1.4
1.5
RE H0

Simulation Studies

Table 2. Simulation study for $W_\mu(d,h)$: estimates (ES) and standard errors (SE) of rejection rates for pixels inside the five ROIs were reported at 2 different scales (h_0, h_{10}), 2 different distributions ($N(0,1)$ and $\chi^2(3)-3$), and 2 different sample sizes ($n=60,80$) at $\alpha=5\%$. For each case, 1,000 simulated data sets were used.

		$N(0,1)$				$\chi^2(3)-3$			
		$n=60$		$n=80$		$n=60$		$n=80$	
$\beta_2(d)$	s	ES	SE	ES	SE	ES	SE	ES	SE
0.2	h_0	0.20	0.066	0.24	0.070	0.08	0.038	0.08	0.037
	h_{10}	0.30	0.126	0.38	0.121	0.10	0.069	0.18	0.081
0.4	h_0	0.56	0.090	0.67	0.079	0.15	0.065	0.18	0.070
	h_{10}	0.93	0.051	0.98	0.030	0.26	0.129	0.35	0.159
0.6	h_0	0.88	0.039	0.95	0.024	0.27	0.057	0.33	0.050
	h_{10}	1.00	0.004	1.00	0.004	0.51	0.091	0.63	0.083
0.8	h_0	0.99	0.015	1.00	0.005	0.43	0.080	0.52	0.080
	h_{10}	0.99	0.010	0.99	0.011	0.78	0.099	0.90	0.006
0.0	h_0	0.07	0.006	0.07	0.006	0.06	0.007	0.07	0.006
	h_{10}	0.08	0.011	0.07	0.011	0.07	0.012	0.08	0.012

Infant Brain Development Data

- **Objective:** We want to assess the brain structure change in the early brain development.
- **Subject:** 38 infants.
- **Image:** Diffusion-weighted images and T1 weighted images were acquired for each subject at 2 weeks, 1 and 2 years old.
- **Method:** Voxel-wise imaging analysis and MARM.

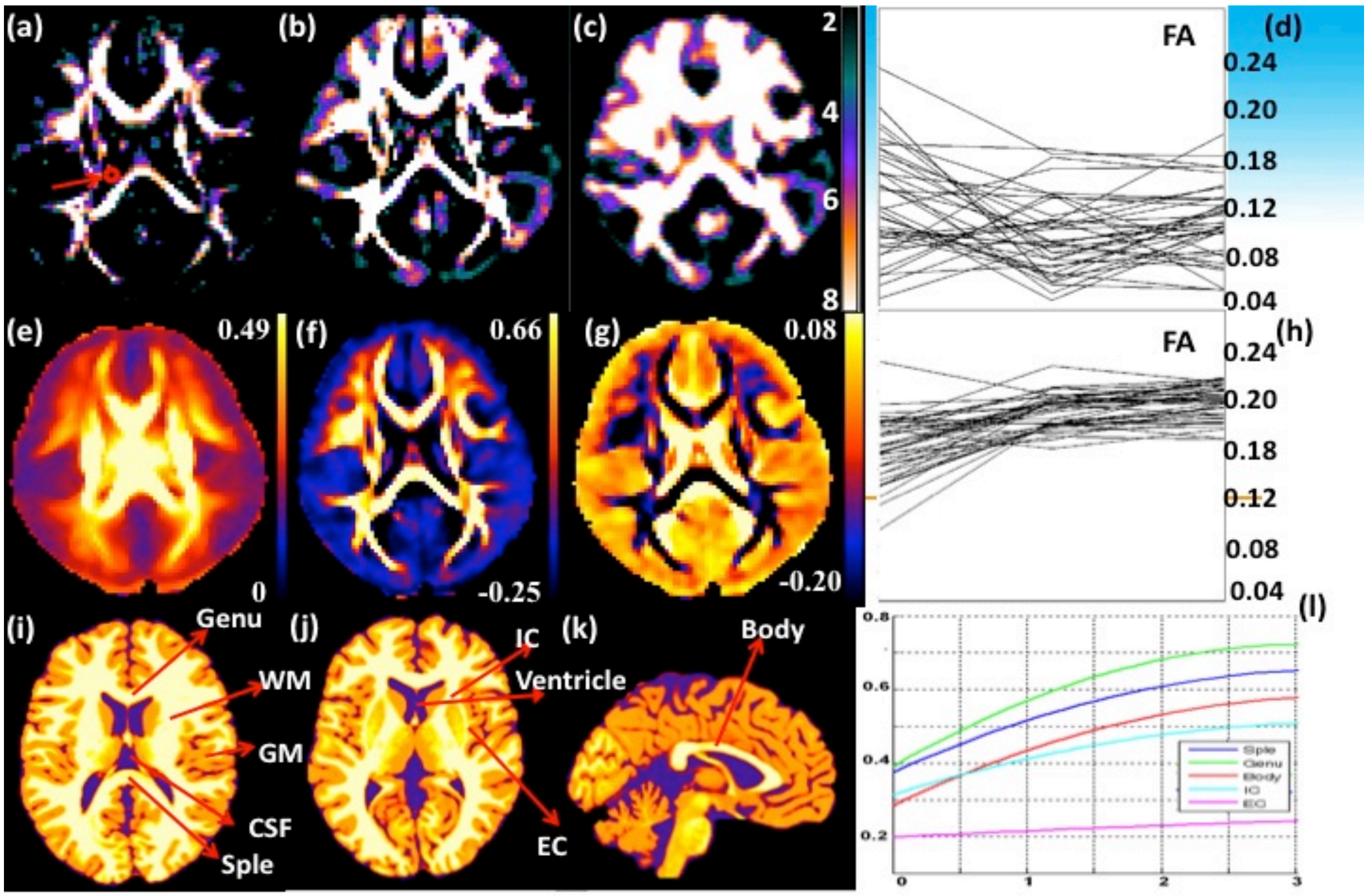

(a)
(b)
(c)
2
4
6
8
FA
(d)
0.24
0.20
0.18
0.12
0.08
0.04
(e)
0.49
0
(f)
0.66
-0.25
(g)
0.08
-0.20
FA
(h)
0.24
0.20
0.18
0.12
0.08
0.04
(i)
Genu
WM
GM
CSF
Sple
(j)
IC
Ventricle
EC
(k)
Body
(l)
0.8
0.6
0.4
0.2
0
1
2
3
Sple
Genu
Body
IC
EC

New Developments

- Adaptive Neighhoods
- Adaptive Weights
- Cross-sectional, longitudinal, twin and family studies
- Robust Procedure
- Parametric and Nonparametric Components

Brain Connectivity Analysis

Penalized Methods, Multivariate Analysis, and Time Series Analysis

How to spatially and temporally quantify the dynamic association among different functional regions?

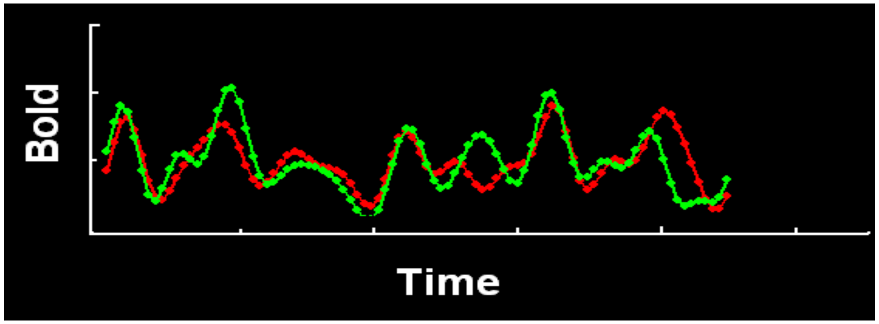

Functional connectivity is the mechanism for the coordination of activity between different neural assemblies in order to achieve a complex cognitive task or perceptual process. (Fingelkurts, Fingelkurts, Seppo Kahkonen, Fingelkurts, 2005)

Resting-State Network:
fMRI for finger tapping task;
fcMRI: contralateral motor cortex showed activation and low frequency (<0.1 Hz) fluctuations in the signal of the resting brain, revealing a high degree of temporal correlation.

fMRI fcMRI

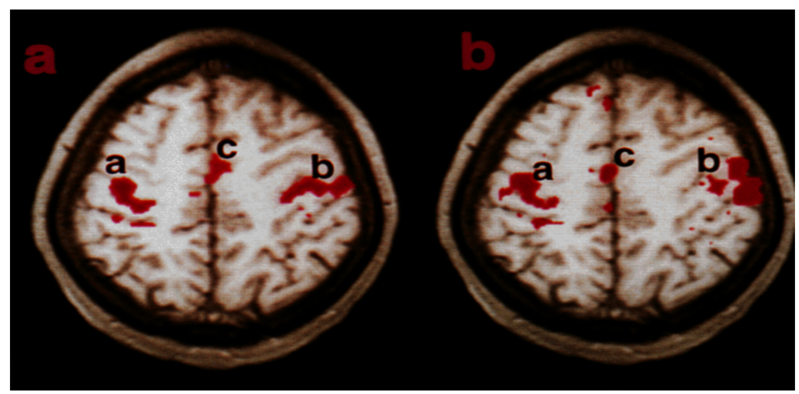

Biswal et al, JCBFM, 17:301-308, 1997

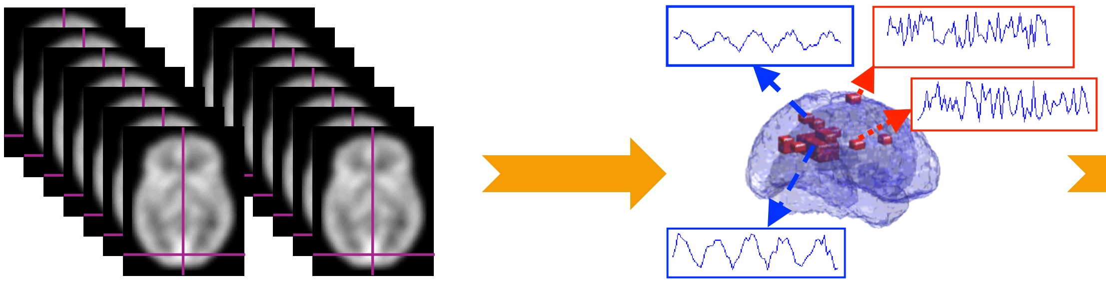

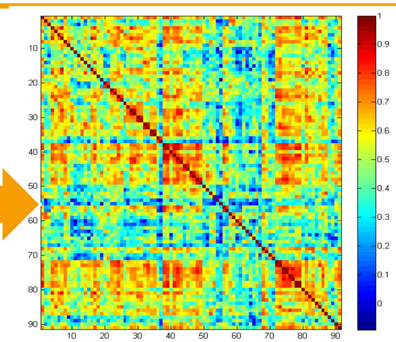

Conventional Analysis

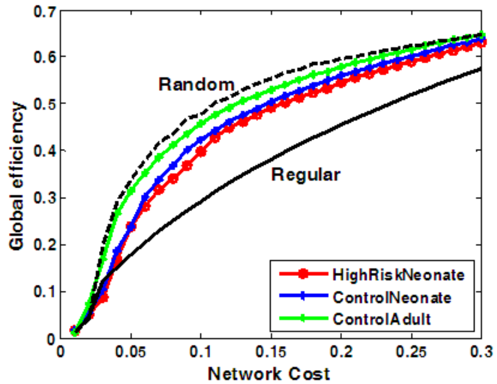

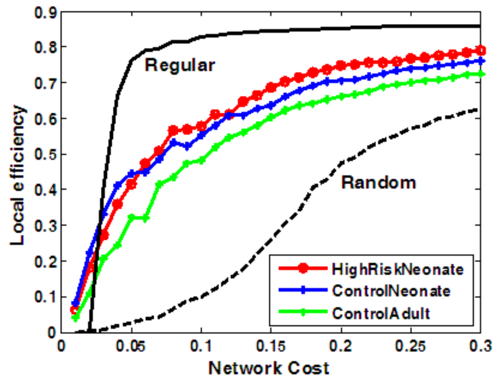

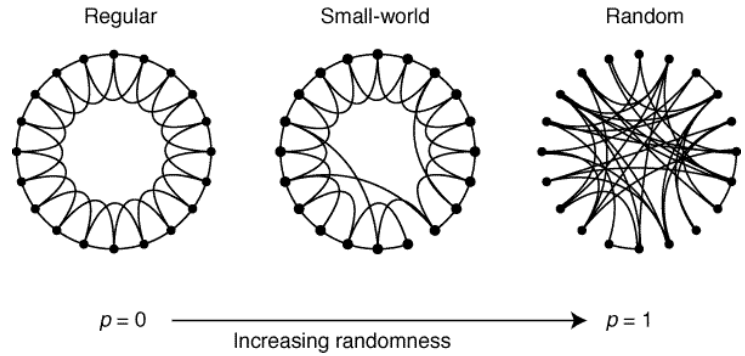

A multivariate network-level approach

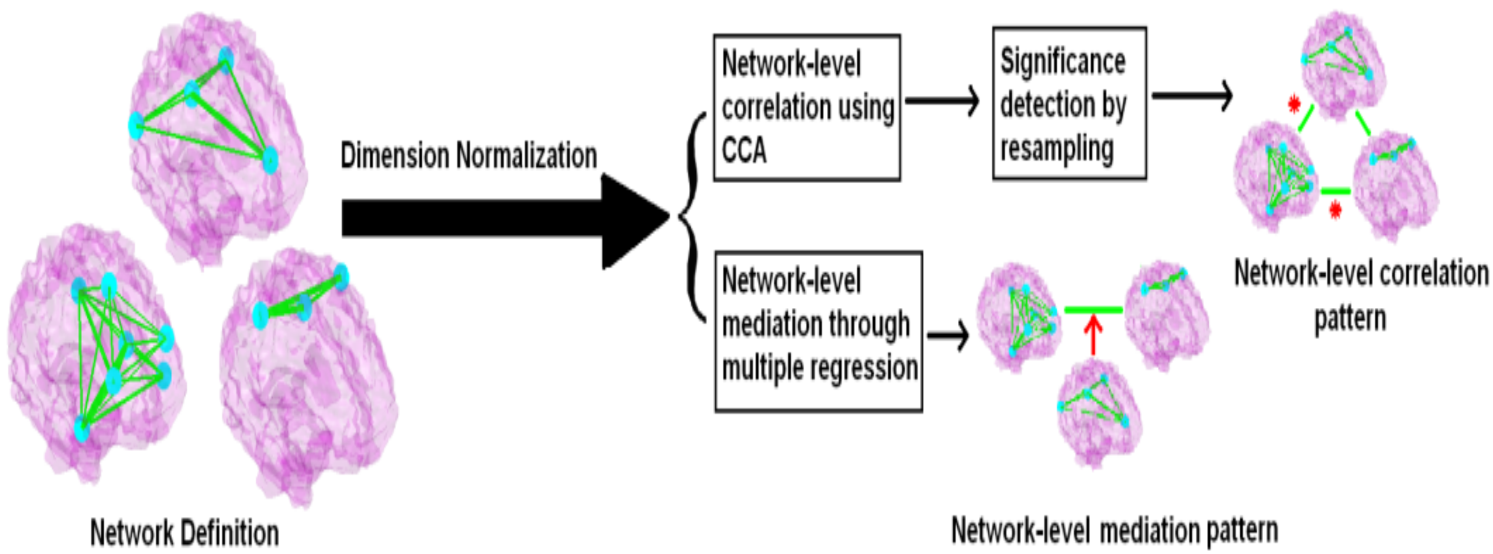

(i) network-level correlation using CCA;
(ii) network-level mediation analysis;
(iii) significance detection by resampling methods;
(iv) Network-level correlation pattern.

Network Definition

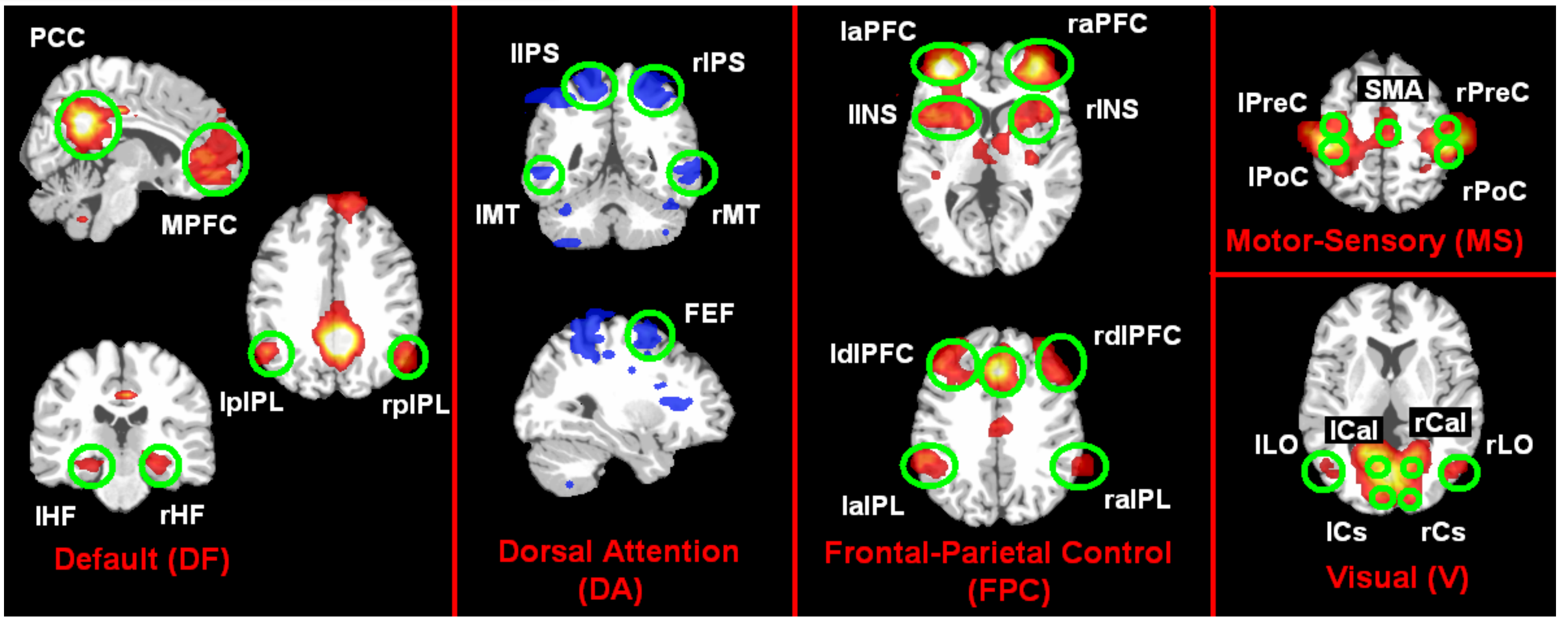

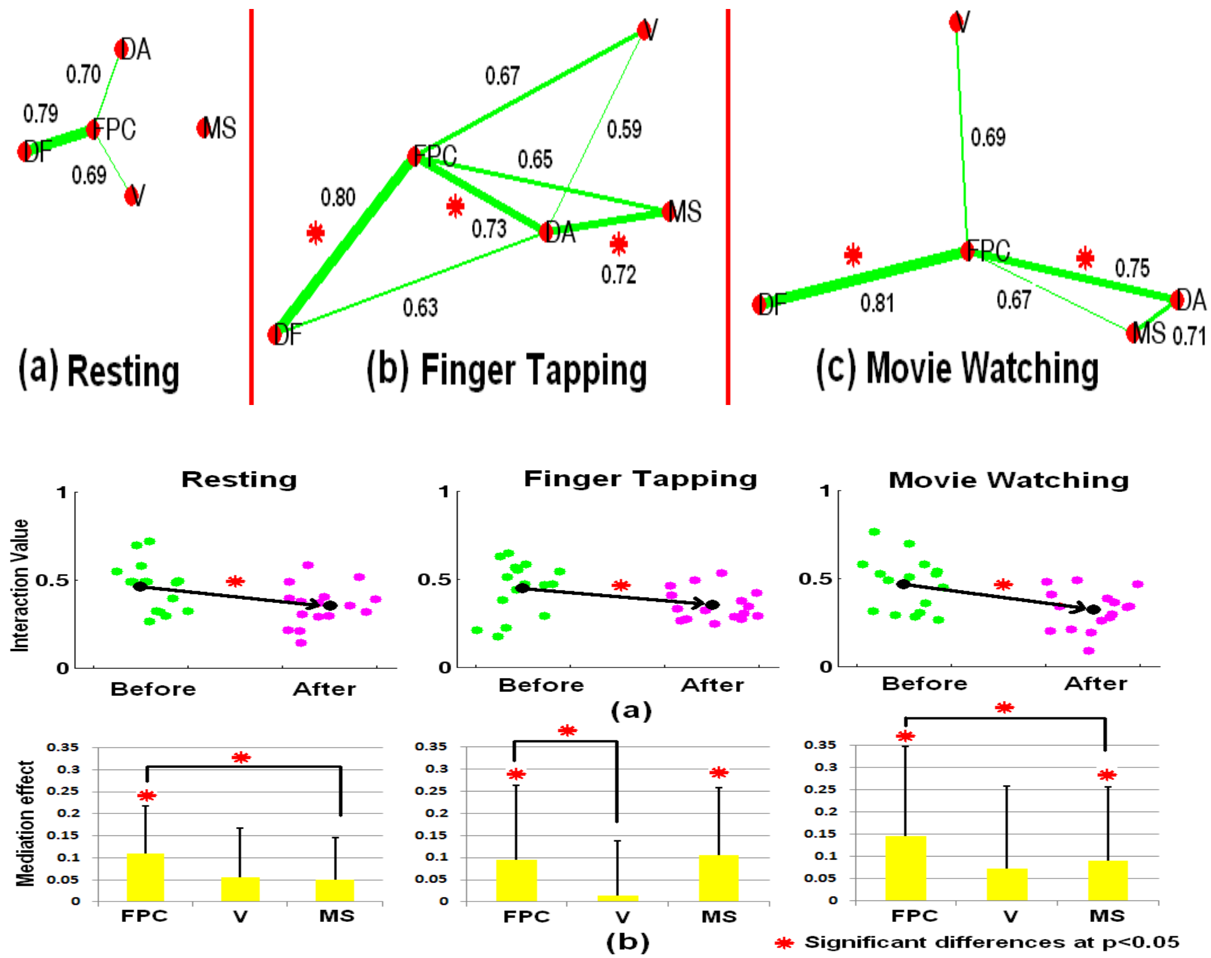

DA
0.70
0.79
FPC
MS
DF
0.69
V
(a) Resting
V
0.67
0.59
FPC
0.65
MS
0.80
0.73
DA
0.72
0.63
DF
(b) Finger Tapping
V
0.69
FPC
0.75
DF
0.81
0.67
DA
MS 0.71
(c) Movie Watching
Resting
Finger Tapping
Movie Watching
Interaction Value
Before
After
(a)
Mediation effect
FPC
V
MS
(b)
Significant differences at p<0.05

Selective regulation of the two opposing networks during different tasks

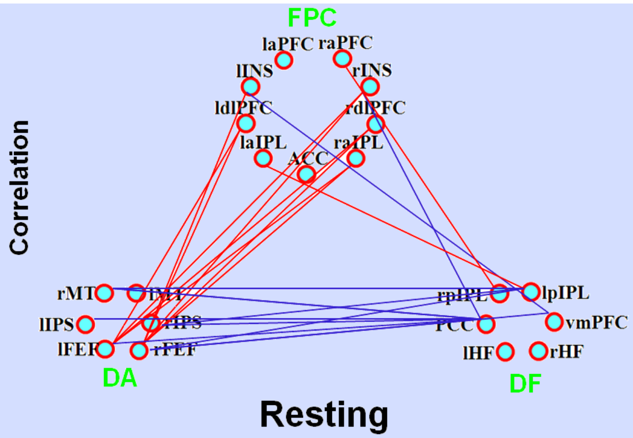

Bayesian Covariance Lasso

Flow Cytometry Data
11 proteins
7466 cells

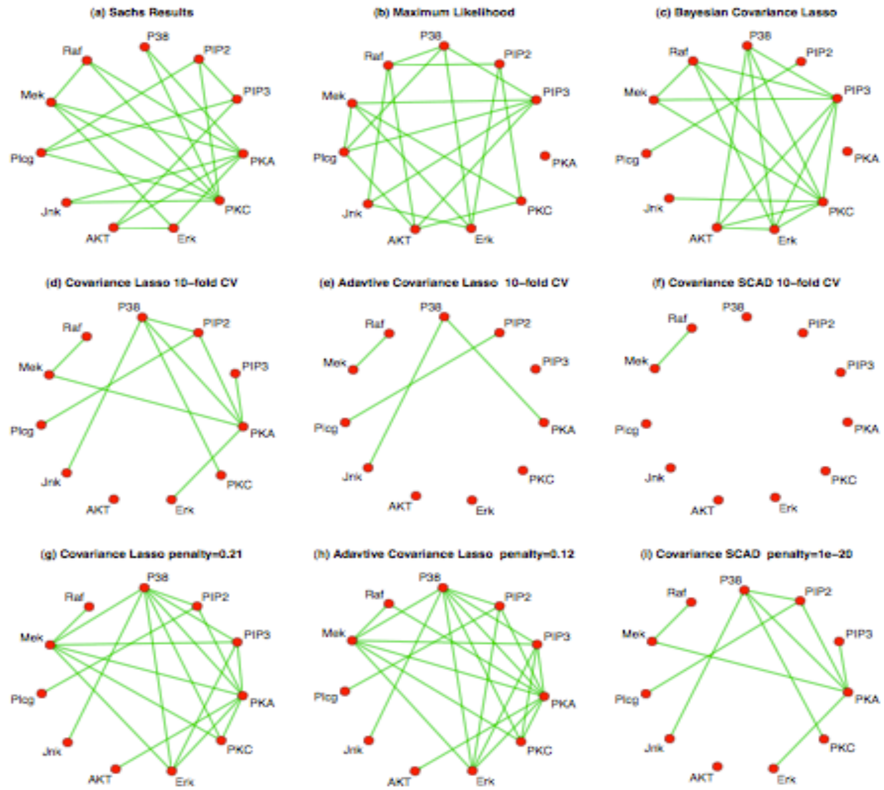

Fig. 5: Networks for 11 proteins from Sachs et al. (2003).

90 ROIs
30 subjects
2-rd fcMRI

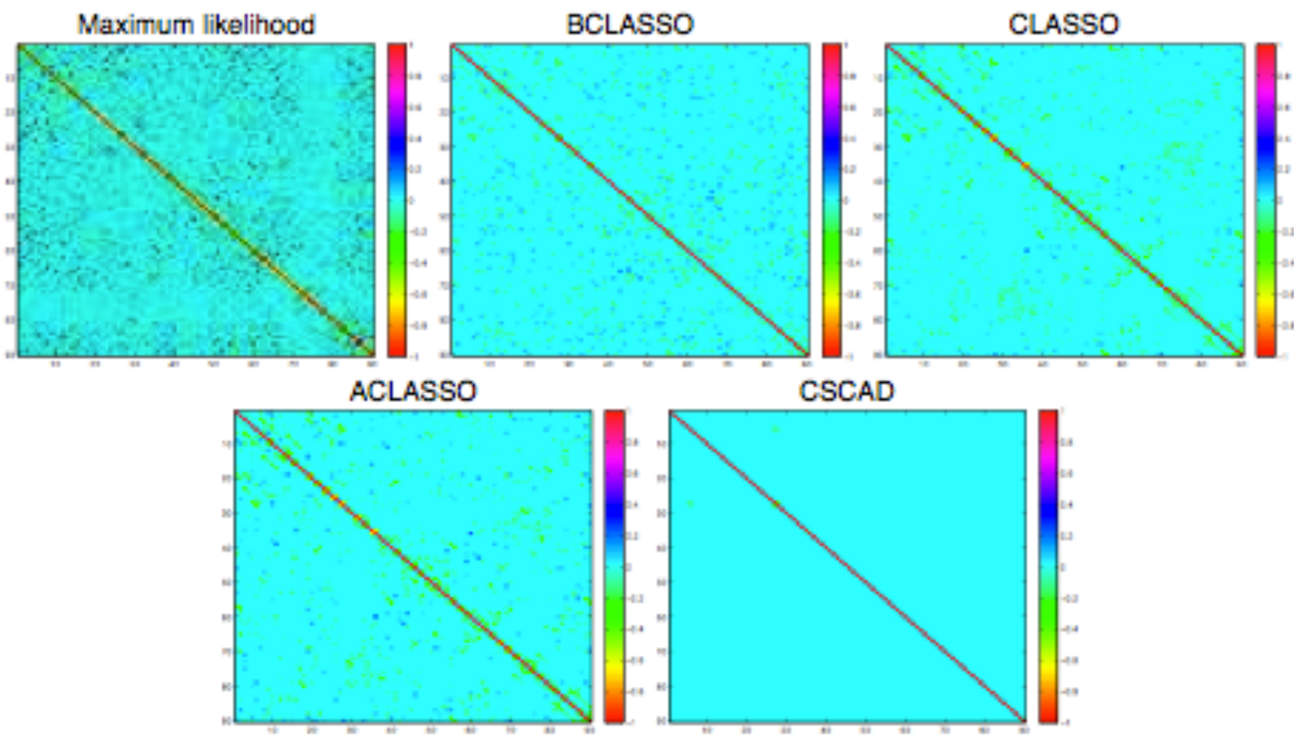

Fig. 6: Image plots of the partial correlation matrices for 90 regions of 2-year old children's brains using the different methods

Acknowledgements